

Simultaneous Localization and Mapping Related Datasets: A Comprehensive Survey

Yuanzhi Liu, Yujia Fu, Fendong Chen, Bart Goossens, Wei Tao, and Hui Zhao

Abstract—Due to the complicated procedure and costly hardware, Simultaneous Localization and Mapping (SLAM) has been heavily dependent on public datasets for drill and evaluation, leading to many impressive demos and good benchmark scores. However, with a huge contrast, SLAM is still struggling on the way towards mature deployment, which sounds a warning: some of the datasets are overexposed, causing biased usage and evaluation. This raises the problem on how to comprehensively access the existing datasets and correctly select them. Moreover, limitations do exist in current datasets, then how to build new ones and which directions to go? Nevertheless, a comprehensive survey which can tackle the above issues does not exist yet, while urgently demanded by the community. To fill the gap, this paper strives to cover a range of cohesive topics about SLAM related datasets, including general collection methodology and fundamental characteristic dimensions, SLAM related tasks taxonomy and datasets categorization, introduction of state-of-the-arts, overview and comparison of existing datasets, review of evaluation criteria, and analyses and discussions about current limitations and future directions, looking forward to not only guiding the dataset selection, but also promoting the dataset research.

Index Terms—Dataset, evaluation, localization, mapping, review, SLAM, survey.

I. INTRODUCTION

Simultaneous Localization and Mapping (SLAM) is a subject with respect to achieving both “internal and external cultivation” in a mobile robot – externally knowing the world by constructing a map and internally knowing itself by tracking the location [1], [2], [3]. Serving as the decisive technology of mobile robotic community, SLAM has attracted significant attention and aroused many productive applications. In self-driving cars [4], navigating robots [5], and unmanned aerial vehicles (UAVs) [6], [7], SLAM maps the surrounding environment and figures out the ego-motion inside the map. In virtual reality/augmented reality (VR/AR) systems [8], SLAM

gives accurate poses of the agent, thus helps to intuitively manipulate virtual objects. In mobile mapping [9], SLAM estimates transformations across adjacent frames and merges together the 3D points into a consistent model. However, from the real-world deployment point of view, such technologies are far from mature, indicating a huge gap between benchmark scores and mature productivity [10], [11].

The research of SLAM related problems has been heavily relying on publicly available datasets. On the one hand, the concrete experiment of SLAM related problems involves quite costly hardware and complicated procedure. One has to employ mobile platforms (such as a wheeled robot), sensors (such as LiDARs and cameras), and ground truth instruments (such as a real-time kinematic (RTK) corrected global navigation satellite system (GNSS) and a set of motion capture system), which are huge financial burdens for individual researchers. And if multi-sensor data are required (in most cases it is), the temporal and spatial calibration is obligatory to be performed before data collection. Overall, it is almost impossible to test every draft in the manner of field experiment. On the other hand, datasets can provide equitable benchmarks for evaluation and comparison. To fairly quantify the algorithm performance, the dataset providers have proposed several consensual evaluation criteria and indicators [12], [13]. By evaluating on the same datasets, researchers worldwide are able to compare their algorithms horizontally. Gradually, public benchmark score has become a fundamental basis of today’s paper publication.

In this context, four major problems arose. Firstly, the usages of existing datasets are quite biased. Actually, over the past decade, a quantity of datasets have been released, whereas the researchers lack a convenient way to know them, thus only test on several best-known ones, such as KITTI [14], TUM RGB-D [12], and EuRoC [15]. This may well result in over-fitting, thus good scores on a certain benchmark cannot ensure equally good results on the others. Secondly, the selection of datasets lacks a clue and is sometimes incorrect. SLAM is an emerging but complicated subject, while still there is no clear taxonomy on related tasks. This causes a two-way selection difficulty: the algorithm researchers have no clue to choose suitable datasets, and the dataset providers have no basis to specify the evaluable tasks of them. Thirdly, the existing datasets are still limited in some dimensions. For example, lack of scene types, data size, and sensor number and modalities, limitation of ground truth, etc. Although different datasets are complementary, still the datasets in their entirety do not reflect all-roundly the real world, thus could easily hide the defects of algorithms. Nevertheless, such limitations are rarely analyzed to recommend future direc-

This work is supported by the National Key R&D Program of China under Grant 2018YFB1305005.

Yuanzhi Liu, Yujia Fu, Wei Tao, and Hui Zhao are with the Department of Instrument Science and Engineering, School of Electronic Information and Electrical Engineering, Shanghai Jiao Tong University, Shanghai 200240, China (e-mail: lyzrose@sjtu.edu.cn, yujiafu@sjtu.edu.cn, taowei@sjtu.edu.cn, huizhao@sjtu.edu.cn).

Fendong Chen is with the School of Instrumentation Science and Engineering, Harbin Institute of Technology, Harbin 150001, China (e-mail: chenfd@hit.edu.cn).

Bart Goossens is with the Department of Telecommunications and Information Processing (TELIN), Ghent University, 9000 Ghent, Belgium, and also with the Interuniversity Microelectronics Center (imec), 3001 Leuven, Belgium (e-mail: bart.goossens@ugent.be).

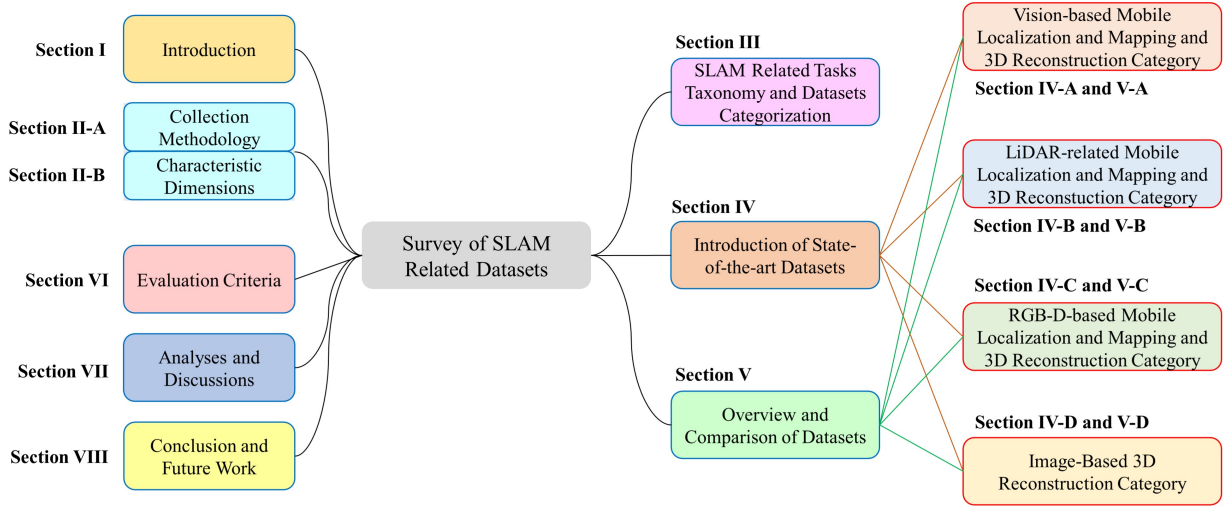


Fig. 1. The schematic diagram of the overall structure of the paper.

tions. Fourthly, the threshold in creating datasets is relatively high. The research of SLAM related datasets is a self-contained subject which can push the limits of algorithms at another level, while still the community cannot access a systematical knowledge about collection methodology and characteristics, which may well affect the widespread releases of new datasets.

To the best of our knowledge, no open literature has addressed the above issues. Even, there is not any survey specializing in SLAM datasets yet. Firman [16] surveyed a total of 102 RGB-D datasets, while out of them, only 9 can be used for SLAM related problems. Cai et al. [17] also surveyed the RGB-D-based datasets, and 46 datasets were categorized into 5 categories, whereas covered only 2 for SLAM usages. Bresson et al. [18] presented a survey about the trends of SLAM in autonomous driving with 10 datasets summarized, nevertheless, they were quite old and mainly collected for LiDAR-based methods, which were far from comprehensive. Yurtsever et al. [19] also presented a survey about autonomous driving, with an overview of 18 datasets. However, the applicable tasks were not specified: many of them cannot be used for SLAM purpose.

To fill the gap, this paper strives to present a structured and comprehensive survey about SLAM related datasets. On the one hand, as there is not any perfect or dominant dataset in SLAM domain over this period (as ImageNet [20] in computer vision field), we believe SLAM related datasets should be used in a manner of complementation. To this end, the primary goal of this paper is to serve as a dictionary to ensure comprehensive, correct, and efficient dataset selections. Based on the proposed SLAM related tasks taxonomy and datasets categorization, we survey a total of 97 datasets with every dataset specified with the applicable tasks, and meanwhile, many dimensions of characteristics are summarized and compared. On the other hand, whether from the perspective of drilling or evaluation, we believe the datasets can push the limits of SLAM related algorithms in another level. Thus, another goal of this paper is to lower the threshold and guide the future directions of dataset research. Therefore, the general collection methodology and fundamental characteristic dimensions of SLAM related

datasets are described, and the current limitations and future directions are analyzed and discussed. Moreover, some state-of-the-art datasets and consensual evaluation criteria are introduced in detail, which are instructive to future releases.

The remainder of this paper is organized into 5 sections (the overall structure is shown in Fig. 1). Section II introduces the general collection methodology and fundamental characteristic dimensions of SLAM related datasets, in order to pave the way for the following introductions. Section III clears the taxonomy of SLAM related tasks, resulting in four broad categories for datasets classification. Section IV introduces 16 state-of-the-art datasets in detail. Section V surveys by category as many as possible existing SLAM related datasets (97 in total), forming into 2 overview and comparison tables for each category, with guidelines on datasets selection. Section VI reviews the key evaluation criteria. Section VII gives analyses and discussions on the current weaknesses and future directions of datasets and evaluation. Finally, Section VIII draws a brief conclusion and arranges the future work.

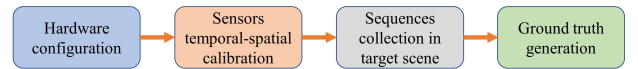


Fig. 2. The general collection methodology of dataset collection.

II. SLAM RELATED DATASETS: GENERAL COLLECTION METHODOLOGY AND FUNDAMENTAL DIMENSIONS

A. General Collection Methodology

The general methodology of dataset collection is shown in Fig. 2: configure the hardware first, then perform temporal-spatial sensor calibration, then collect data sequences in a target testing scene, finally generate accurate ground truth. As can be seen, the procedure is more complicated than the other kinds of dataset, such as object detection, which does not require strictly sensor calibration or high-end ground truth generation techniques. To lower the threshold of the research, and pave the way for the following introductions, this part will give a concrete description of the general methodology. It should be noted that, in addition to the real-world data collection, there is also a virtual and synthetic

manner, just like the rendering of some realistic 3D computer games. However, the methodology of such manner is mainly a software issue (such as using AirSim¹ and POV-Ray²), hence we will not introduce it in detail.

1) Hardware Configuration

Hardware configuration involves the selection of mobile platforms and perception sensors. For the mobile platforms, the selection mainly depends on the target applications, for example: using a handheld carrier for VR/AR and smartphone applications, a backpack for mobile mapping, an automobile for autonomous driving, a wheeled robot for service and navigation robotics, and an UAV for aerial applications.

For the perception sensors, the selection is required by the sensor type that the algorithm is based on. However, one is quite possible to try different modalities and fusions of sensors to fill a certain gap. Therefore, to support such demands, the collection systems are typically equipped with non-single sensors and multiple modalities, such as cameras (mono, stereo, grayscale, color, and event-based [21]), LiDARs (single- and multi-beam), RGB-D sensor [22], and Inertial Measurement Unit (IMU). Here we mainly refer to commercial-level IMU since it is cheap and ubiquitous, while some high-end IMUs (such as a fiber-optic gyroscope (FOG)) are too expensive and are mainly used as ground truth instruments rather than perception sensors.

2) Sensors Calibration

Under the context of multiple sensors configuration (in most cases it is), spatial-temporal calibration among different sensors is obligatory to be performed.

The spatial calibration aims to find a rigid transformation (also called extrinsic parameter) between different sensor frames, enabling to unify all the data into a single coordinate system. Usually, extrinsic parameter calibration may appear in pairs of camera-to-camera, camera-to-IMU, camera-to-LiDAR, and can be extended group-by-group in multiple sensors situation. For stereo camera calibration, the most widely used in machine vision field could be Zhang's method [23] proposed in 2000. It is quite flexible as the technique only requires to freely take images at several different orientations of a printed planar checkerboard. The algorithm will detect corner points on the board among each shot image, serving as the constraints of a closed-form solution, and then a set of coarse values will be solved. Finally, the results will be furtherly refined by minimizing the reprojection error. So far, the intrinsic, lens distortion, and extrinsic parameters are calibrated. The algorithm has been implemented in Matlab³, OpenCV⁴, and ROS⁵, proved to be highly accurate and reliable, significantly lowering the bound of 3D vision research. For camera-to-IMU calibration, the best-known framework is the Kalibr⁶ toolbox [24], [25], [26]. While calibrating, it only requires to wave the visual-inertial sensor suite in front of the calibration pattern. The framework parameterizes both the transformation matrix and time-offset into a unified principled

maximum-likelihood estimator, thus by minimizing the total objective errors, the Levenberg-Marquardt (LM) algorithm can estimate all unknown parameters at once. For camera-to-LiDAR calibration, the general methodology is to find the mutual correspondences between 2D images and 3D point clouds, thus compute a rigid transformation between them (an example is shown in Fig. 3). Two commonly used frameworks are the KIT Camera and Range Calibration Toolbox⁷ [27] and the Autoware Calibration Toolbox⁸ [28], and they respectively present a fully automatic and an interactive implementation.

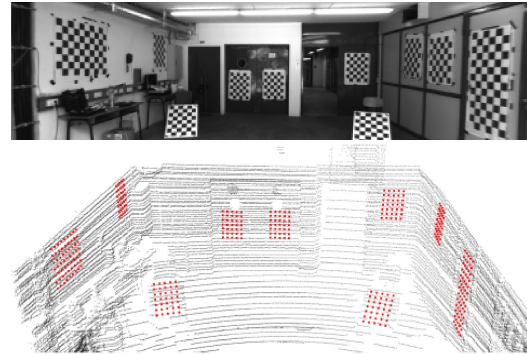


Fig. 3. An example implemented by KIT Range Calibration Toolbox: the top image shows the arrangement of the markers and the bottom shows the result of camera-LiDAR calibration [27].

The temporal calibration aims to synchronize the clocks or data packets of different sensors, or estimate the time-offsets between them. The most desirable solution is to synchronize with the hardware support, such as external trigger (industrial cameras usually have), GNSS timing, and Precision Time Protocol [29] (PTP, also known as IEEE-1588) synchronizing. However, such features can hardly be found on consumer-level products, especially for normal cameras and IMUs. To this end, a feasible approach is to estimate the time-offset caused by unsynchronized clocks or communication delay among different sensors. Solving such problems, the general methodology is to parameterize the time-offset, and furtherly perform optimization by maximizing the cross correlation or minimizing a designed error function between different sensor processes. For example, as mentioned above, the Kalibr toolbox opens an implementation on unified temporal and spatial calibration for camera-to-IMU.

Overall, the procedure and techniques for spatial-temporal alignment among different sensors are quite common, hence we will not detail the calibration process of each dataset in the following sections.

3) Sequence Collection In Target Scene

The selection of target scene depends on the expected test scenarios of the algorithms. For example, we can select urban, rural, and highway scenes for autonomous driving test. For data sequence collection, to duplicate the real world better, larger quantity of sequences, various routes, and longer paths are expected. Moreover, if you want to test the possible place recognition and loop closure functions of the algorithm, the route should traverse several times the same location.

¹ <https://microsoft.github.io/AirSim/>

² <http://www.povray.org/>

³ <https://www.mathworks.cn/help/vision/ref/cameracalibrator-app.html>

⁴ https://docs.opencv.org/master/dc/dbb/tutorial_py_calibration.html

⁵ http://wiki.ros.org/camera_calibration

⁶ <https://github.com/ethz-asl/kalibr>

⁷ <http://www.cvlibs.net/software/calibration/>

⁸ <https://www.autoware.ai/>



Fig. 4. The motion capture system from OptiTrack [30]. The high-rate cameras mounted around the room are tracking the location and posture of the actors by detecting the reflective markers.

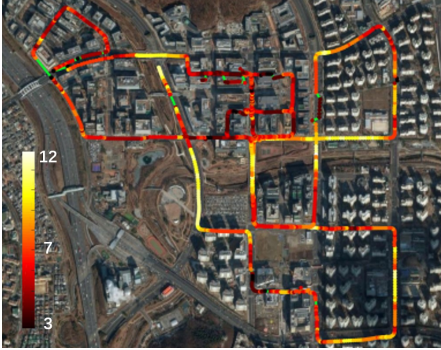


Fig. 5. The GPS reception rate during a data collection route of Complex Urban dataset. Trajectory color represents the number of received satellites: Yellow more, Red fewer, and Green represents invalid. In complex urban area, it is challenging for GNSS to work interrupted by high-rise buildings [39].



Fig. 6. The FARO X130 large-scale 3D scanner that we used to get the ground truth 3D model of a football court. It scans scene geometry by rotating its laser emitter globally and measuring the return wave to compute each 3D point.

4) Ground Truth Generation

Ground truth is the accurate reference data to be compared against in evaluation. To make it clear, within the range of SLAM related problems, we only talk about two kinds of ground truth: pose (namely position and orientation) and 3D structure, respectively for localization and mapping evaluation.

- *Position and Orientation:*

The technique employed for pose measurement could differ regarding different scenarios. For small-scale and indoor scenes, the most effective solution is motion capture system (MoCap) (e.g., VICON⁹, OptiTrack¹⁰, and MotionAnalysis¹¹) (as shown in Fig. 4), which works at a rather high rate, and meantime provides incredible accuracy both on position and orientation. But there are still drawbacks of it: it is quite costly and cannot work well outdoors, as the excessive interference of infrared light will

affect the camera tracking. For large-scale outdoor scenarios, GNSS with RTK correction and dual-antenna could be the most mature solution [31]. However, the applicable condition is also strict – the mobile agent should be under an open sky, otherwise the accuracy will drift significantly. So quite commonly, inside a single data sequence, there could be some segments that cannot be trusted, which will dramatically influence the quality of the dataset (as shown in Fig. 5). Another high-precision solution supporting both indoor and outdoor environment is laser tracker (e.g., FARO¹² and Leica¹³). It provides with superior positioning accuracy (up to sub-mm level), while occlusion-free should be ensured to make way for the laser emitted from instrument to the target, which is hard to achieve in many situations. There are also some alternatives for localization, such as Fiducial Marker [32], Global System for Mobile Communications (GSM) [33], ultra-wide band (UWB) [34], Wi-Fi (we refer to the wireless network technology based on the IEEE 802.11 family of standards) [35], and Bluetooth [36], all of which are widely deployed in industry. However, although more ubiquitous, these solutions are either with insufficient accuracy or struggle in certain conditions. Moreover, sometimes the environments could be too complex to measure ground truth (e.g., urban canyon and indoor-outdoor integration scene), then it is a compromise to use the results of multi-sensor fusion algorithms (e.g., fuse LiDAR odometry or SLAM with high-end INS and wheel odometry) as a baseline [37] or directly measure the start-to-end drift [38] for evaluation.

- *3D Structure:*

Chronically, it is a bit unusual to provide 3D-structure ground truth in SLAM datasets [12], [40], [41], although mapping is an integral and crucial part of research. One primary reason could be the hardware burden – high-accuracy 3D-scanners (as shown in Fig. 6) that provide dense scene model are hard to afford for many institutes, let alone individual researchers. For objects or small-scale scenes, a portable 3D-scanner powered by structured light or laser could be the best choice (e.g., GOM ATOS¹⁴, Artec 3D¹⁵, and Shining 3D¹⁶), providing with an accuracy of 10-um level. For large-scale scenes, the best solution is to use a professional surveying instrument (e.g., FARO, Leica¹⁷, and Trimble¹⁸), with an mm-level accuracy in hundreds of meters. The scanners are able to cover very huge area by registering multiple stations, with each individual scan consuming several to tens of minutes. Moreover, sometimes the area could be too large, then if the pose data are accurate, it is also applicable to use a mobile mapping system (MMS, e.g., RIEGL¹⁹, which fuses high-precision RTK, LiDAR, and IMU) or take the mapping results of LiDAR-based mapping/SLAM algorithms as 3D structure baseline [37].

B. Fundamental Characteristics Dimensions

As reflected by the collection methodology, the characteristics of SLAM related datasets are mainly decided by 5 fundamental

¹² <https://www.faro.com/>

¹³ <https://www.hexagonmi.com/products/laser-tracker-systems>

¹⁴ <https://www.gom.com/metrology-systems/atos.html>

¹⁵ <https://www.artec3d.com/>

¹⁶ <https://www.shining3d.com/>

¹⁷ <https://leica-geosystems.com/products/laser-scanners>

¹⁸ <https://www.trimble.com/3d-laser-scanning/3d-scanners.aspx>

¹⁹ <http://www.riegl.com/nc/products/mobile-scanning/>

⁹ <https://www.vicon.com/>

¹⁰ <https://optitrack.com/>

¹¹ <https://www.motionanalysis.com/>

dimensions: mobile platform, sensor setup (calibrated perception sensors), target scene, data sequence, and ground truth. Therefore, these dimensions will also be the basis of datasets introduction, comparison, and analyses in the following sections. The descriptions of each dimension are given below.

1) Mobile Platform

Mobile platform decides the motion pattern of a dataset. The general characteristics of several common platforms are listed in Table I, explaining the degree of freedom (DoF), speed, and motion properties. Such characteristics are identified to impact algorithm performance, for example, rapid motion (e.g., shake, sharp turn/rotation/shifting, and high-speed) can affect the data quality, such as camera motion blur (see Fig. 7-left), and LiDAR distortion (both 2D/3D LiDARs are designed to sweep the laser emitter to scan massive points asynchronously, which are packed into a single frame but with indeed different coordinates in the motion, badly messing the result, see Fig. 7-right). Besides, pure rotation will cause fundamental matrix degeneration in monocular case, and fast speed may cause narrow overlap between adjacent frames. As shown in the table, generally 6-DoF platforms (handheld, backpack, UAV) are more difficult to algorithms.

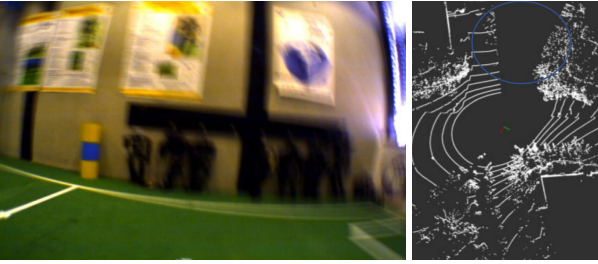


Fig. 7. Camera motion blur under walking shake (left), and LiDAR motion distortion under rapid rotation (right) [42], [43].

TABLE I
THE CHARACTERISTICS OF DIFFERENT MOBILE PLATFORMS

Platform	DOF	Speed	Motion Properties
Handheld	6	$\approx 1\text{m/s}$	Frequent shake, sharp turn, rapid rotation, sharp shifting
Backpack	6	$\approx 1\text{m/s}$	Frequent shake
Automobile	3	10-25m/s	Smooth forward/turn/shifting, constant speed
Wheeled robot	3	1-5m/s	Smooth forward/turn/shifting, constant speed
UAV	6	1-15m/s	Turn, rotation, sharp shifting

2) Sensor Setup

Sensor setup refers to the number and modalities of calibrated perception sensors, thus decides the supported algorithm types of a dataset. As illustrated in the methodology, we can assume that all the perception sensors have been calibrated well, thus they can be used in any combinations. For example, if the dataset is with the sensor setup of binocular stereo cameras, a LiDAR, and an IMU, then it can support algorithms based on stereo vision, vision-inertial fusion (VI), vision-LiDAR fusion (VL), vision-LiDAR-inertial fusion (VIL), etc. When building or selecting a dataset, it is the primary factor to be considered.

3) Target Scene

Target scene involves the type, condition, and scale of the expected test environment. The type of the scene decides the data appearance and structure, which are exactly what the algorithms rely on to estimate motions, thus directly affect the performance.

Imagine that if a camera is moving in front of a pure-white wall (namely weak texture), then it is impossible for a vision-based algorithm to extract salient features to track the motion. Besides, if a LiDAR-based method is working in a long corridor (namely repetitive structure), then it is quite tough to get match between LiDAR scans. Likewise, scene type can also drag in some other challenging elements include repetitive texture (grassland, sand, etc.), weak structure (open field, farmland, etc.), and interference feature and structure (reflection of water and glass, etc.).

Scene condition mainly include illumination, dynamic objects, weather, season, and time. These elements all have impacts on algorithms performance, for example, under bad illumination or at dark night a camera cannot acquire good images.

Scene scale is also important, as it indirectly affect the volume and variety of data sequences. It is largely determined by scene type, for example, an urban or campus scene can usually cover a large scale, while a room scene usually has a small area.

4) Data Sequence

Data sequence involves the quantity of sequences, the length of paths, and the variety of collection routes. Usually, datasets with greater quantity, longer trajectories, and various routes have more complete coverage of the scene, thus have more chance to inspect the weaknesses of the algorithms.

5) Ground Truth

Ground truth involves the types and quality of the reference data, it decides the evaluable tasks of a dataset. The previous methodology part has given a comprehensive introduction on the existing ground truth techniques, while they are quite different in applicable scenario, requirements, and accuracy. Here a characteristics comparison among them is given in Table II. It should be noted that, although with different accuracy, mostly the ground truth data are already quite enough for SLAM-related evaluation.

TABLE II
THE COMPARISON OF THE CHARACTERISTICS AMONG SOME COMMONLY USED GROUND TRUTH TECHNIQUES

Technique	GT	Scenario	Accuracy
MoCap	6-DoF pose	Indoor (small scale)	High: sub- mm/deg
RTK-GNSS (&INS)	6-DoF pose	Outdoor	High: cm level (open sky) Low: denied area
Laser Tracker	3D position	In/outdoor	High: sub- mm (occlusion free)
SLAM-based algorithm	6-DoF pose	In/outdoor	Low/Medium
Marker, WiFi, ...	6-DoF pose/ 3D position	In/outdoor (middle scale)	Medium: cm-dm level
Start-to-end drift	0 loop-drift	In/outdoor	Low
Large-scale 3D scanner	3D structure	Scene/object	High: mm level
Small-scale 3D scanner	3D structure	Object	High: sub-mm level
SLAM-based algorithm	3D structure	Scene/object	Low/Medium

III. SLAM RELATED TASKS TAXONOMY AND DATASETS CATEGORIZATION

This section provides a clear SLAM related tasks taxonomy and datasets categorization, in the hope of resolving the two-way selection difficulty between algorithm researchers and datasets providers.

The proposed taxonomy of SLAM related tasks takes into account 2 principles: sensor-oriented, and functionality-oriented.

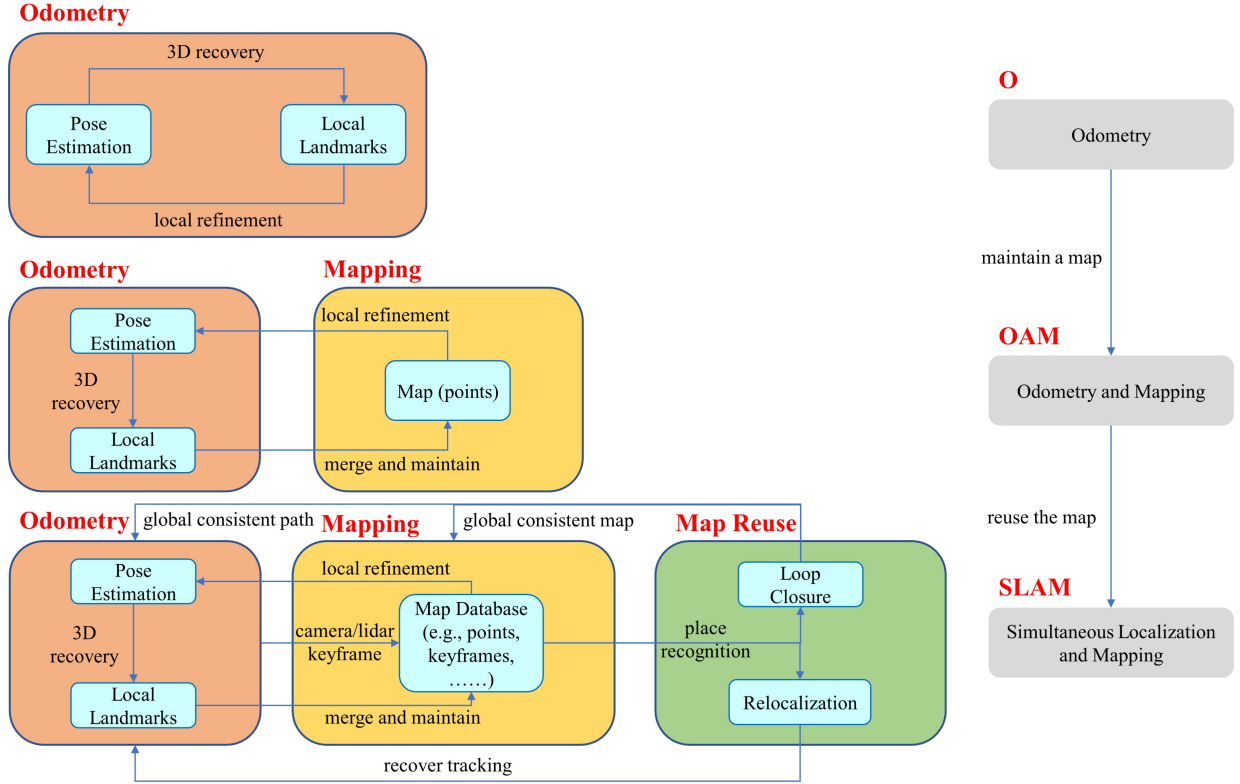


Fig. 8. The technical architecture and hierarchical relationship among odometry, mapping, and SLAM.

TABLE III
THE OVERALL TAXONOMY OF SLAM RELATED TASKS

Sensor Setup					Functionality
Based Sensor	Sub-sensor-modality		Aiding Sensor		
Vision-based (V)	Monocular, Stereo, Fisheye, Omnidirectional, Thermal, Event, ...	\oplus	IMU (I)/	\oplus	Odometry (O)/
LiDAR-based (L)	2D LiDAR, 3D LiDAR		GNSS/		Odometry and Mapping (OAM)/
Vision-LiDAR-based (VL)	Combination of the above		Wheel Encoder/		Simultaneous Localization and Mapping (SLAM)/
RGB-D-based	N/A			3D Reconstruction (3DR)
Image-based	N/A		N/A		Structure from Motion (SfM)/ Multiple View Stereo (MVS)

Oriented by sensor setup, there are mainly five branches for SLAM related tasks: LiDAR-based, vision-based, vision-LiDAR fusion, RGB-D-based, and image-based. Benefiting from the high-accuracy ranging of laser sensors, LiDAR-based methods (2D [44] and 3D [45]) are widely employed, acting as a mature solution. However, the price of LiDAR is too high, with multi-beam editions (3D) costing at least thousands of dollars [46]. As the visual sensors become ubiquitous, along with the improvements of computing hardware, vision-based methods have greatly attracted the efforts of SLAM community [47], [48], [49]. More specifically, due to the diversity of visual modalities, there has emerged many sub-classes, including monocular, stereo, fisheye, event-based [50] methods, etc., suitable for different application scenarios. Although not as robust nor accurate as LiDAR-based methods [45], [51], [52], still vision methods are proved to have huge potentials and are steadily on its way forward [53]. In order

to combine the advantages of the both modalities, vision-LiDAR fusion has become a hot topic that attracts significant attention [54]. RGB-D is a novel modality that also combines the imaging and ranging sensor. It collects color images along with a depth channel which make it much easier to perform 3D perception. Since the Microsoft Kinect [22] was first introduced, RGB-D sensors have been widely adopted in SLAM research due to the low-cost and complementary nature [55], [56]. Additionally, there is another branch named image-based which is popular in 3D computer vision. Compared with vision-based methods, it does not require specifically arranged sensor setup or sequential images, photos that collected from the Internet can also be used to recover the 3D model of a scene or an object. For the other modalities, such as IMU, GNSS, and wheel odometry, they can provide a priori and be fused into optimization thus enhance the accuracy and robustness of motion estimation. Since they are

adopted mainly to play aiding roles, the related fusions are categorized into the above five branches.

In the context of the above sensor setups, oriented by functionality, there are two main branches of SLAM related problems: mobile localization and mapping, and 3D reconstruction.

Within the range of mobile localization and mapping, there are 3 specific tasks: odometry, mapping (here we refer to a real-time or quasi real-time sequential manner), and SLAM. The 3 terms are with a hierarchical relationship at technical level, as shown in Fig. 8. Odometry means to track the position and orientation of an agent incrementally over time [57]. The abbreviation of such system is usually named as “O”, such as VO, VIO, and LO, which refers to Visual Odometry, Visual-Inertial Odometry, and LiDAR Odometry respectively. It was proposed to serve as an alternative or supplement to wheel odometry due to the better performance especially in uneven or other adverse terrains [58], [59], [60]. In the strict sense, besides tracking the path, odometry also recovers 3D points, whereas these landmarks are only used for local optimization rather than a map. Mapping means to build a map of the environment in a particular format through mobile collection. Normally, mapping works along with odometry, thus named as odometry and mapping (OAM) (we avoid using the term mobile mapping as it usually refers to a more professional procedure in surveying and mapping domain [61]), since it relies on pose estimation to recover 3D points and merge together scene structures. As for SLAM, intuitively, it has both functions of odometry and mapping, but it is not a simple combination of the two. SLAM means to keep a track of an agent’s location while at the same time building a global consistent and reusable map [57], [62]. This implies two core functions of SLAM: loop closure and relocalization, which rely on the map database to query the previous visited places. Loop closure means to add new constraints around revisited places to perform global optimization, thus eliminate accumulated drift of the path and ensure a global consistent map. Relocalization means to recover positioning within the prebuilt map after the robot lose its track. As can be seen, the “SLAM map” is not only a model, but also a database for query, which supports the map reuse capability that draws a line between SLAM and the other two. It should be noted that, the map does not have to be dense or good looking, the point is whether the robot can recognize. After all, sparse map points can also store features and descriptors [63], [64].

3D reconstruction means to recover a high-quality 3D map or model of a scene or an object from sequential data or data of different locations and perspectives. The general methodology is similar with mobile localization and mapping, but it does not require sequential data and real-time running. It can establish as many as possible constraints among any co-visible data frames and does much more optimization, thus no doubt achieve better accuracy and density. It can be achieved with many modalities of sensors (e.g., camera, LiDAR, and RGB-D), but here we want to emphasize image-based approach a bit, which does not require sequential data or a fixed sensor. There are mainly two specific tasks in image-based field: structure from motion (SfM) and multiple view stereo (MVS). SfM is a process of recovering 3D structure from 2D images of different locations and views [65], by estimating camera poses among any co-visible views. Usually,

the output models are composed of sparse point cloud. MVS can be regarded as a generalization of the two-view stereo, it assumes known camera poses of each view (just as the extrinsic parameter between binocular cameras) to recover dense 3D models. Since SfM already estimates the camera poses beforehand, MVS can directly serve as a post process of SfM to build an accurate and dense model [66].

Overall, comprehensively considering the above principles and the consensus of this field, we propose the taxonomy as the combination of the based sensor, aiding sensor, and functionality, as shown in Table III. For example, if an algorithm is based on LiDAR and the functionality is Odometry and Mapping (OAM), then the task will be categorized as LOAM (this coincides with the name of the algorithm proposed by Zhang et al. [45]); if the algorithm is based on Vision (V), aided with an IMU (I), and the functionality is Odometry (O), then the task will be categorized as VIO. It should be noted that, within the aiding sensors, usually GNSS and wheel odometry are used for generating ground truth, but to fuse them into SLAM process is also doable and effective.

As for datasets categorization, logically, to match the datasets with corresponding algorithm types, we mainly follow the sensor setup as the basis. Although some methods will require specific datasets (such as event-based VO/VSLAM [50]), considering that typically a dataset is not only designed for one task, to maintain the compatibility and selection coverage, we avoid categorizing the datasets too fine, but instead resulting in 4 broad categories: 1. Vision-based mobile localization and mapping and 3D reconstruction datasets, 2. LiDAR-related mobile localization and mapping and 3D reconstruction datasets, 3. RGB-D-based mobile localization and mapping and 3D reconstruction datasets, and 4. Image-based 3D reconstruction datasets. This criterion coincides with the sensor setup of the proposed SLAM tasks taxonomy, whereas the only difference is that the datasets suitable for LiDAR-based and vision-LiDAR-based algorithms are merged together into LiDAR-related category. Because, from the dataset point of view, if the platform is equipped with LiDAR, then it can also accommodate cameras. It should be noted that, RGB-D datasets and LiDAR-related datasets that contain camera data can also support vision-based methods. For example, the best-known KITTI dataset [14] and TUM RGB-D dataset [12] are usually used for benchmarking VO and VSLAM algorithms. Moreover, some datasets with IMU data [67] and 6-DoF motions could be originally designed for IMU fusion algorithms, thus are typically with higher difficulty. To avoid possible confusions, we will further provide a considerate dataset selection guideline in Section V.

IV. STATE-OF-THE-ART DATASETS

This section gives a structured and detailed introduction of 16 state-of-the-art datasets by the above 4 broad categories, which we believe can well represent the whole datasets entirety, to help understand current datasets and also to serve as a good lesson for future releases. Many deep insights that even not covered by the original papers are given, making the enumeration worthy. Note that, limited by space, we avoid introducing more cases minutely, which on the other hand will also not make more sense due to the homogeneous information. Hence, such selection does not mean

any recommendation bias, and it is exactly one main goal of this paper to remove the biased usage. To achieve clear descriptions, the datasets are introduced in a structured way, mainly attending to general information, platform and sensor setup, scenes and sequences, ground truth, and highlights. Although introduced individually, we do follow a chronological order, and emphasize the features and progresses compared with previous works. For a holistic comparison and analysis, we will arrange a concise but comprehensive overview covering all the datasets in Section V, and give analyzation and discussion in Section VII.

A. Vision-based Mobile Localization And Mapping And 3D Reconstruction Category

1) EuRoC MAV [15]

The EuRoC MAV dataset was collected under the context of the European Robotics Challenge (EuRoC), in particular, for the Micro Aerial Vehicle competitions of visual-inertial algorithms. Since the publication in 2016, it has been tested by a great many teams and cited by massive literature, becoming one of the most widely used datasets in SLAM scope.

TABLE IV
THE PROPERTIES OF THE SENSORS AND GROUND TRUTH INSTRUMENTS

Sensor/Instrument	Type	Rate	Characteristics
Camera	2 × MT9V034	20 Hz	WVGA, monochrome, global shutter
IMU	ADIS16448	200 Hz	MEMS, 3D accelerometer, 3D gyroscope
Laser Tracker	Leica MS50	20 Hz	1mm accuracy
Motion Capture	Vicon	100 Hz	sub-(mm/deg) accuracy
3D Scanner	Leica MS50	30 kHz	3mm accuracy

- *Platform and sensor setup*: The dataset was collected using an MAV, logically designed to provide 6-DoF motions with slow to high speed. Two grayscale cameras (stereo setup) and an IMU were equipped and with strictly spatial-temporal alignment (the properties are listed in Table IV), thus ideal for vision (mono and stereo) and especially IMU fusion algorithms.

- *Scenes and sequences*: The dataset consists of two portions: machine hall and room, with 5 and 6 sequences respectively. Varying in terms of texture, motion, and illumination conditions, the datasets were recorded in 3 difficulty levels: easy, medium, and difficult. This has been proved to be challenging for many algorithms [49], [68], [69], enabling researchers to locate the weakness and enhance their algorithms effectively.

- *Ground truth*: The dataset has reliable ground truth data of both positioning and 3D mapping, thus support both kinds of evaluation. For the first batch collected in the machine hall, the 3D position ground truth was provided by laser tracker. For the second batch in the room, both 6D pose and 3D map ground truth were provided, respectively by motion capture system and laser scanner. All the ground truth is with extreme quality, as shown in Table IV from the instrument properties.

- *Highlights*: Vision-IMU setup, multiple complexity-levels, highly accurate ground truth, 3D map ground truth.

2) TUM MonoVO [38]

TUM MonoVO dataset, released in 2016, was specifically for testing long-range tracking accuracy of O/SLAM, complementing previous datasets with larger scale. Markedly, all the images have been photometrically calibrated.

- *Platform and sensor setup*: The dataset was collected through a handheld carrier, which makes the motion pattern challenging. Two grayscale cameras were used, but merely with wide and narrow-angle lenses rather than forming a stereo pair, so can only be used for monocular algorithms. The cameras have up to 60Hz frame rate, which are far above normal to enable handling quick and unsmooth motions while designing algorithms.

- *Scenes and sequences*: The dataset provides 50 sequences in a variety of scenes from indoor to outdoor. The indoor scenes were mainly recorded in a school building, covering office, corridor, large hall, and so on. The outdoor scenes were mainly recorded in a campus area, including building, square, parking lot, and the like. Many sequences have extremely long distances, which are expected by researchers to perform long-range tests.

- *Ground truth*: Due to the massive collections in indoor and outdoor integration environments, it was almost impossible to measure ground truth using GNSS/INS or motion capture system. So this dataset was designed to record each sequence starting and ending at the same position, and generated a set of “ground truth” poses at the start and end segments, allowing to evaluate the tracking accuracy based on the loop drift. Note that, you have no chance to inspect the exact locations where the errors occur, hence not recommended if you target frame-by-frame accuracy. And you must disable the “loop closure” function for SLAM usages, otherwise the zero drift will invalid the evaluation.

- *Highlights*: Handheld motion pattern, diverse scenes various sequences, photometrically calibration, in-outdoor integration.

3) UZH-FPV Drone Racing [70]

The UZH-FPV Drone Racing dataset, published in 2019, is officially used in IROS 2020 Drone Racing Competition. Among the existing real-world datasets, it contains the most aggressive motions, complementing previous 6-DoF datasets further.

- *Platform and sensor setup*: The dataset was collected using a quadrotor controlled by an expert pilot to make extreme speeds, accelerations, and fast rotations, proved to be far beyond the capabilities of existing algorithms [71]. It equipped a grayscale event camera, and a grayscale binocular stereo camera, both with hardware synchronized IMU (properties are listed in Table V), thus can support quite well vision-based (mono and stereo), IMU fusion, and event-based methods.

TABLE V
THE PROPERTIES OF THE SENSORS AND GROUND TRUTH INSTRUMENT

Sensor/Instrument	Type	Rate	Characteristics
Event Camera	mDAVIS	50 Hz	346 × 260, grayscale + events, 120° FOV
IMU #1	mDAVIS built-in	500Hz	3D accelerometer, 3D gyroscope
Stereo Camera (binocular)	OV7251	120 Hz	640 × 480, grayscale, global shutter, 186° FOV
IMU #2	Snapdragon built-in	1000Hz	3D accelerometer, 3D gyroscope, 3D magnetometer
Laser Tracker	Leica MS60	20 Hz	1mm accuracy

- *Scenes and sequences*: The dataset was collected in an indoor airplane hangar and an outdoor grassland edged by trees, forming a total of 27 sequences. It has a 340.1/923.5 (m) max distance and a 12.8/23.4 (m/s) top speed for indoor/outdoor scene (both the top speeds are larger than any existing sequences).

- *Ground truth*: The ground truth were generated by tracking the 3D position using the Leica MS60 total station, with below 1mm accuracy. However, due to the aggressive flights, laser lost tracking could always occur causing trajectory broken, thus only complete sequences were selected for publication.

- *Highlights*: Aggressive motion, highly accurate ground truth, event data.

4) OpenLORIS-Scene [41]

OpenLORIS-Scene, published in 2019, is the official dataset of IROS 2019 Lifelong SLAM Challenge. Compared with previous datasets, it is a real-world collection in dynamic and daily-changing scenarios specialized for long-term robot navigation.

- *Platform and sensor setup*: The dataset was collected by wheeled robots (with odometry) with an RGB-D camera and a color binocular stereo camera (both with hardware synchronized IMU), and a 2D/3D LiDAR (all properties are listed in Table VI). It well supports monocular, binocular, RGB-D, and IMU fusion methods, but not recommended for LiDAR-based, since LiDAR is already used for generating ground truth.

TABLE VI
THE PROPERTIES OF THE SENSORS AND GROUND TRUTH INSTRUMENTS

Sensor/Instrument	Type	Rate	Characteristics
RGB-D Camera	RealSense D435i	30 Hz	848 × 480, RGB + Depth, global shutter, 69 × 42 FOV, 6-axis IMU
Stereo Camera (binocular)	RealSense T265	30 Hz	640 × 480, RGB, global shutter, 186° FOV, 6-axis IMU
LiDAR #1	Hokuyo UTM-30LX	40 Hz	2D LiDAR, 270° Horizontal, 30m range, 5cm accuracy
LiDAR #2	RoboSense RS-LiDAR-16	20 Hz	16-beam LiDAR, 360° H × 30° V, 150m range, 2cm accuracy
Motion Capture	OptiTrack	240 Hz	sub-(mm/deg) accuracy

- *Scenes and sequences*: The dataset was collected in 5 scenes: office, corridor, home, café, and market, which are quite typical application scenarios for service robots but rarely appeared in previous datasets. Thanks to the real-life record, many dynamic people and objects were brought inside, fulfilling the pressing expectation of such data. It also targets long-term SLAM, thus many sequences of each same scene but at different time slots were captured, which incorporates ever-change of illumination, viewpoints, and those caused by human activities (see Fig. 9).



Fig. 9. 5 Different environments: office, corridor, home, café, and market from left to right collected at different time (top and bottom row) [41].

- *Ground truth*: For office scene, the ground truth was provided by Motion Capture System at 240 Hz, ideal for frame-by-frame evaluation. For the other scenes, the ground truth was generated by LiDAR SLAM and partly accompanied with sensor fusion, reported to have cm-level accuracy, which are not that strict but enough for vision methods evaluation.

- *Highlights*: Service robot platform, multi-modal sensors, typical scenes, ever-changing environments, long-term data.

5) TartanAir [72]

TartanAir, published in 2020, is the official dataset of CVPR 2020 Visual SLAM Challenge. It is a synthetic dataset collected via simulation, thus accomplish to design many challenging effects, with the mission of pushing the limits of visual SLAM.

- *Platform and sensor setup*: TartanAir is a simulated dataset, thus there is no practical platform or sensor setup. However, it created random motion patterns with high complexity, which are good for testing whereas not realistic as real-world motions. Also, multi-modal sensors are simulated: two color cameras (stereo setup), an IMU, a depth camera, and a 3D LiDAR, supporting many modals of SLAM related tasks, whereas such data are quite perfect, which fail to mimic the real-world camera blur or motion distortion of LiDAR, implying the weakness of such manner.

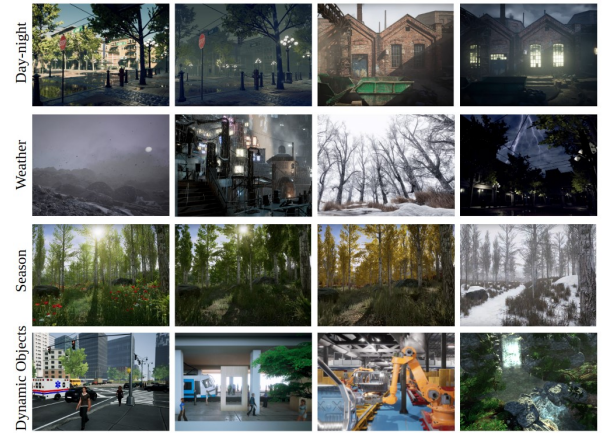


Fig. 10. Some representative images of different categories: Urban, Rural, Nature, Domestic, Public, and Sci-fi from left column to right [72].

- *Scenes and sequences*: TartanAir has simulated diverse scenes (30 in 6 categories): Urban, Rural, Nature, Domestic, Public, and Sci-fi. As shown in Fig. 10, the scenes were designed with many challenging effects, such as light changing, bad illumination, adverse weather, time and season effects, and dynamic objects. The dataset has a total of 1037 long sequences, resulting in more than 1M frames, which are much larger than existing datasets. However, although seem plentiful the images, when inspecting at a full resolution, still you will find the quality far from realistic.

- *Ground truth*: Both camera poses and 3D map ground truth are provided. Notably, they are absolutely accurate thanks to the simulation manner. Besides, some other labels are also provided, such as semantic segmentation, stereo disparity, depth map, and optical flow.

- *Highlights*: Diverse motion patterns, diverse scenes, wealthy sequences, challenging effects, perfect ground truth.

B. LiDAR-related Mobile Localization And Mapping And 3D Reconstruction Category

1) KITTI Odometry [14]

The KITTI Odometry dataset, released by Karlsruhe Institute of Technology (KIT) and Toyota Technological Institute in 2012, is the most popular dataset in SLAM domain. Except for the high-quality dataset itself, it is also largely because of the famous public benchmark.

- *Platform and sensor setup*: KITTI was collected using a car with binocular stereo color and monochrome cameras (both pairs triggered via hardware and with a long baseline), a LiDAR (synchronized per sweep with camera frames), and an RTK-GPS&INS device (for ground truth). All the sensors are top-level (the properties are listed in Table VII) and offer high-quality data, supporting vision-based (mono and stereo) and LiDAR related O/SLAM, whereas conversely the smooth motion, clear images, and dense point clouds do make the algorithms easy to handle, which may be insufficient for the demonstration of normal cases.
- *Scenes and sequences*: The dataset was collected around a mid-size city of Karlsruhe, in rural areas and on highways. It contains a huge volume of raw data, while considering the long trajectories, varying speeds, and reliable GPS signal, a total of 39.2km's driving distance were selected, forming 22 sequences with frequent loop closures, ideal for SLAM validation purpose. However, although collected in real life, still KITTI is generally known to be easy: good lighting and weather, sufficient texture and structure, and static scene in most sequences, leading to an impressive result of 0.53% error in translation [73]. It is worth noting that, the 21th and 22th sequences captured on the highway are highly dynamic (see Fig. 11), which could be challenging for motion estimation algorithms.



Fig. 11. A frame from the 21th sequence that crowded with moving cars.

TABLE VII
THE PROPERTIES OF THE SENSORS AND GROUND TRUTH DEVICES

Sensor/Devices	Type	Rate	Characteristics
Camera (monochrome)	2 × PointGrey Flea2 FL2-14S3M-C	10 Hz	1392 × 512, 8-bit gray, global shutter, 90° × 35° FOV
Camera (color)	2 × PointGrey Flea2 FL2-14S3C-C	10 Hz	1392 × 512, 8-bit RGB, global shutter, 90° × 35° FOV
LiDAR	Velodyne HDL-64E	10 Hz	64-beam LiDAR, 360° H × 26.8° V, 120m range, 2cm accuracy
RTK-GPS&INS	OXTS RT3003	100 Hz	cm/sub-deg accuracy

- *Ground truth*: A high-end RTK-GPS&INS device was used to generate pose ground truth. Trajectories with good GPS signal were selected to ensure cm level accuracy. But note that, due to the GPS nature of absolute measurement, the ground truth was not smooth locally, which will cause biased evaluation results if studying very small sub-sequence. An intuitive understanding is you cannot measure accurately the thickness of a single piece of paper, but are able to measure 100 pages together. So, in 2013, KITTI changed the minimum evaluated length from 5 to 100 and counting longer sequences, leading to a better indication on performance. This also gives us a lesson: if your technique cannot give accurate ground truth, focus longer segments for evaluation (to study start-to-end drift is an extreme version of this concept, such as TUM MonoVO).

- *Highlights*: High quality vision-LiDAR data, accurate ground truth, wealthy sequences, loop closures, public benchmark.

2) Oxford RobotCar [40]

The Oxford RobotCar dataset, presented in 2016, was recorded by traversing a same route twice a week in around one year, resulting in over 1000km's trajectories. Various time slots, weather, and scene change were covered inside, complementing previous datasets (such as KITTI) greatly with long term and challenging data.

- *Platform and sensor setup*: There are 4 cameras (1 trinocular stereo and 3 monocular), two 2D-LiDARs, a 3D-LiDAR, and a set of RTK-GPS&INS device (for ground truth) equipped on a car, thus supports vision-based (mono and stereo) and LiDAR related O/SLAM. The sensor properties are listed in Table VIII.

TABLE VIII
THE PROPERTIES OF THE SENSORS AND GROUND TRUTH DEVICES

Sensor/Devices	Type	Rate	Characteristics
Stereo Camera (trinocular)	FLIR Bumblebee XB3	16 Hz	1280 × 960, 8-bit RGB, global shutter, 66° HFOV, 12/24cm baseline
Camera	3 × FLIR GS2-FW-14S5C-C	12 Hz	1024 × 1024, 8-bit RGB, global shutter, 180° HFOV
2D LiDAR	SICK LMS-151	50 Hz	270° Horizontal, 50m range, 3cm accuracy
3D LiDAR	SICK LD-MRS (4 planes)	12.5 Hz	85° H × 3.2° V, 50m range, 3cm accuracy
RTK-GPS&INS	NovAtel SPAN-CPT	10 Hz	cm/sub-deg accuracy



Fig. 12. The variation of conditions at the very same locations caused by time slots, weather, season, and human activities [74].

- *Scenes and sequences*: Due to the long-term frequent collection, a wide variety of scene appearances and structures caused by illumination change, diverse weather, dynamic objects, seasonal effects, and construction works were collected, covering inside pedestrian, cyclist, and vehicle traffic, light and heavy rain, direct sun, snow, and down, dusk and night. Compared with KITTI, RobotCar is more comprehensive at the level of mimicking the real world, thus will be more persuasive if algorithms can handle such variation and challenge with good scores. Several example images are shown in Fig. 12 to give an intuitive feel.

- *Ground truth*: Separated from the dataset, the ground truth of RobotCar was released in 2020 [75]. After well selected from the whole dataset, a sample of 72 traversals were provided 6D-pose ground truth at 10Hz by post-processing the high-end GNSS/INS with RTK correction, resulting in a cm/sub-deg accuracy.

- *Highlights*: Long-term dataset, long trajectory, vision-LiDAR setup, repeatedly traverse, various and challenging conditions.

3) Complex Urban [37]

The Complex Urban dataset, released in 2019, was recorded in diverse and complex urban environments suffering from denied

or inaccurate GNSS, complementing KITTI and RobotCar with a totally different urban style.

- *Platform and sensor setup*: The dataset was collected using a car equipped with multi-modal sensors of different levels: two color cameras (binocular stereo), two 2D-LiDARs, two 3D-LiDARs, a consumer-level GPS, a VRS-RTK GPS (for ground truth), a 3-axis FOG (for ground truth), a consumer-level IMU, and two wheel encoders (for ground truth), supporting a wide range of SLAM related tasks based on vision (mono and stereo), LiDAR, and IMU/GNSS fusion. The sensors properties are listed in Table IX. But note that, due to the non-overlap, it does not support to project LiDAR points to the exact position on camera frames while building vision-LiDAR fusion algorithms.

TABLE IX
THE PROPERTIES OF THE SENSORS AND GROUND TRUTH DEVICES

Sensor/Devices	Type	Rate	Characteristics
Camera	2 × FLIR FL3-U3-20E4C-C	10 Hz	1280 × 560, 8-bit RGB, global shutter
2D LiDAR	2 × SICK LMS-511	100 Hz	190° Horizontal, 80m range, 5cm accuracy
3D LiDAR	2 × Velodyne VLP-16	10 Hz	16-beam LiDAR, 360° H × 30° V, 100m range, 3cm accuracy
GPS	U-Blox EVK-7P	10 Hz	2.5m accuracy, consumer-grade
FOG	KVH DSP-1760	1000 Hz	3-axis, 0.05°/h bias
IMU	Xsens MTi-300	200 Hz	9-axis AHRS, 10°/h bias
Encoder	2 × RLS LM13	100 Hz	4096 resolution
RTK-GPS	SOKKIA GRX2	1 Hz	H: 10mm, V: 15mm accuracy

- *Scenes and sequences*: The dataset was collected in diverse and complex urban scenes such as metropolitan area, residential area, complex apartment, highway, tunnel, bridge, and campus. It covered inside many complex and high-rise buildings (shake the GNSS performance), multi-lane roads, and crowded moving objects, which are totally different with the European urban style of KITTI and the like, posing new challenge for algorithms. All the sequences have kilometers of trajectory length, enabling realistic and thorough tests. A sample frame and associated 3D point cloud are shown in Fig. 13, well illustrating “complex”.



Fig. 13. A sample frame and associated 3D point cloud, containing dense moving objects and high-rise buildings, well illustrating “complex” [39].

- *Ground truth*: Due to the severe occlusion of high-rise buildings, bridges, and tunnels, it was impossible for VRS-GPS to calculate complete and accurate ground truth trajectories. To this end, the dataset has generated a baseline using an iSAM pose-graph SLAM framework [76], employing constraints from FOG, encoder, VRS-GPS, and ICP-based loop closure. See Table IX, the sensors and devices are in good properties, thus will not bias too much under such rigorous post-processing.

- *Highlights*: Multi-modal and multi-level sensors, complex urban environments, diverse scenes.

4) *Newer College* [77]

Newer College (the upgrade version of the 2009 New College dataset [78]), released in 2020, is the first LiDAR-related dataset collected in handheld motion pattern while at the same time with both trajectory and 3D mapping ground truth, complementing previous vehicular datasets significantly, thus is very precious.

- *Platform and sensor setup*: The dataset was collected using a handheld carrier, with 6-DoF motion containing vibration which can cause motion blur and LiDAR distortion. It was equipped an RGB-D sensor (only used as binocular stereo camera), and one 3D-LiDAR, both embedded with IMU, supporting vision-based (mono and stereo), LiDAR-related, and also IMU fusion SLAM related tasks. The sensors properties are shown in Table X.

- *Scenes and Sequences*: The dataset was collected in the New College of Oxford, with one sequence of 2.2km trajectory length. It was recorded at walking speeds (around 1 m/s) with several designed loop closures, thus can support the validation of SLAM and other place recognition algorithms quite well. The 3D map of the environment are shown in Fig. 14.

TABLE X
THE PROPERTIES OF THE SENSORS AND GROUND TRUTH INSTRUMENT

Sensor/Instrument	Type	Rate	Characteristics
RGB-D Sensor (only used as binocular stereo camera)	RealSense D435i	30 Hz	2 × 848 × 480, RGB + Depth, global shutter, 69° × 42° FOV, 6-axis IMU @650hz
LiDAR	Ouster OS1-64	10 Hz	64-beam LiDAR, 360° H × 45° V, 120m range, 5cm accuracy, 6-axis IMU @100hz
3D scanner	Leica BLK360	360 kHz	8mm accuracy

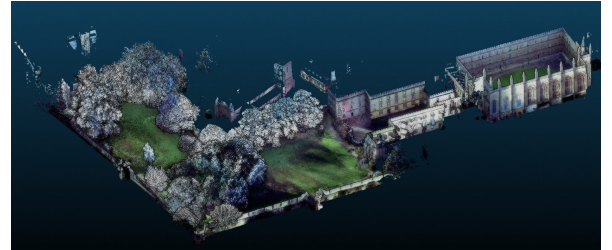


Fig. 14. The pre-build ground truth 3D map of the environment [77].

- *Ground truth*: The dataset provides both accurate pose and 3D map ground truth, thus support both localization and mapping evaluation, which is quite rare in previous datasets. As we have analyzed, it is not always accurate nor smooth to generate ground truth pose using GNSS, thus Newer College employed a novel method: first scan a dense ground truth 3D map of the scene with a survey-grade 3D laser scanner (as shown in Fig. 14), and then localize by registering the LiDAR data against the prebuild map (ICP was used here), thus a high-rate and accurate 6D-pose could be calculated. As listed in Table X, the 3D scanner has an <1cm accuracy while the LiDAR has cm-level, thus we can infer that the pose ground truth is also cm-level accurate. This is also a lesson for us to get ground truth pose when building middle-scale or indoor-outdoor integrated dataset.

- *Highlights*: Handheld LiDAR dataset, accurate pose and 3D map ground truth, long trajectory, loop closures.

C. RGB-D-based Mobile Localization And Mapping And 3D Reconstruction Category

1) TUM RGB-D [12]

TUM RGB-D, released by Technical University of Munich in 2012, has become a top popular SLAM related dataset in the past decade. Though captured with RGB-D sensor, it is also widely used in pure vision-based methods. Remarkably, this dataset has proposed a set of evaluation criteria and indicators, becoming the consensus of localization evaluation till today (will be illustrated in Section VI).

- **Platform and sensor setup:** There are two recording platforms: handheld and robot, thus covering a wide range of motions. Both of them were equipped with an RGB-D sensor (Table XI lists the properties), supporting vision and RGB-D based O/SLAM.

TABLE XI

THE PROPERTIES OF THE SENSOR AND GROUND TRUTH INSTRUMENT

Sensor/Instrument	Type	Rate	Characteristics
RGB-D Camera	Kinect v1	30 Hz	640 × 480, RGB + Depth, rolling shutter, 70° × 60° FOV, 3-axis accelerometer
Motion Capture	MotionAnalysis Raptor-E	100 Hz	sub-(mm/deg) accuracy

- **Scenes and sequences:** The dataset was recorded in 2 different indoor scenes: an office (for handheld), and an industrial hall (for robot). A total of 39 sequences were captured, with and without loop closures, supporting SLAM validation.

- **Ground truth:** Both the scenes were fully covered by a motion capture system (Table XI lists the properties), providing high-rate and accurate 6D pose ground truth, supporting frame-by-frame evaluation. For ease of use, a set of automatic evaluation tools were provided. However, this dataset lacks 3D map ground truth, which could be the only glaring weakness.

- **Highlights:** Handheld and robot platforms, highly-accurate ground truth.

2) ICL-NUIM [79]

ICL-NUIM, released in 2014, is a synthetic dataset with both camera pose and 3D map ground truth, complementing the TUM RGB-D dataset with mapping evaluation.



Fig. 15. Two example images: living room (left), and office room (right) [79].

- **Platform and sensor setup:** Different with many other synthetic datasets (e.g., TartanAir), ICL-NUIM duplicated a real-world handheld trajectory to make the motion pattern realistic. Then, an RGB-D sensor was simulated to capture the data within the 3D models in the POV-Ray software.

- **Scenes and sequences:** The dataset simulated 2 indoor scenes: a living room, and an office room. Each scene has 4 sequences, one of which designed with a small loop trajectory to support SLAM usage. Remarkably, noises were added to the RGB and depth images to mimic the real-world sensor noise. Such proce-

dures made the data quite realistic, which is a good lesson for the datasets afterwards. As can be seen in Fig. 15, the rendered quality was even better than some later-released datasets, e.g., TartanAir. Whereas, it is a pity that both the scenes cover a relatively small area, with a maximal sequence length of only 11m.

- **Ground truth:** Since the collection already followed some pre-defined routes, they directly serve as perfect ground truth. The routes were obtained by running Kintinuous SLAM [80] from handheld data in a real living room, thus are quite realistic. For the office room scene, additionally the 3D model was provided as 3D mapping ground truth.

- **Highlights:** Realistic trajectory and data, accurate ground truth, 3D scene ground truth.

3) InteriorNet [81]

InteriorNet, presented in 2018, is a photo-realistic, large-scale, and highly variable synthetic dataset of interior scenes, complementing previous synthetic datasets (e.g., ICL-NUIM) markedly.

- **Platform and sensor setup:** To overcome the weakness of lacking trajectory realism in previous datasets, InteriorNet proposed to generate random trajectories first, and then augment them with a learned style model to mimic realistic motions. Compared with ICL-NUIM's duplicating real-world trajectories, this method is more flexible and efficient. As for sensor setup, except for RGB-D sensor, it also simulated IMU (noise available), stereo, events, and so on. Remarkably, the final frames were obtained by averaging between shutter open and close renderings, accomplishing to mimic motion blur, outperforming many other datasets.

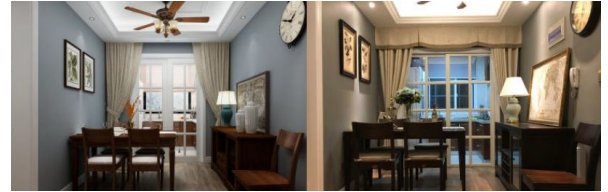


Fig. 16. The Rendering results (left) vs. real-world decorations (right) [81].

- **Scenes and sequences:** The dataset was rendered in various interior scenes and layouts collected from world-leading furniture manufacturers with fine geometric details and high-resolution texture, ranging from small studio to large 42-room apartment. A total of 15k sequences with 1k frames in each are provided, along with many challenging conditions, including various lighting, moving objects, and motion blur. The rendered images are very close to the real world, as depicted in Fig. 16.

- **Ground truth:** The 3D scene ground truth was provided by the pre-designed CAD models. The camera poses ground truth can be easily accessed with perfect accuracy from the simulator.

- **Highlights:** Diverse scenes, wealthy sequences, realistic data, accurate ground truth, 3D scene ground truth.

4) BONN Dynamic [82]

Bonn Dynamic, released in 2019, is a specially designed highly dynamic RGB-D dataset collected in real world, enabling the investigation under such challenge. Both camera poses and 3D mapping ground truth are provided for evaluation.

- **Platform and sensor setup:** The dataset was captured using an RGB-D sensor (Table XII lists the properties) by a handheld carrier, and exactly in this case, motion blur could easily occur due to the 6-DoF motion pattern together with rolling shutter.

TABLE XII
THE PROPERTIES OF THE SENSORS AND GROUND TRUTH INSTRUMENTS

Sensor/Instrument	Type	Rate	Characteristics
RGB-D Camera	ASUS Xtion Pro LIVE	30 Hz	1280 × 1024, RGB + Depth, rolling shutter, 58° × 45° FOV
Motion Capture	OptiTrack Prime 13	240 Hz	<0.2cm/0.5° error
3D Scanner	Leica BLK360	360 kHz	8mm accuracy

- *Scenes and sequences*: A total of 24 sequences were captured under highly-dynamic conditions, such as manipulating box and playing balloon, which was known to be challenging for motion estimation, and 2 sequences were captured under static condition. Three dynamic frames are shown in Fig. 17, as can be seen, the dynamics also add effects on motion blur.

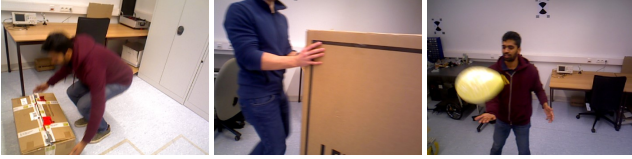


Fig. 17. Two example dynamic frames in the dataset: manipulating boxes (left), and playing with balloons (right) [82].

- *Ground truth*: The pose ground truth was measured by motion capture system with high rate and accuracy. Additionally, the 3D scene ground truth was also provided, containing only the static parts of the scene, enabling 3D reconstruction evaluation. Table XII lists the properties of the ground truth instruments.
- *Highlights*: Highly dynamic environments, wealthy sequences, accurate ground truth, 3D scene ground truth.

D. Image-based 3D Reconstruction Category

1) Middlebury [13]

Middlebury, published in 2006, is a top famous multi-view stereo dataset with known 3D shape ground truth. Novel evaluation metrics were proposed to enable quantitative comparison on mapping accuracy and completeness, which has been dominantly used by the community in past decades.

- *Platform and sensor setup*: The dataset was collected using a CCD camera mounted on a Stanford Spherical Gantry robotic arm. The robotic arm has a high motion flexibility that enables the camera shooting at any viewpoints on a one-meter sphere, with a rather high positioning accuracy within 0.2mm and 0.02 degrees. The properties of the sensor are listed in Table XIII.

TABLE XIII
THE PROPERTIES OF THE SENSORS AND GROUND TRUTH INSTRUMENTS

Sensor/Instrument	Type	Resolution	Characteristics
Camera	CCD sensor	640 × 480	RGB
3D Scanner	Cyberware Model-15	0.25mm	0.2mm accuracy

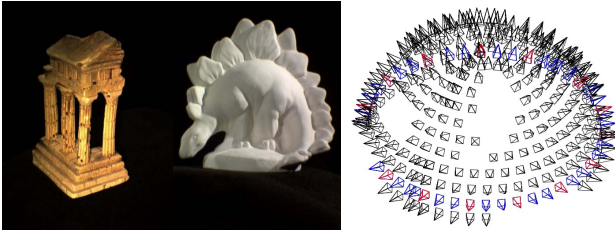


Fig. 18. The object models and viewpoints of dataset: Temple and Dino (left), and different viewpoints (right) [13].

- *Scenes and sequences*: The dataset well selected two target objects for study: Temple and Dino (as shown in the left 2 parts of Fig. 18), both of which are plaster models. Many challenging characteristics were included in the dataset, such as both sharp and smooth features, complex topologies, strong concavities, and both strong and weak surface texture. For each model, there are 3 sets of data provided (see the right part of Fig. 18): hemisphere views (black), ring views (blue), and sparse ring views (red).

- *Ground truth*: The camera poses ground truth were provided by the high-precision robotic arm. Then based on the accurate poses, for each object, about 200 individual scans acquired by a 3D scanner were merged into a whole model, which has a 0.25 mm resolution and better than 0.2mm accuracy (as listed in Table XIII), serving as 3D reconstruction ground truth.

- *Highlights*: 3D model ground truth, challenging model, novel evaluation metrics.

2) BigSfM²⁰

The BigSfM Project is a gathering of massive internet photos datasets, stimulating the growth of many large-scale reconstruction methods in recent years. It offers a seminal way to get huge data resource to support large-scale 3D reconstruction study.

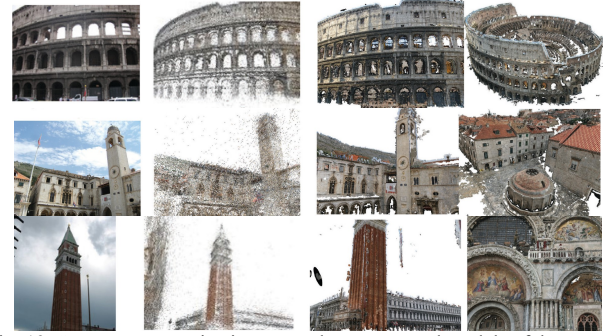


Fig. 19. Some representative images and reconstructed models of the scenes: Colosseum (Rome), Dubrovnik, and San Marco Square (Venice) from top to bound [83].

- *Platform and sensor setup*: This kind of datasets were normally collected on the internet, e.g., Flickr and Google images, thus the platforms and sensors vary. Most of the photos were captured via hand-held smartphone or digital camera, so there was not a fixed resolution or camera intrinsic, which on the other hand, can also serve as a challenge for 3D reconstruction algorithms.

- *Scenes and sequences*: BigSfM contains a variety of community photo datasets. Some famous ones are Rome [83], Venice [84], Dubrovnik [85], NotreDame [86], Landmarks [87], etc. For each scene, there could be hundreds of to tens of thousands of images shot at massive viewpoints. Some representative images and reconstructed models are shown in Fig. 19.

- *Ground truth*: Due to the unorganized nature that the photos could be collected using random cameras, by different persons, and under different conditions, it is normally impractical to provide ground truth 3D models for evaluation. As an alternative, sometimes the GPS tags along with the photos (when available) could be used to verify the camera poses, indicating the reconstruction quality, although not accurate that much.

- *Highlights*: Large-scale scenes, massive photos, web resource.

²⁰ <https://research.cs.cornell.edu/bigsfm/>

3) Tanks and Temples [88]

Tanks and Temples, published in 2017, is a large-scale image-based 3D reconstruction dataset which covers both outdoor and indoor scenes. The most significant contribution is the provided large-scale and high-quality ground truth 3D models, which were long missing in previous datasets [83], [89], [90].

- *Platform and Sensor Setup*: There are two setups for capturing the data, both using a stabilizer with a professional digital camera. As listed in Table XIV, both cameras captured 4k videos at 30hz, and the images were in high-quality thanks to the stabilizer, all of which enable high-fidelity scene reconstruction.

TABLE XIV
THE PROPERTIES OF THE SENSORS AND GROUND TRUTH INSTRUMENT

Sensor/Instrument	Type	Rate	Characteristics
Camera #1	DJI Zenmuse X5R	30 Hz	3840 × 2160, 8-bit RGB, rolling shutter, 84° FOV
Camera #2	Sony a7S II	30 Hz	3840 × 2160, 8-bit RGB, rolling shutter, 90° FOV
3D Scanner	FARO Focus 3D X330	976 kHz	330m range, 2mm accuracy

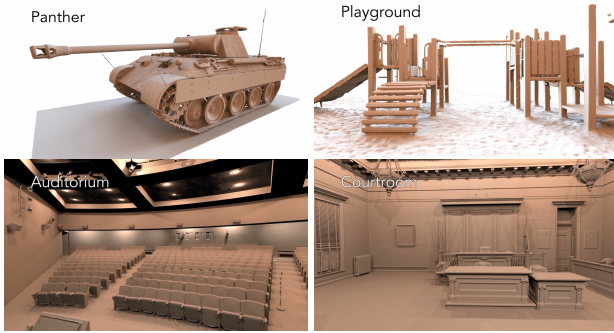


Fig. 20. 4 representative scene models: Panther and Playground - Intermediate group (up), Auditorium and Courtroom - Advanced group (bound) [91].

- *Scenes and sequences*: There is a total of 21 sequences (1 per scene) provided, categorized as 3 groups: intermediate group, advanced group, and training group, covering scenes including Panther, Playground, Auditorium, Courtroom, and so on (see Fig. 20), with an area of up to 4295m². The advanced group are more challenging due to the scale, complexity, illumination, and other factors, as can be felt from the Auditorium model.
- *Ground truth*: The 3D scene ground truth was acquired by an industrial-grade large-scale laser scanner (Table XIV lists the properties), by registering multiple individual scans together via overlap areas. Furthermore, the ground truth camera poses were estimated using the ground truth point cloud [88].
- *Highlights*: 3D scene ground truth, multiple complexity levels, large-scale scenes, diverse scenes.

V. OVERVIEW AND COMPARISON OF EXISTING DATASETS

In this section, based on the proposed 4 broad categories, we comprehensively survey 97 SLAM related datasets, and provide concise but comprehensive overview and comparison tables by category (in a chronological order, for several datasets proposed in the same year, we follow the alphabet order) to serve as a dictionary. We cover the 5 fundamental dimensions of datasets introduced in Section II, and clearly specify the applicable tasks

and challenging elements of each dataset. For each category of datasets, two tables are provided: in the first table, except for the dataset name and released/published year, we arrange cited number, perception sensor setup, ground truth, applicable tasks, and tested methods, for a general selection; in the second table, we arrange mobile platform, collection scenes, data sequences, challenging elements, and dataset links, enabling a finer selection and easy access. The details of each dimension are illustrated below.

- *Name*: The dataset names (usually from the providers) and the corresponding references. If a dataset is collected by synthetic and virtual manner, then we will annotate it as “V”. If a dataset is collected from the web, then we will annotate it as “W”.
- *Year*: The released or published year of the datasets.
- *Cited Number*: The citation number of the dataset (we refer to the statistics on Google Scholar), which could partly indicate the utilization. We use “partly” here because: on the one hand, many datasets do not have self-contained publications [83], then the citation shares together with the corresponding algorithm papers; on the other hand, some datasets are not specifically designed for SLAM related tasks [92], thus the citation could be contributed by other usages.
- *Perception Sensor Setup*: This dimension lists the calibrated perception sensors, framing into 3 columns: camera (we also put RGB-D sensor into this class), IMU, and LiDAR. The camera column lists the specific camera types, such as color, grayscale, event, depth, RGB-D, plenoptic, thermal, and intensity, along with some features to be emphasized such as stereo, fisheye, omnidirectional, wide-angle (WA), narrow-angle (NA), global shutter (GS), and rolling shutter (RS). For image-based 3D reconstruction datasets, we point out either the camera type is professional, consumer, or random to indicate the image source and quality. The IMU column shows whether perception purpose IMU is available, that means we will not cover an IMU that mainly used for ground truth generation. The LiDAR column shows the LiDAR type (2D or 3D) and number of beam (e.g., 4, 16, 32, and 64). For the very few datasets with Radar, we also put it in the LiDAR column, since they are all ranging sensors.
- *Ground truth*: This dimension is framed into 2 columns: pose and 3D. Each column shows whether such type of ground truth is available, and if available the generation technique will be shown, indicating the accuracy.
- *Applicable tasks*: This dimension clearly specifies the applicable tasks of each dataset. For vision-based, LiDAR-related, and RGB-D-based categories, the tasks are framed into 4 columns: O, OAM, SLAM, and 3DR. If the pose ground truth is available, then we will give a “✓” in the blank of O, OAM, and SLAM; if the 3D ground truth is available, then we will give a “✓” in 3DR. In addition, based on the definition of the proposed taxonomy, SLAM has loop closure or relocalization features, hence to well support them, we will give another “✓” if the sequences contain revisited places. However, we will not give a “✓” if the loop is used for evaluation, because SLAM can close the loop and bias the result. For image-based category, 2 columns are listed: SfM and MVS. We will give a “✓” to SfM and MVS first, as it is already a success to reconstruct to 3D from massive individual 2D images. And if either pose or 3D ground truth is available, we

will give another “✓” in the blank of SfM; if the 3D ground truth is available, we will give another “✓” to MVS.

- *Tested methods*: This dimension lists some tested methods on corresponding datasets, in the hope of indicating the usage status and providing useful references. Limited by the space, we cannot list all these contents, which can be further indexed via database. IMU fusion methods (e.g., VINS-mono [102]) are underlined.
- *Mobile Platform*: In this dimension, the mobile platform of collection is given, indicating different motion patterns.
- *Collection Scene*: This dimension shows the collection scenes of data sequences, framed into 3 columns: indoor, outdoor, and indoor-outdoor integration (I-O) scenes. The indoor and outdoor columns list the specific scenes, such as urban, office, room, and so on. If there are many types of scenes employed, we will fill the blank as various or multiple. The I-O column reveals whether the data sequence is traversed between indoor and outdoor scenes (if yes, we will give a “✓” in the blank).
- *Data Sequence*: This dimension is framed into 2 columns: number and volume. The number column lists the total sequence

number of the datasets, indicating the variety of collection routes. To avoid misunderstanding, the dataset will be annotated a “r” if the sequences have repeated routes. The volume column shows the length, duration, or frame number of the data sequences.

- *Challenging element*: In this dimension, challenging elements within the datasets are listed, which could be resulted by motion pattern, scene type, and scene conditions. Overall, elements caused by motion pattern will be annotated with an “M”, mainly including rapid motion, pure rotation, motion blur, and LiDAR distortion; for elements resulted by scene type, namely weak, repetitive, and interference of feature and structure, we will mark as “F” and “S” respectively; for scene conditions, we will mark dynamic objects as “D”, varying, bad, and changing illumination as “I”, various and adverse weathers as “W”, different time-slots as “T”, multiple seasons as “SE”. For image-based datasets, we will additionally mark complex geometry as “C”, and large-scale sequences (more than 1k frames in each) as “L”.
- *Dataset Link*: The web links of datasets. One can easily access detailed information and download the datasets via the links.

* Dataset Selection Guideline

We recommend the dataset users to follow our guideline to select useful datasets using our “dictionary” (the following tables).

- 1) Determine which broad category your algorithm belongs to (refer to Section III) and go to the corresponding session (A~D). E.g., if you are building vision-based SLAM related algorithms, then go to session A, B, and C.
- 2) Consider the specific task you are building (refer to Section III), and see the applicable tasks columns (O/OAM/SLAM/3DR or SfM/MVS) to find available datasets (normally you can find many candidates in this step).
- 3) Consider the specific sensors you want to use (camera, stereo, event, IMU, LiDAR, etc.), and see the perception sensor setup columns to further find some suitable datasets. E.g., if you want to build stereo-vision algorithm with IMU fusion, you can locate EuRoC, Blackbird, Complex Urban, etc.; if you want event-based vision datasets, you can locate UZH-event, MVSEC, etc. Note that, some datasets with IMU data and 6-DoF motions could be with higher difficulty.
- 4) Consider the indicator you want to evaluate (pose or 3D structure), and see the ground truth columns to choose datasets with expected ground truth quality (refer to Section II-B-5)). E.g., if you want to study the frame-by-frame accuracy of VO, then better to choose those datasets with MoCap or LasTrack.
- 5) Choose your expected mobile platform (they are with different motion pattern, refer to Section II).
- 6) Choose your expected testing scene (indoor, outdoor, indoor-outdoor, or specifically office, campus...).
- 7) Choose your desired data volume (100 frames or thousands of frames per sequence).
- 8) Choose your expected challenging elements within the datasets (weak texture, bad illumination, adverse weather, and so on).
- 9) Go to the dataset link to get detailed information and download for use.

Notice: Except for “demand-oriented” selection, from the algorithm testing point of view, one had better choose multiple datasets (with different platform, scene, etc.) for evaluation to avoid over-fitting and hidden defects on certain benchmarks. We will later analyze the necessity of complementary usage in Section VI-C.

A. Vision-based Mobile Localization and Mapping and 3D Reconstruction Category

In this part, we collect 34 datasets for vision-based mobile localization and mapping and 3D reconstruction tasks. The overview and comparison are given in Table XV and Table XVI. Note that we also include several datasets that equipped with LiDAR sensors, such as OpenLORIS and TartanAir, because such datasets are mainly designed for vision-based algorithms, and the LiDARs are mainly employed to generate ground truth [41] or merely serve as a kind of ground truth label [72].

TABLE XV
OVERVIEW AND COMPARISON TABLE-I OF VISION-BASED MOBILE LOCALIZATION AND MAPPING AND 3D RECONSTRUCTION DATASETS

Name	Year	Cited	Perception Sensor Setup			Ground Truth		Applicable Tasks				Tested Methods
			Camera	IMU	LiDAR	Pose	3D	O	OAM	SLAM	3DR	
UTIAS MultiRobot [93]	2011	56	1×color (per-robot)	N/A	N/A	MoCap ^a	N/A	✓	✓	✓	✓	[94], [95]
Devon Island [96]	2012	55	2×color (stereo)	N/A	N/A	DGPS	N/A	✓	✓	✓		[97], [98]
TUM Omni [99]	2015	206	1×fisheye-gray	N/A	N/A	MoCap (P ^b)	N/A	✓	✓	✓	✓	[99], [100]
EuRoC MAV [15]	2016	682	2×gray (stereo)	Y	N/A	MoCap LasTrack ^c	3D Scanner	✓	✓	✓	✓	[49], [53], [101], [102]
(V) SYNTHIA [92]	2016	1031	2×omni-color (stereo) 2×omni-depth (stereo)	N/A	N/A	Simulated	N/A	✓	✓	✓	✓	[103], [104]
TUM monoVO [38]	2016	135	1×NA-gray 1×WA-gray	N/A	N/A	Loop Drift	N/A	✓	✓	✓		[98], [101]

(V) Virtual KITTI [105]	2016	628	1×color 1×depth	N/A	N/A	Simulated	N/A	✓ ✓ ✓✓	[103], [106]
PennCOSYVIO [107]	2017	57	4×color (4-orien ^a) 2×gray (stereo) 1×fisheye-gray	Y	N/A	Fuducial Marker	N/A	✓ ✓ ✓✓	[102], [108]
UZH Event [109]	2017	204	1×event	Y	N/A	MoCap (P)	N/A	✓ ✓ ✓✓	[50], [110], [124]
Zurich Urban [111]	2017	63	1×color	Y	N/A	GPS+Pix4D	N/A	✓ ✓ ✓✓	
ADVIO [112]	2018	31	1×color 1×gray	Y	N/A	Tango+IMU+ Fixed-points	N/A	✓ ✓ ✓✓	[49], [101], [113], [114]
Apollo Scapes [115]	2018	36	2×color	N/A	2×Rigel-2D	RTK-GNSS	MMS	✓ ✓ ✓✓ ✓	[115], [116]
(V) Blackbird [117]	2018	24	2×gray (stereo) 1×gray	Y	N/A	MoCap	N/A	✓ ✓ ✓✓	[49], [102], [118]
VI Canoe [119]	2018	14	2×color (stereo)	Y	N/A	GPS&INS	N/A	✓ ✓ ✓✓	[120]
Mount Etna [121]	2018	11	2×gray (stereo)	Y	N/A	DGPS	N/A	✓ ✓ ✓✓	[122]
MVSEC [123]	2018	91	2×event (stereo) 2×gray (stereo)	Y	1×Velodyne-16	MoCap/ LiDAR+IMU+GPS	N/A	✓ ✓ ✓✓	[124]
SPO [125]	2018	5	2×gray (stereo) 1×plenoptic	N/A	N/A	Loop Drift	N/A	✓ ✓ ✓	[49], [101]
TUM VI [126]	2018	90	2×gray (stereo)	Y	N/A	MoCap (P)	N/A	✓ ✓ ✓✓	[53], [102], [113]
Upenn Fast Flight [127]	2018	190	2×gray (stereo)	Y	N/A	GPS	N/A	✓ ✓ ✓✓	[102], [128]
AQUALOC [129]	2019	13	2×gray (1 for each scene)	Y	N/A	COLMAP	N/A	✓ ✓ ✓✓	[53], [130]
Dynamic Scenes [131]	2019	5	2×color (stereo)	N/A	N/A	Loop Drifts	N/A	✓ ✓ ✓✓	
OpenLORIS [41]	2019	21	1×RGB-D 2×fisheye-RGB (stereo)	Y	1×Hokuyo-2D 1×Robosense-16	MoCap/ LiDAR SLAM	N/A	✓ ✓ ✓✓	[49], [101], [102]
Rosario [132]	2019	14	2×color (stereo)	Y	N/A	RTK-GPS	N/A	✓ ✓ ✓✓	[49], [127], [133]
TUM RS [134]	2019	6	1×GS-gray 1×RS-gray	Y	N/A	MoCap	N/A	✓ ✓ ✓✓	[134], [135]
UZH-FPV [70]	2019	47	1×event 2×gray (stereo)	Y	N/A	LasTrack	N/A	✓ ✓ ✓✓	[50], [102]
ViViD [136]	2019	1	1×thermal 1×RGB-D 1×event	Y	1×Velodyne-16	MoCap/ LiDAR SLAM	N/A	✓ ✓ ✓✓	
ZJU&SenseTime [137]	2019	12	1×color (per scene)	Y	N/A	MoCap	N/A	✓ ✓ ✓✓	[49], [101], [102], [128]
4-Seasons [138]	2020	6	2×gray (stereo)	Y	N/A	RTK-GNSS+SLAM	SLAM	✓ ✓ ✓✓ ✓	
FinnForest [140]	2020	2	4×color (2 for stereo)	Y	N/A	GNSS&INS	N/A	✓ ✓ ✓✓	[49], [133]
PanoraMIS [141]	2020	0	1×omni-color/ 1×dual-fisheye-color	Y	N/A	Robot Odometry/ GPS	SLAM	✓ ✓ ✓✓ ✓	
(V) TartanAir [72]	2020	11	2×color (stereo) 1×depth	Y	1×Simulated-32	Simulated	Simulated	✓ ✓ ✓✓ ✓	[49], [101]
(V) Virtual KITTI2 [142]	2020	17	2×color (stereo) 1×depth	N/A	N/A	Simulated	N/A	✓ ✓ ✓✓	
DSEC [143]	2021	8	2×color (stereo) 2×event (stereo)	N/A	1×Velodyne-16	RTK-GNSS	N/A	✓ ✓ ✓✓	[124]
SeRM [144]	2021	0	1×color	N/A	N/A	RTK-GPS+ Wheel encoder	N/A	✓ ✓ ✓✓	

^aMoCap means Motion Capture System, ^bP means partially coverage, ^cLasTrack means Laser Tracker. Within the tested methods, [49] denotes ORB-SLAM2, [50] Ultimate SLAM, [53] ORB-SLAM3 (dot-lined if both w/ and w/o IMU are tested), [101] DSO, [102] VINS-mono, [113] ROVIO, [124] ESVO, [128] MSCKF.

TABLE XVI
OVERVIEW AND COMPARISON TABLE-II OF VISION-BASED MOBILE LOCALIZATION AND MAPPING AND 3D RECONSTRUCTION DATASETS

Name	Mobile Platform	Collection Scene			Data Sequence		Challenging	Dataset Link
		Indoor	Outdoor	I-O	Number	Volume		
UTIAS MultiRobot	Wheeled Robot	Workspace			9	900-4400s per seq		http://asrl.utias.utoronto.ca/datasets/mrclam/index.html
Devon Island	Rover		Island (planetary)		23	10km in total	F, T	http://asrl.utias.utoronto.ca/datasets/devon-island-rover-navigation/
TUM Omni	Handheld	Office			5	79-165s per seq	M	https://vision.in.tum.de/data/datasets/omni-lsdlam
EuRoC MAV	UAV	Machine hall, room			11	37-131m per seq	M, I	https://projects.asl.ethz.ch/datasets/doku.php?id=kmavvi_sualinertialdatasets
(V) SYNTHIA	Car		Urban		51(r)	1k frames per seq	D, T, W, SE	https://synthia-dataset.net/
TUM monoVO	Handheld	Building	Campus	✓	50	105min in total	M	https://vision.in.tum.de/data/datasets/mono-dataset
(V) Virtual KITTI	Car		Urban		50(r)	233-837 frames per seq	W, T	https://europe.naverlabs.com/research/computer-vision-research-naver-labs-europe/proxy-virtual-worlds-vkitti-1/
PennCOSYVIO	Handheld	Building	Campus	✓	4	150m per seq	F, I	https://daniilidis-group.github.io/penncosyvio/
UZH Event	Handheld	Objects, office	Building		24	2-133s per seq		http://rpg.ifi.uzh.ch/davis_data.html
Zurich Urban	UAV		Urban		1	2km in total		http://rpg.ifi.uzh.ch/zurichmavdataset.html
ADVIO	Handheld	Office, mall, metro	Urban, campus		7	4.5km in total	M, F	https://github.com/AaltoVision/ADVIO
ApolloScape	Car		Urban		6	28km in total	D, T, I	http://apolloscape.auto/self_localization.html
(V) Blackbird	UAV	Various			168(r)	860.8m max	M	https://github.com/mit-fast/Blackbird-Dataset
VI Canoe	Canoe		River		10	2.7km in total	F	https://databank.illinois.edu/datasets/IDB-9342111
Mount Etna	Rover		Mountain		2	1km per seq	F	https://www.robex-allianz.de/datasets/
MVSEC	Multiple	Workspace, building	Workspace, building, urban, highway	✓	14	9.8-18293m per seq	I	https://daniilidis-group.github.io/mvsec/
SPO	Handheld	Building	Park		11	25-274m per seq		https://www.hs-karlsruhe.de/odometry-data/
TUM VI	Handheld	Building	Campus	✓	28	67-2656m per seq	F, I	https://vision.in.tum.de/data/datasets/visual-inertial-dataset
Upenn Fast Flight	UAV	Warehouse	Wooded area	✓	4(r)	700m per seq	M, F, I	https://github.com/KumarRobotics/msckf_vio

AQUALOC	Underwater vehicle		Underwater		17	10.7-122.1m per seq	F, I, D	http://www.lirmm.fr/aqualoc/
Dynamic Scenes	Car		Urban		2	6.4k frames per seq	D, I	https://dataverse.harvard.edu/dataset.xhtml?persistentId=doi:10.7910/DVN/NZETVT
OpenLORIS	Wheeled Robot	Multiple			22(r)	2244s in total	I, T, D	https://lifelong-robotic-vision.github.io/dataset/scene
Rosario	Wheeled Robot		Agriculture		6	152-709m per seq	F, I	https://www.cifasis-conicet.gov.ar/robot/doku.php
TUM RS	Handheld	Office			10	30-57m per seq	M	https://vision.in.tum.de/data/datasets/rolling-shutter-data-set
UZH-FPV	UAV	Hangar	Field		27	59-736m per seq	M	http://rpg.ifi.uzh.ch/uzh-fpv.html
ViViD	Handheld	Room	Urban		9	Up to 50m per seq	M, I, T	https://sites.google.com/view/dgbicra2019-vivid
ZJU&SenseTime	Handheld	Room			16	40-119s per seq	M, F, D	http://www.zjuvgy.net/eval-vislam/
4-Seasons	Car		Urban, rural, sub-urban		30	350km in total	I, T, W, D, SE	https://www.4seasons-dataset.com/
FinnForest	Car		Forest		11	1.3-6.5km per seq	F, I, W, T, SE	https://etsin.fairdata.fi/dataset/06926f4b-b36a-4d6e-873c-aa3e7d84ab49
PanoraMIS	Wheeled Robot/ UAV		Urban, park, field		4	Up to 4.2km per seq	F, I	https://home.mis.u-picardie.fr/~panoramis/
(V) TartanAir	Random	Various	Various		1037	1M frames in total	I, D, W, SE	https://theairlab.org/tartanair-dataset/
(V) Virtual KITTI2	Car		Urban		50(r)	233-837 frames per seq	W, T	https://europe.naverlabs.com/research/computer-vision-research-naver-labs-europe/proxy-virtual-worlds-vkitti-2/
DSEC	Car		Urban		53	3193s in total	I, T	https://dsec.ifi.uzh.ch/
SeRM	Car		Urban		3	26km in total	D	https://github.com/SeRM-dataset/dataset

B. LiDAR-related Mobile Localization And Mapping And 3D Reconstruction Category

In this part, we collect 25 datasets for LiDAR-related mobile localization and mapping and 3D reconstruction usages. The overview and comparison are given in Table XVII and Table XVIII.

TABLE XVII
OVERVIEW AND COMPARISON TABLE-I OF LiDAR-RELATED MOBILE LOCALIZATION AND MAPPING AND 3D RECONSTRUCTION DATASETS

Name	Year	Cited	Perception Sensor Setup			Ground Truth		Applicable Tasks				Tested Methods
			Camera	IMU	LiDAR	Pose	3D	O	OAM	SLAM	3DR	
DARPA [145]	2007	58	4×color (stereo) 1×WA-color	N/A	12×Sick-2D 1×Velodyne-64	DGPS+IMU+DMI	N/A	✓	✓	✓✓		
New College [78]	2009	308	2×gray (stereo) 5×color (panor ^a)	Y	2×Sick-2D	Segway Odometry	N/A	✓	✓	✓✓	[146], [147]	
Rawseeds [148]	2009	153	3×gray (stereo) 1×color 1×omni ^b -color	Y	2×Hokuyo-2D 2×Sick-2D	VisualTag/ LiDAR-ICP/ RTK-GPS	N/A	✓	✓	✓✓	[149]	
Marulan [150]	2010	78	1×color 1×IR-thermal	N/A	4×Sick-2D	RTK-DGPS&INS	N/A	✓	✓	✓✓	[151]	
Ford Campus [152]	2011	253	6×color (omni)	Y	1×Velodyne-64 2×Riegl-2D	DGPS	N/A	✓	✓	✓✓	[153], [154]	
ASL Challenging [155]	2012	102	N/A	Y	1×Hokuyo-2D (tilting as 3D)	Total Station	N/A	✓	✓	✓✓	[153], [156]	
Gravel Pit [157]	2012	12	1×intensity (LiDAR)	N/A	1×Autonosys-3D	DGPS	N/A	✓	✓	✓✓	[158]	
KITTI [14]	2012	6341	2×color (stereo) 2×gray (stereo)	N/A	1×Velodyne-64	RTK-GPS&INS	N/A	✓	✓	✓✓	[45], [49], [51], [53], [54], [154]	
Canadian Planetary [159]	2013	40	3×color (stereo)	Y (P ^c)	1×Sick-2D	DGPS+IMU/ DGPS+VO	N/A	✓	✓	✓✓	[160]	
Institut Pascal [161]	2013	20	4×gray (2 for stereo) 1×omni-color 1×fisheye-color 1×webcam-color	Y	2×Sick-2D	RTK-GPS	N/A	✓	✓	✓✓	[162]	
Malaga Urban [163]	2014	178	2×color (stereo)	Y	2×Sick-2D 3×Hokuyo-2D	GPS	N/A	✓	✓	✓✓	[49], [164]	
NCLT [165]	2016	166	6×color (omni)	Y	1×Velodyne-32 1×Hokuyo-2D	FOG+RTK-GPS+ EKF-Odometry	N/A	✓	✓	✓✓	[166], [167]	
Sugar Beets 2016 [168]	2016	75	1×RGB/NIR 1×RGB-D	N/A	2×Velodyne-16 1×Nippon-2D	RTK-GPS	3D Scanner	✓	✓	✓✓	✓ [169]	
Chilean Underground [170]	2017	16	3×color (stereo)	N/A	1×Rigel-3D	Registration	3D Scanner	✓	✓	✓✓	✓	
Oxford RobotCar [40]	2017	631	3×color (stereo) 3×fisheye-color	N/A	2×Sick-2D 1×Sick-4	RTK-GPS&INS	N/A	✓	✓	✓✓	[48], [49], [171], [172]	
KAIST Day/Night [173]	2018	63	2×color (stereo) 1×thermal	N/A	1×Velodyne-32	RTK-GPS&INS	N/A	✓	✓	✓✓	[174]	
Katwijk Beach [175]	2018	17	2×color (stereo) 2×color (stereo)	N/A	1×Velodyne-16	RTK-DGPS	N/A	✓	✓	✓✓		
MI3DMAP [176][177]	2018	29	1×color 2×fisheye-color	Y	2×Velodyne-16	SLAM	3D Scanner	✓	✓	✓✓	✓ [178]	
Urban@CRAS [179]	2018	12	2×color (stereo)	Y	1×Velodyne-16	RTK-GPS	N/A	✓	✓	✓✓	[49], [133]	
Complex Urban [37]	2019	50	2×color (stereo)	Y	2×Velodyne-16 2×Sick-2D	RTK-GPS+ FOG+SLAM	SLAM	✓	✓	✓✓	✓ [172]	
Mulran [180]	2019	17	N/A	N/A	1×Radar 1×Sick-2D 1×Velodyne-16	RTK-GPS+ FOG+SLAM	SLAM	✓	✓	✓✓	✓ [181]	
Newer College [77]	2020	6	1×RGB-D (used as binocular)	Y	1×Ouster-64	ICP Map Matching	3D Scanner	✓	✓	✓✓	✓ [49], [182]	
Oxford Radar [184]	2020	58	3×color (stereo) 3×fisheye-color	N/A	1×Radar 2×Sick-2D 2×Velodyne-32	GPS&INS+SLAM	N/A	✓	✓	✓✓	[185], [192]	

UrbanLoco [186]	2020	14	1×fisheye-color/ 6×RGB	Y	1×Velodyne-32/ 1×Robosense-32	RTK-GNSS&INS	N/A	✓	✓	✓✓	[45], [102]
Naver Labs Indoor* [187]	2021	1	6×color 4×color (smartphone)	N/A	2×Velodyne-16	SLAM+SfM	SLAM+SfM	✓	✓	✓✓	✓

*panor means panoramic, ^bomni means omnidirectional, ^p means partially coverage. *Naver Labs has released 2 datasets, whereas the outdoor dataset is only opened to Korean users, thus has not been listed here. Within the tested methods, [45] denotes LOAM, [48] LSD-SLAM, [49] ORB-SLAM2, [51] LeGO-LOAM, [53] ORB-SLAM3, [54] V-LOAM, [102] VINS-mono, [146] ORB-SLAM, [154] OverlapNet.

TABLE XVIII
OVERVIEW AND COMPARISON TABLE-II OF LiDAR-RELATED MOBILE LOCALIZATION AND MAPPING AND 3D RECONSTRUCTION DATASETS

Name	Mobile Platform	Collection Scene			Data Sequence		Challenging	Dataset Link
		Indoor	Outdoor	I-O	Number	Volume		
DARPA	Car		Urban	✓	3	90km in total	D, I	http://grandchallenge.mit.edu/wiki/index.php/PublicData
New College	Wheeled Robot		Campus		1	2.2km in total	I	http://www.robots.ox.ac.uk/NewCollegeData
Rawseeds	Wheeled Robot	Building	Campus	✓	11	10km in total	D	http://www.rawseeds.org/
Marulan	UGV		Field		40	66s-357s per seq	W, T	http://sdi.acfr.usyd.edu.au/
Ford Campus	Car		Campus		2	6km and 37km		http://robots.engin.umich.edu/SoftwareData/Ford
ASL Challenging	Custom Base	Multiple	Multiple		8	31-45 scans per seq	S	https://projects.asl.ethz.ch/datasets/doku.php?id=laserregistration:laserregistration
Gravel Pit	Rover		Field (planetary)		10(r)	1.1km per seq	F, S, T	http://asl1.utias.utoronto.ca/datasets/abl-sudbury/
KITTI	Car		Urban, sub-urban		22	39.2km in total	D	http://www.cvlibs.net/datasets/kitti/index.php
Canadian Planetary	UGV	Workspace (planetary)	Workspace (planetary)		4	272 scans in total	F, S	http://asl1.utias.utoronto.ca/datasets/3dmap/#Datasets
Institut Pascal	Car		Workspace		6	0.6-7.8km per seq		http://ipds.univ-bpclermont.fr/
Malaga Urban	Car		Urban		1	36.8km in total	D	https://www.mrpt.org/MalagaUrbanDataset
NCLT	Wheeled Robot	Building	Campus	✓	27	147.4km in total	D, T, I, W, SE	http://robots.engin.umich.edu/nclt/
Sugar Beets 2016	Field Robot		Agriculture		27	2-5km per seq	F, S, T	http://www.ipb.uni-bonn.de/data/sugarbeets2016/
Chilean Underground	UGV	Mine			43	2km in total	I, S	http://dataset.amtc.cl/
Oxford RobotCar	Car		Urban		100(r)	10km per seq	D, I, T, W, SE	https://robotcar-dataset.robots.ox.ac.uk/
KAIST Day/Night	Car		Campus, urban, residential		18(r)	42km in total	I, T, D	https://sites.google.com/view/multispectral/home
Katwijk Beach	Rover		Beach (planetary)		3	2km in total	I	https://robotics.estec.esa.int/datasets/katwijk-beach-11-2-015/
MI3DMap	Backpack	Building			8	Up to 500m per seq		http://mi3dmap.net/
Urban@CRAS	Car		Urban		5	1.8-5km per seq	I, D	https://rdm.inesctec.pt/dataset/nis-2018-001
Complex Urban	Car		Urban, campus		19	1.6-22km per seq	D	https://sites.google.com/view/complex-urban-dataset
Mulran	Car		Urban		12	4.9-23.4km per seq	D, T	https://sites.google.com/view/mulran-pr/home
Newer College	Handheld		Campus		1	2.2km in total		https://ori-drs.github.io/newer-college-dataset/
Oxford Radar	Car		Urban		32	9km per seq	I, D, T, W	https://oxford-robotics-institute.github.io/radar-robotcar-dataset/
UrbanLoco	Car		Urban		13	Up to 13.8km per seq	D	https://advdataset2019.wixsite.com/urbanloco
Naver Labs Indoor	Wheeled Robot	Mall, metro			5	~137k frames in total	F, D, I, T	https://www.naverlabs.com/en/storyDetail/194

C. RGB-D-based Mobile Localization And Mapping And 3D Reconstruction Category

In this part, we collect 20 datasets for RGB-D-based mobile localization and mapping and 3D reconstruction tasks. The overview and comparison are given in Table XIX and Table XX.

TABLE XIX
OVERVIEW AND COMPARISON TABLE-I OF RGB-D-BASED MOBILE LOCALIZATION AND MAPPING AND 3D RECONSTRUCTION DATASETS

Name	Year	Cited	Perception Sensor Setup			Ground Truth		Applicable Tasks				Tested Methods
			Camera	IMU	LiDAR	Pose	3D	O	OAM	SLAM	3DR	
KinectFusion [189]	2012	82	1×RGB-D	N/A	N/A	SLAM	SLAM/3D Scanner	✓	✓	✓✓	✓	[55]
TUM RGB-D [12]	2012	2131	1×RGB-D	N/A	N/A	MoCap ^a	N/A	✓	✓	✓✓		[48], [49], [146], [190], [212]
7-Scenes [191]	2013	477	1×RGB-D	N/A	N/A	SLAM	SLAM	✓	✓	✓✓	✓	[192]
SUN 3D [193]	2013	511	1×RGB-D	N/A	N/A	SfM	SfM	✓	✓	✓✓	✓	[80], [193], [194], [240]
Stanford 3D Scene [195]	2013	181	1×RGB-D	N/A	N/A	SLAM	SLAM	✓	✓	✓✓	✓	[195]
(V) ICL-NUIM [79]	2014	626	1×RGB-D	N/A	N/A	SLAM	Simulated	✓	✓	✓✓	✓	[56], [80], [190], [194], [240]
RGB-D Scenes [196]	2014	294	1×RGB-D	N/A	N/A	SLAM	SLAM	✓	✓	✓✓	✓	
CoRBS [197]	2016	79	1×RGB-D	N/A	N/A	MoCap	3D Scanner	✓	✓	✓✓	✓	[198], [240]
SceneNN [199]	2016	152	1×RGB-D (per scene)	N/A	N/A	SLAM	SLAM	✓	✓	✓✓	✓	[200]
ETH RGB-D [201]	2017	153	1×RGB-D	N/A	N/A	MoCap	3D Scanner	✓	✓	✓✓	✓	[201]
Robot@Home [202]	2017	49	4×RGB-D	N/A	1×Hokuyo-2D	SLAM	N/A	✓	✓	✓✓		[203]
(V) SceneNet [204]	2017	158	1×RGB-D	N/A	N/A	Simulated	Simulated	✓	✓	✓✓	✓	[205]
(V) SUNCG [206]	2017	648	1×RGB-D	N/A	N/A	Simulated	Simulated	✓	✓	✓✓	✓	[49], [207]
ScanNet [208]	2017	823	1×RGB-D (custom)	Y	N/A	SLAM	SLAM	✓	✓	✓✓	✓	[192], [209]
(V) InteriorNet [81]	2018	82	1×RGB-D	Y	N/A	Simulated	Simulated	✓	✓	✓✓	✓	[49], [56]
Bonn [82]	2019	18	1×RGB-D	N/A	N/A	MoCap	3D Scanner	✓	✓	✓✓	✓	[82], [210], [211]
ETH3D SLAM [212]	2019	39	1×color+depth	Y	N/A	MoCap/SfM	N/A	✓	✓	✓✓		[49], [80], [190], [212], [240]
(V) Replica [213]	2019	69	1×RGB-D	N/A	N/A	Simulated	Simulated	✓	✓	✓✓	✓	[49], [210]
VINS-RGBD [215]	2019	14	1×RGB-D	Y	N/A	MoCap	N/A	✓	✓	✓✓		[102], [215]
VCU-RVI [67]	2020	0	1×RGB-D	Y	N/A	MoCap (P ^b)	N/A	✓	✓	✓✓		[102], [215], [216]

^aMoCap means Motion Capture System, ^bP means partially coverage. Within the tested methods, [48] denotes LSD-SLAM, [49] ORB-SLAM2 (visual and RGB-D), [55] KinectFusion, [56] ElasticFusion, [80] Kintinous, [102] VINS-mono, [146] ORB-SLAM, [190] BundleFusion, [212] BAD-SLAM, [215] VINS-RGBD.

TABLE XX
OVERVIEW AND COMPARISON TABLE-II OF RGB-D-BASED MOBILE LOCALIZATION AND MAPPING AND 3D RECONSTRUCTION DATASETS

Name	Mobile Platform	Collection Scene			Data Sequence		Challenging	Dataset Link
		Indoor	Outdoor	I-O	Number	Volume		
KinectFusion	Handheld	Various			57	500-900 frames per seq		https://hci.iwr.uni-heidelberg.de/benchmarks/KinectFusion/Capture_Tool_and_Example_Datasets
TUM RGB-D	Handheld Wheeled Robot	Office, workshop			39	1.5m-40m per seq	M	https://vision.in.tum.de/data/datasets/rgbd-dataset
7-Scenes	Handheld	Multiple			14	1k-7k frames per seq		https://www.microsoft.com/en-us/research/project/rgb-d-dataset-7-scenes/
SUN 3D	Handheld Wheeled Robot	Indoors			415	Tens of thousands of frames in total		http://sun3d.cs.princeton.edu/
Stanford 3D Scene (V) ICL-NUIM	Handheld	Multiple	Multiple		8	72s-432s per seq		http://qianyi.info/scenedata.html
RGB-D Scenes	Handheld	Room, office			8	2m-11m per seq		https://www.doc.ic.ac.uk/~ahanda/VaFRIC/iclnuim.html
CoRBS	Handheld	Objects, furniture			23	85-1128 frames per seq		http://rgbd-dataset.cs.washington.edu/dataset.html
SceneNN	Handheld	Objects			20	5m-59m per seq	M	http://corbs.dfki.uni-kl.de/
ETH RGB-D	Handheld	Rooms			100	2k-10k frames per seq	I	http://www.scenenn.net/
Robot@Home	MAV	Room			1	142s		https://projects.asl.ethz.ch/datasets/doku.php?id=iros2017
(V) SceneNet	Wheeled Robot	Rooms			81	75min in total	I, F	http://mapir.isa.uma.es/mapirwebsite/index.php/mapir-downloads/2013-robot-at-home-dataset
(V) SUNCG	Random	Rooms			16k	5M frames in total	M, I	https://robotvaul.bitbucket.io/scenenet-rgbd.html
ScanNet	Custom	Rooms			46k	400k frames in total		https://sscn.cs.princeton.edu/
(V) InteriorNet	Handheld	Rooms			1513	2.5M frames in total		http://www.scan-net.org/
Bonn	Custom	Rooms			15k	1k frames per seq	M, I, D	https://interiomnet.org/
ETH3D SLAM	Handheld	Office			26	332-11k frames per seq	D	http://www.ipb.uni-bonn.de/data/rgbd-dynamic-dataset
(V) Replica	Handheld	Various	Multiple		96	70-4601 frames per seq	M, I	https://www.eth3d.net/slam_datasets
VINS-RGBD	Custom	Rooms			Custom	Custom rendered		https://github.com/facebookresearch/Replica-Dataset
VCU-RVI	Handheld Wheeled Robot	Lab, Workspace			9	32-271s per seq	M, F	https://robotics.shanghaitech.edu.cn/datasets/VINS-RGBD
	Handheld Wheeled Robot	Lab, Hall, Corridor			39	3.7km in total	M, I, D	https://github.com/rising-turtle/VCU_RVI_Benchmark

D. Image-based 3D Reconstruction Category

In this part, we collect 18 datasets that mainly focus on image-based 3D reconstruction usages. The overview and comparison are given in Table XXI and Table XXII.

TABLE XXI
OVERVIEW AND COMPARISON TABLE-I OF IMAGE-BASED 3D RECONSTRUCTION DATASETS

Name	Year	Cited	Perception Sensor Setup			Ground Truth		Applicable Tasks		Tested Methods
			Camera	IMU	LiDAR	Pose	3D	SfM	MVS	
Middlebury [13]	2006	2656	Professional	N/A	N/A	Robot Arm	3D Scanner	✓✓	✓✓	[217], [218], [219], [221]
(W) Notre Dame [86]	2006	3899	Random	N/A	N/A	N/A	N/A	✓	✓	[86], [229], [232]
EPFL [220]	2008	865	Professional	N/A	N/A	2D-3D Alignment	3D Scanner	✓✓	✓✓	[218], [219], [226]
(W) Rome [83]	2009	2150	Random	N/A	N/A	N/A	N/A	✓	✓	[83], [86], [90], [219]
SAMANTHA [89]	2009	156	Professional	N/A	N/A	Control Points (P ^a)	3D Scanner (P)	✓✓	✓✓	[86], [89]
TUM multiview [221]	2009	174	Professional	N/A	N/A	N/A	3D Scanner	✓✓	✓✓	[221], [222]
(W) Dubrovnik [85]	2010	457	Random	N/A	N/A	GPS	N/A	✓✓	✓	[83], [86], [90], [219]
Quad [223]	2011	349	Professional/consumer	N/A	N/A	GPS+DGPS	N/A	✓✓	✓	[86], [87], [90], [225]
San Francisco [224]	2011	444	6×color (panor ^b)	N/A	1×Velodyne-64	GPS+INS	N/A	✓✓	✓	[87], [225]
Tsinghua University [226]	2011	153	Professional	N/A	N/A	N/A	3D Scanner	✓✓	✓✓	[226]
(W) Landmarks [87]	2012	383	Random	N/A	N/A	GPS+INS	N/A	✓✓	✓	[87]
(W) Large-Scale Collections [227]	2012	22	Random	N/A	N/A	SIFT matching	N/A	✓✓	✓	[228]
(W) SfM-Disambig [229]	2013	58	Random	N/A	N/A	N/A	N/A	✓	✓	[229]
DTU Robot [230]	2014	146	Professional	N/A	N/A	Robot Arm	3D Scanner	✓✓	✓✓	[219], [231]
(W) IDSIM [232]	2014	259	Random	N/A	N/A	N/A	N/A	✓	✓	[86], [90]
COLMAP [90]	2016	1306	Professional	N/A	N/A	N/A	N/A	✓	✓	[90], [219]
ETH3D MVS [233]	2017	245	1×Digital 2×NA-gray (stereo) 2×WA-gray (stereo)	Y	N/A	2D-3D Alignment	3D Scanner	✓✓	✓✓	[90], [219]
Tanks and Temples [88]	2017	219	1×color (per scene)	N/A	N/A	2D-3D Registration	3D Scanner	✓✓	✓✓	[86], [90], [219]

^aP means partially coverage, ^bpanor means panoramic. Within the tested methods, [86] denotes Bundler, [90] COLMAP, [219] PMVS.

TABLE XXII
OVERVIEW AND COMPARISON TABLE-II OF IMAGE-BASED 3D RECONSTRUCTION DATASETS

Name	Mobile Platform	Collection Scene			Data Sequence		Challenging	Dataset Link
		Indoor	Outdoor	I-O	Number	Volume		
Middlebury	Robot Arm	Objects			6	802 views in total	F, C	https://vision.middlebury.edu/mview/data/
(W) Notre Dame	N/A		Landmark		1	715 images		http://phototour.cs.washington.edu/datasets/
EPFL	N/A		Buildings		12	203 images in total	F	https://documents.epfl.ch/groups/c/cv/cvlab-unit/www/data/multiview/index.html
(W) Rome	N/A		Landmarks		1	16k images	L	https://www.cs.cornell.edu/projects/p2f/
SAMANTHA	N/A		Landmarks		8	39-380 images per seq		http://www.diegm.uniud.it/~fusiello/demo/samantha/
TUM Multiview	N/A	Objects			5	21-33 images per seq	F	https://vision.in.tum.de/data/datasets/3dreconstruction
(W) Dubrovnik	N/A		Landmarks		1	6k images	L	https://www.cs.cornell.edu/projects/p2f/
Quad	N/A		Landmarks		1	6k images	L	http://vision.soic.indiana.edu/projects/disco/
San Francisco	Vehicle		Landmarks		1	1.7M images	L	https://purl.stanford.edu/vn158kj2087

Tsinghua University	N/A		Buildings, temples		9	68-636 images per seq	T	http://vision.ia.ac.cn/data/
(W) Landmarks	N/A		Landmarks		10k	massive	L	http://landmark.cs.cornell.edu/Landmarks3/
(W) Large-Scale Collections	N/A		Landmarks		5	4k-7k images per seq	L	https://research.cs.cornell.edu/matchlearn/
(W) SfM-Disambig	N/A		Landmarks		4	839-8032 images per seq	L	https://www.cs.cornell.edu/projects/disambig/
DTU Robot	Robot Arm	Objects			80	49/64 views per seq	F, C	http://roboimagedata.compute.dtu.dk/?page_id=36
(W) IDSfM	N/A		Landmarks		13	227-2152 images per seq	L	https://research.cs.cornell.edu/1dsfm/
COLMAP	N/A	Landmarks	Landmarks	✓	4	100-1273 images per seq	L	http://colmap.github.io/datasets.html
ETH3D MVS	Tripod/Handheld	Various	Multiple		82	11k images in total	F	https://www.eth3d.net/datasets
Tanks and Temples	Stabilizer	Various	Various		14	4k-22k images per seq	F, C, L	https://www.tanksandtemples.org/

VI. EVALUATION CRITERIA

Although reliable ground truth are the decisive premise, evaluation criteria are also indispensable for benchmarks. They play important roles in correctly quantifying and fairly comparing the algorithm performances, identifying potential failure modes, and thus looking for breakthroughs. In this section, we will focus on 2 indicators: positioning and mapping, which are the main functionalities of SLAM related problems. Some other non-functional concerns like time consuming, CPU&RAM usage, and GPU requirement, although have been investigated by some efforts [234], [235], [236], will not be covered due to the immaturity and poor utilization. In part C, we compare top results on 2 different benchmarks to illustrate the necessity of complementary usage.

A. Positioning Evaluation

Due to the limitation of large-scale surveying techniques in earlier years, it was rather difficult to obtain ground truth 3D maps. Therefore, it has been a long while to evaluate SLAM related algorithms by examining the positioning performance. The most widely used evaluating indicators could be the two proposed within the TUM RGB-D benchmark – relative pose error (*RPE*), and absolute trajectory error (*ATE*) [12].

The relative pose error (*RPE*) investigates the local accuracy of the motion estimation systems across a fixed time interval Δ . If the estimated trajectory poses are defined as $\mathbf{P}_1, \dots, \mathbf{P}_n \in \text{SE}(3)$ and the ground truth poses are defined as $\mathbf{Q}_1, \dots, \mathbf{Q}_n \in \text{SE}(3)$, then the *RPE* at time step i could be defined as:

$$\mathbf{E}_i := (\mathbf{Q}_i^{-1} \mathbf{Q}_{i+\Delta})^{-1} (\mathbf{P}_i^{-1} \mathbf{P}_{i+\Delta}).$$

Considering a sequence of n camera poses, there could be $(m = n - \Delta)$ individual *RPE*s. Then how to measure the performance on the whole trajectory? TUM RGB-D benchmark proposed to compute the root mean square error (RMSE) over all time intervals of the translational component as:

$$\text{RMSE}(\mathbf{E}_{1:m}, \Delta) := \left(\frac{1}{m} \sum_{i=1}^m \|\text{trans}(\mathbf{E}_i)\|^2 \right)^{1/2},$$

where the $\text{trans}(\mathbf{E}_i)$ refers to the translational component of the *RPE*. Note that due to the amplification effect of the Euclidean norm, the RMSE could be sensitive to the outliers. So if desired, it is also reasonable to evaluate the mean or median errors as an alternative. Although only the translational errors are measured here, the rotational errors can also be reflected together inside. Additionally, the selection of time interval Δ could vary with different systems and conditions. For instance, the Δ can be set to 1 to examine real-time performance, resulting as per frame drift; as for systems inferring via several previous frames, performing local optimization, and focusing on large-scale navigation, it is

not necessary nor reasonable to count on the estimation of each individual frame. However, it is not appropriate to set Δ to n directly, because it penalizes early rotational errors much more than the occurrences near to the end. Instead, it is recommended to average the RMSEs over a wide range of time intervals, but to avoid excessive complexity, an approximation that counts on a fixed number of intervals could also reach a compromise.

Absolute trajectory error (*ATE*) measures the global accuracy by comparing the estimated trajectory against the ground truth to get absolute distances. As the 2 trajectories could lie in different coordinates, an alignment via a rigid-body transformation \mathbf{S} that maps the estimated poses $\mathbf{P}_{1:n}$ onto the ground truth poses $\mathbf{Q}_{1:n}$ is prerequisite. Then the *ATE* at time step i could be computed as:

$$\mathbf{F}_i := \mathbf{Q}_i^{-1} \mathbf{S} \mathbf{P}_i.$$

Similar with *RPE*, the root mean square error (RMSE) over all time indices of the translational component is also proposed as one possible metric for *ATE*:

$$\text{RMSE}(\mathbf{F}_{1:n}) := \left(\frac{1}{n} \sum_{i=1}^n \|\text{trans}(\mathbf{F}_i)\|^2 \right)^{1/2}.$$

It should be noted that *ATE* considers only the translational errors, but actually the rotational errors will also result in wrong translations. Compared with *RPE*, *ATE* has an intuitive visualization for inspecting the actual accidental area of the algorithm. An example visualization of *ATE* and a comparison between *ATE* and *RPE* are shown in Fig 21. As shown in the comparison, *RPE* could be slightly larger than *ATE* due to the more impact from rotational errors.

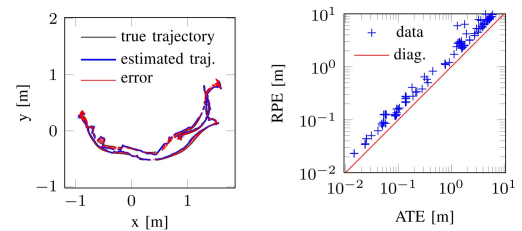


Fig. 21. An example visualization of *ATE* on the “fr1/desk2” sequence of the TUM RGB-D Dataset (left) and a comparison between *RPE* and *ATE* (right). Both plots were generated by RGB-D SLAM system [12].

There are many mainstream datasets [126], [41], [134] sharing the same evaluation criteria with the above, or developing some extended versions based on the same mechanism. For instance, KITTI Odometry benchmark²¹ extends *RPE* to study rotational errors also to enable deeper insights; TartanAir defines success rate (SR) as the ratio of non-lost frames against total sequence length, as the lose-trackings cannot be calculated *RPE* and *ATE*.

²¹ http://www.cvlibs.net/datasets/kitti/eval_odometry.php

However, as we have mentioned in Section II, not all datasets are able to provide complete ground truth trajectory [126], [38]. In this case, normally the start and end segments are available, then after alignment, still RPE and ATE can be evaluated.

B. Mapping Evaluation

In the existing SLAM algorithm publications, it is quite unusual to come across evaluations on mapping performance. But indeed, the evaluation criteria on 3D reconstruction have existed for a long time, which mainly originated from the Middlebury dataset [13]. Denoting the ground truth geometry as G and the reconstruction result as R , there are generally two indicators to be considered: accuracy, and completeness.

The accuracy measures how close R is to G by computing the distances between the corresponding points, which are usually determined by finding the nearest match. If the reconstructions or ground truth models are in other formats like triangle meshes, then the vertices could be used for comparison. One issue will be encountered where the G is incomplete, resulting the nearest reference points to fall on the boundary or a distant part. In this case, a hole-filled version G' is proposed for computing the distance, and the points matched to the repaired region will be discounted. Fig. 22 well illustrates the principle.

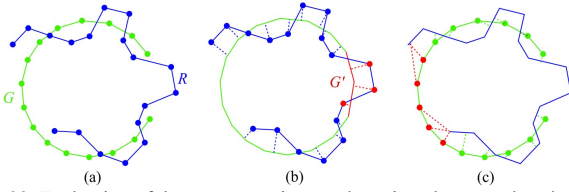


Fig. 22. Evaluation of the reconstruction result against the ground truth model. (a) the representation of the two models, both with incomplete surface. (b) to measure the distance, the nearest matches are found, and the matches related to the hole-filled area will not be included. (c) to measure the completeness, the distances between point matches are computed, those run beyond the threshold will be regarded as “not covered” [13].

The completeness investigates how much of G is modeled by R . Opposite from the accuracy indicator’s comparing R against G , the completeness measures the distances from G to R . Intuitively, if the matching distance runs beyond a threshold, we can deem there is no corresponding point on R , hence the point on G can be logically regarded as “not covered”, as illustrated in Fig. 22.

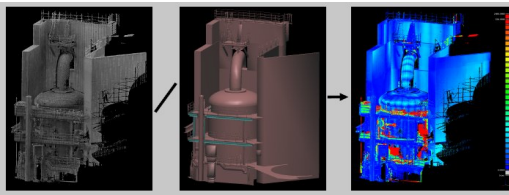


Fig. 23. An example of cloud/mesh computation module investigating the reconstruction accuracy in CloudCompare software [237], the different colors represent different distance values.

For the convenience of the evaluation, ICL-NUIM proposed to exploit the open-source software CloudCompare²² to compute the distances between the reconstruction and the ground truth models. Five standard statistics can be obtained: Mean, Median, Std., Min., and Max. An evaluation demo is shown in Fig. 23.

C. Complementary usage of datasets

As shown in Section V, SLAM related datasets can vary in many dimensions, which cause different impacts (motion pattern, scene appearance and structure, etc.) on algorithm performance and lead to many challenging effects. However, as revealed by the citation statistics, the usages of the datasets are quite biased, which will potentially lead to over-fitting on certain benchmark and hidden defects. To illustrate such risk effectively, here we choose the most widely used KITTI odometry benchmark (only vision-based methods shown) and UZH-FPV benchmark (results of IROS 2020 competition) to give a comparison on the TOP 7 results using the RPE metric proposed by KITTI benchmark (as shown in Table XXIII and Table XXIV). The 2 datasets are with totally different platforms, scenes, sequences, and with a huge contrast on citations (KITTI 6341 vs. UZH-FPV 47).

TABLE XXIII
THE BENCHMARK RESULTS ON KITTI DATASET (VISION ONLY) [73]

Ranking	Name	Translation (%)	Rotation (deg/m)
1	SOFT2	0.57	0.0010
2	SOFT-SLAM	0.65	0.0014
3	RADVO	0.82	0.0018
4	LG-SLAM	0.82	0.0020
5	Rotrocc++	0.83	0.0026
6	GDVO	0.86	0.0031
7	SOFT	0.88	0.0022

TABLE XXIV
THE BENCHMARK RESULTS OF THE UZH-FPV DATASET [71]

Ranking	Name	Translation (%)	Rotation (deg/m)
1	MEGVII-3D	6.819	0.263
2	VCU Robotics	6.891	0.265
3	LARVIO	6.919	0.266
4	Lenovo_LR_ShangHai	7.005	0.282
5	Basalt	7.494	0.268
6	Xin Zhang	9.140	0.219
7	QuetzalC++	34.273	1.635

As can be seen, the TOP results on the two benchmarks have a huge contrast: compared with KITTI, the translational error on UZH-FPV benchmark is one order of magnitude larger, and the rotational error is two orders of magnitude larger. This happens even in the context that the methods from UZH-FPV all fuse the IMU data, whereas the listed methods from KITTI only use pure vision data. Of course, not all the datasets are going to form this big of a contrast on algorithm performance, but it is a truth that the results will vary. Thus, from this point of view, one should not be overconfident on a certain benchmark, since many defects could be hidden. But this never means the datasets produce good scores should be given up: on the one hand, the mechanisms of algorithms indeed vary, and one cannot ensure the algorithm will not encounter certain challenges in “easier” datasets (especially for learning-based methods); on the other hand, from the application point of view, the results in different scenarios all make sense. To this end, we do not encourage to draw biases on dataset selection based on benchmark results (most datasets even have not been tested and evaluated comprehensively after all), instead,

²² <https://www.danielgm.net/cc/>

we should use the datasets in a complementary manner and take advantage of the unbalanced results to look for breakthroughs.

VII. ANALYSES AND DISCUSSIONS

As mentioned repeatedly in the paper, SLAM related datasets complement each other and together form the dataset community. Thus except for understanding the datasets and their difference, to study the whole makes another big sense. Therefore, based on the overview and comparison in Section V, this section studies the whole and give the current limitations and future directions of datasets and evaluation criteria. In the end, we discuss about how to build comprehensive datasets for SLAM community.

A. Datasets limitations and directions

For the datasets limitations and directions, we mainly choose 7 dimensions to analyze and discuss, respectively on the 5 fundamental dimensions including mobile platform, sensor setup, target scene, data sequence, and ground truth, and 2 hot topics recently namely challenging elements, and virtual and synthetic datasets.

1) Mobile platform

For current limitations, the first is the deficiency in the variety of mobile platforms. Fig. 24 shows the distribution of different mobile platforms in each dataset category (we have not shown image-based category because normally good image quality are ensured while collection, e.g., using a stabilizer, thus the motion pattern will not affect too much). As can be seen, vision-based category has a relatively balanced distribution, whereas LiDAR-related category mainly draws on car and wheeled robot (both with 3-DoF motion) and RGB-D-based category mainly draws on handheld and wheeled robot. Although this is partly resulted by the application scenario, from the algorithm developing point of view, the deficiency in the variety of motion patterns will potentially hide the defects. Another limitation is that, most of the datasets only employed single mobile platform for collection. Although they can be used in a complementation way, it is really unfair to make horizontal comparisons if one want to investigate the impacts of different motion patterns.

For future directions, firstly, more diverse platforms are encouraged, e.g., boat [119], motorcycle [123], and backpack [177]. Secondly, we expect more 6-DOF platforms in LiDAR-related datasets, e.g., UAV and backpack [9] are increasingly used in mobile surveying and badly in need of validation. Thirdly, it is highly recommended to deploy various platforms in each single scenario and route to enable fair horizontal comparisons.

2) Sensor setup

Considering that the mainstream sensors can be effectively calibrated temporally and spatially, the limitation of sensor setup

mainly draws on the deficiency of number and types. Leveraging multiple sensors and modalities fusion is an inevitable trend to improve system accuracy and reliability, especially stereo-vision and IMU fusion methods, which have been widely employed and proved to be effective. However, as shown in Section V, many datasets only use basically required sensors: TUM MonoVO [38] only equips monocular cameras, and most of the RGB-D datasets do not have IMU data. Moreover, at present, event-based vision is earning rapid developments and playing a crucial role in robust and high-speed robotics, while are suffering from acute shortage in related datasets, in need of more dedication.



Fig. 25. An approach to convert existing vision datasets to events [238].

In the future, we encourage every dataset to equip redundant and diverse sensors (e.g., event and thermal), to enable possible development and comparison. Then specifically, we hope every future dataset to setup at least stereo cameras and an IMU, which are ubiquitous and affordable. In addition, more dedicated works are needed for event datasets, not only real-world collections, but also convert normal vision data to events (see Fig. 25).

3) Collection scene

For current limitations, firstly, there is still a deficiency in the variety of scene type. For example, only 3 datasets [41], [112], [187] have covered shopping mall, which is highly dynamic and quite common in real life. Secondly, there is a serious lack of indoor-outdoor integrated scenes. Whereas in daily life, it is quite usual for a robot or a human to traverse back and forth. Thirdly, datasets with large-scale indoor scenes are still not enough. Most of the interior scenes are office and room, which cannot meet the demands of applications like factory robots and BIM.

Accordingly, for future directions, firstly, more diverse scenes are expected to complement current datasets, especially typical scenarios like shopping mall, ruins, and industrial park. Secondly, more indoor-outdoor integrated scenes are urgently demanded to research seamless navigation. Thirdly, more large-scale indoor scenes are expected, such as big buildings and large factory hall.

4) Data sequence

The limitation of data sequence mainly draws on the shortage of sequence number and variety and length of single session. For example, Zurich Urban [111] only collected single sequence in

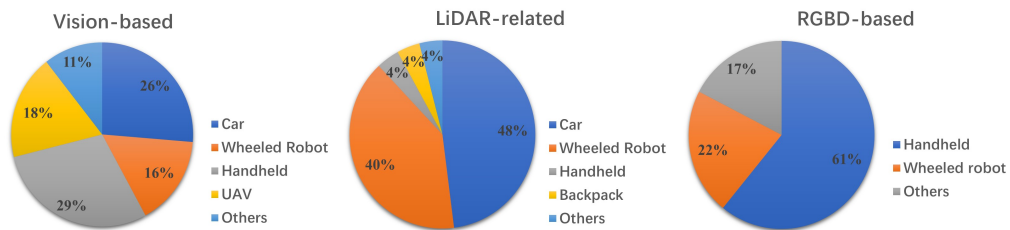


Fig. 24. The distribution of different mobile platforms in each dataset category (except for image-based).

large-scale urban environment; ICL-NUIM [79] only traversed 2m-11m's length per session, which is even too short compared with other indoor datasets. Such datasets have not made full use of the scene and wasted the chance of more thorough testing.

To this end, making full use of the scenes is expected in future datasets, namely collecting as many as possible data sequences and traverse various and longer routes. This is especially doable in large-scale environments. Besides, we expect every dataset to post the session length statistic.

5) Ground truth

For pose ground truth, the limitation mainly lies on the low accuracy and incomplete coverage in some datasets. For example, Complex Urban [37] (in outdoor GNSS-denied areas) has to use SLAM to generate a baseline; TUM VI [126] (long-range indoor and outdoor integrated) only has ground truth data in the start and end segments. For 3D ground truth, the primary limitation is that most datasets (62/97) have not provided such data, and there are also some datasets using SLAM-based algorithm to generate 3D baselines, which could be less accurate.

In the future, we expect there could emerge novel techniques and approaches for generating pose ground truth, especially those with versatility both indoors and outdoors. For 3D structure, we expect future datasets to provide ground truth as far as possible, to enable mapping evaluation. Besides, more types of ground truth are expected, such as depth image and semantic labels.

6) Challenging elements

To date, there has already been many challenging elements identified and embedded in the datasets, proven to shake the performance of algorithms (Fig. 26 shows some failure cases on TartanAir [72]). But there is still a deficiency in some expressly designed elements, such as dense dynamics, multiple time slots, extreme weather, and different seasons. For example, in RGB-D category, only InteriorNet [81] and Bonn [82] have designed sequences with moving objects, whereas such situation are quite commonly encountered in real-world deployments.

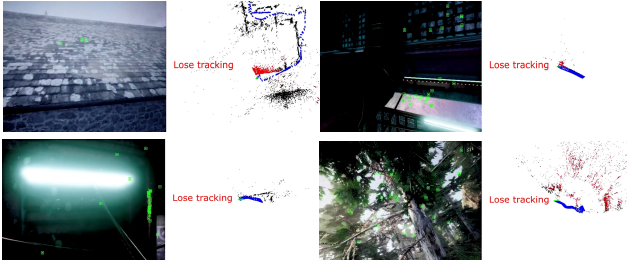


Fig. 26. Some failure cases of ORB-SLAM-Stereo under challenging conditions such as weak and repetitive texture, and bad illumination [239].

In the future, firstly, more and more datasets with dense and various challenging elements are expected, especially those as mentioned above. Then, rigorous studies on the failure modes of algorithms are highly demanded, which will help to quantify the impacts of challenges and identify more such elements.

7) Virtual and synthetic datasets

Synthetic datasets open a new route to handle the drawbacks of real-world datasets, such as complicated collection procedure, limited scenes and sequences, and inaccurate ground truth. For such datasets, the limitation mainly draws on the deficiency of data reality. Firstly, the rendered images are still far from realistic

sometimes [72], [92]. Secondly, it is still quite rare to mimic real-world sensor latency and noises, e.g., camera motion blur and LiDAR motion distortion, which will make the data too ideal.

Therefore, in the future, considering that synthetic datasets can generate boundless sequences under various scenes, especially with perfect ground truth, more such datasets are encouraged to bridge certain gap, but with higher data reality.

B. Evaluation limitations and directions

For limitations and directions of evaluation criteria, we mainly choose 3 dimensions to analyze and discuss, respectively on the 2 functional dimensions namely localization and mapping, and 1 non-functional dimension namely hardware consumption.

1) Localization evaluation

With the wide implementations and test of time in past years [240], [241], [242], the evaluation criteria on localization are relatively mature, which mainly consists of ATE, RPE, and the related variations. However, such dimensions are still quite limited, because SLAM tasks contain many processes, such as initialization, loop-closure, and relocalization. To this end, in the future, more diversified and detailed indicators are expected, such as the accuracy and speed of initialization, the accuracy and success rate of relocalization, the detection rate of loop-closure [41], and the localization accuracy under challenging conditions [243]. These dimensions will definitely be of great significance for inspecting an algorithm deeply and all-roundly.

2) Mapping evaluation

As reflected in the literature, mapping performance is rarely measured in SLAM, whereas sometimes, building an accurate map can even be more important than localization, e.g., path planning, barriers avoidance, and making high-definition (HD) map and light-weight semantic map [144], [244] as virtual sensor for localization. Besides, the existing criteria only investigate the 3D geometry [79], [13], overlooking other dimensions. Hence in the future, the algorithms should be widely evaluated in mapping, and novel criteria that combine geometry, texture, and semantic labeling are desiderated by the community.

3) Hardware consumption evaluation

The current evaluation criteria and algorithms mainly focus on the functional level – localization and mapping, overlooking the hardware consumption, which is a sharply decisive part for the transition from laboratory to application. Thus in the future, more such criteria are expected to be proposed and especially widely employed, such as CPU and RAM usage, GPU requirement, and time consumption [234]. These indicators determine whether an algorithm can be widely deployed in real world, namely, whether can be embedded lightweightly, whether can work in real time, and whether the total cost is reasonable.

C. How to build comprehensive datasets?

Comprehensive datasets are the powerhouse of improvements and breakthrough of algorithms. Before the release of ImageNet in 2009 [20], no one had imaged a vision Artificial Intelligence can be like today within 10 years' trip: The accuracy of objects classifying rose from 71.8% to 97.3%, surpassing human ability and proving that datasets can push the limits of algorithms to another level [245]. However, compared with machine learning, to

collect SLAM datasets is more complicated and time consuming, thus it is almost impossible to build an ImageNet in SLAM field.

In such condition, we mainly advocate 2 approaches to bridge the gap. One is to develop mature techniques and pipeline to generate high-reality synthetic datasets. This is exactly what many datasets are trying hard to do, such as Replica (using Habitat-Sim) [213], [246] and InteriorNet [81]. Moreover, surprisingly, from RTX20 series, NVIDIA has released their ray-tracing GPUs with RT Cores [247]. Such hardware-level ray-tracing technology enables users to get high-quality photo renderings in real-time (see Fig. 27, a screenshot of Red Dead Redemption 2 game rendered by RTX3090), leading to a more convenient and boundless way to generate realistic SLAM datasets.



Fig. 27. A screenshot of Red Dead Redemption2 rendered by RTX3090 [248].

The other is to build a set of standards of datasets and call for distributing the data collections (e.g., different platforms, scenes, and weathers, etc.) to the community, and finally the standard-compliant datasets are released to public. In this way, both individuals and institutes can join collections and enjoy the feedbacks.

It is worth noting that, it is a matter of principle that simulation cannot replace experiment of real-world data, especially for tasks like SLAM, which are close related to life safety issues. Thus it is recommended to use them jointly: Use the synthetic datasets as preliminary testing purposes to validate a certain assumption, then after getting supportive results, the corresponding real-world datasets can be proposed. We believe in the next few years, the datasets community can witness a prosperity and drive SLAM technology significantly.

VIII. CONCLUSION AND FUTURE WORK

This paper is the first comprehensive survey specialized on SLAM related datasets. We treat SLAM related dataset as a research branch rather than merely a tool, thus except for the normal review dimensions of datasets, we also introduce the collection methodology, which distinguishes our survey from many others. By presenting a range of cohesive topics, two major concerns have been addressed: one is to remove the biased usage of datasets and ensure a comprehensive, correct, and efficient selection; the other is to lower the threshold and promote future directions of datasets research. We believe by making full use of the existing datasets and exploiting new ones, SLAM related algorithms can attend key breakthroughs soon afterwards. Moreover, to maintain the benefit of the paper, we will keep updating the datasets dictionary and comments periodically on GitHub at: https://github.com/robot-pesg/SLAM_Datasets_Survey_JAS.

The paper itself is already comprehensive and concrete which well accomplishes its missions about datasets, but afterwards,

another key topic arises namely the study of “dataset-algorithm-evaluation”. Although many qualitative challenging elements are pointed out in each dataset, how to quantify such elements? What are the quantitative impacts of them on algorithms? We do not want to crowd this survey too much which may cause emanative structure, instead we believe such issues deserve a self-contained research paper, which is exactly our main goal in the coming few months, attending to thorough evaluations of diverse algorithms against massive datasets. Besides, we are also building a new vision-LiDAR dataset in typical, large-scale, and indoor-outdoor integration scenes with both accurate localization and mapping ground truth.

ACKNOWLEDGMENT

To achieve a better illustration, this survey has reused many photos from the internet, dataset holders, and journals. The authors would like to acknowledge them all for the public licenses and copyright permissions. The authors would also like to acknowledge Dr. Yassine Selami for the refinement on English writing. Yuanzhi Liu would like to thank Prof. Bart Goossens and Prof. Wilfried Philips for the guidance and suggestions on the research when he served as a guest researcher in Ghent University, Belgium.

REFERENCES

- [1] C. Cadena, L. Carlone, H. Carrillo, Y. Latif, D. Scaramuzza, J. Neira, I. Reid, and J. J. Leonard, "Past, present, and future of simultaneous localization and mapping: Toward the robust-perception age," *IEEE Trans. Robot.*, vol. 32, no. 6, pp. 1309-1332, 2016.
- [2] H. Durrant-Whyte and T. Bailey, "Simultaneous localization and mapping: Part I," *IEEE Robot. Automat. Mag.*, vol. 13, no. 2, pp. 99-110, 2006.
- [3] T. Bailey and H. Durrant-Whyte, "Simultaneous localization and mapping (SLAM): Part II," *IEEE Robot. Automat. Mag.*, vol. 13, no. 3, pp. 108-117, 2006.
- [4] Singandhupe and H. M. La, "A Review of SLAM Techniques and Security in Autonomous Driving," in *2019 Third IEEE Int. Conf. Robot. Comput. (IRC)*, Naples, Italy, 2019, pp. 602-607.
- [5] M. Milford and G. Wyeth, "Persistent Navigation and Mapping using a Biologically Inspired SLAM System," *Int. J. Robot. Res.*, vol. 29, no. 9, pp. 1131-1153, 2010.
- [6] M. Blösch, S. Weiss, D. Scaramuzza, and R. Siegwart, "Vision based MAV navigation in unknown and unstructured environments," in *2010 IEEE Int. Conf. Robot. Automat. (ICRA)*, Anchorage, AK, USA, 2010, pp. 21-28.
- [7] Cvišić, J. Česić, I. Marković, and I. Petrović, "SOFT-SLAM: Computationally efficient stereo visual simultaneous localization and mapping for autonomous unmanned aerial vehicles," *J. Field Robot.*, vol. 35, no. 4, pp. 578-595, 2018.
- [8] D. Chekhlov, A. P. Gee, A. Calway, and W. Mayol-Cuevas, "Ninja on a Plane: automatic discovery of physical planes for augmented reality using visual SLAM," in *2007 6th IEEE and ACM Int. Symp. Mix. Augment. Real. (ISMAR)*, Nara, Japan, 2007, pp. 153-156.
- [9] S. Karam, G. Vosselman, M. Peter, S. Hosseinyalamdary, and V. Lehtola, "Design, Calibration, and Evaluation of a Backpack Indoor Mobile Mapping System," *Remote Sens.*, vol. 11, no. 8, p. 905, 2019.
- [10] N. E. Boudette, "Despite High Hopes, Self-Driving Cars Are 'Way in the Future'." *The New York Times*. <https://www.nytimes.com/2019/07/17/business/self-driving-autonomous-cars.html> (accessed Jun. 7, 2020).
- [11] D. Wakabayashi, "Self-Driving Uber Car Kills Pedestrian in Arizona, Where Robots Roam." *The New York Times*. <https://www.nytimes.com/2018/03/19/technology/uber-driverless-fatality.html> (accessed May. 13, 2020).
- [12] J. Sturm, N. Engelhard, F. Endres, W. Burgard, and D. Cremers, "A benchmark for the evaluation of RGB-D SLAM systems," in *2012*

- IEEE/RSJ Int. Conf. Intell. Robot. Syst. (IROS)*, Vilamoura, Portugal, 2012, pp. 573-580.
- [13] S. M. Seitz, B. Curless, J. Diebel, D. Scharstein, and R. Szeliski, "A Comparison and Evaluation of Multi-View Stereo Reconstruction Algorithms," in *2006 IEEE Comput. Society Conf. Comput. Vis. Pattern Recognit. (CVPR)*, New York, NY, USA, 2006, pp. 519-528.
 - [14] Geiger, P. Lenz, and R. Urtasun, "Are we ready for autonomous driving? the kitti vision benchmark suite," in *2012 IEEE Conf. Comput. Vis. Pattern Recognit. (CVPR)*, Providence, RI, USA, 2012, pp. 3354-3361.
 - [15] M. Burri, J. Nikolic, P. Gohl, T. Schneider, J. Rehder, S. Omari, M. W. Achtelik, and R. Siegwart, "The EuRoC micro aerial vehicle datasets," *Int. J. Robot. Res.*, vol. 35, no. 10, pp. 1157-1163, 2016.
 - [16] M. Firman, "RGBD datasets: Past, present and future," in *Proc. IEEE Conf. Comput. Vis. Pattern Recognit. Workshops (CVPRW)*, Las Vegas, NV, USA, 2016, pp. 19-31.
 - [17] Z. Cai, J. Han, L. Liu, and L. Shao, "RGB-D datasets using microsoft kinect or similar sensors: a survey," *Multimed. Tools Appl.*, vol. 76, no. 3, pp. 4313-4355, 2017.
 - [18] G. Bresson, Z. Alsayed, L. Yu, and S. Glaser, "Simultaneous Localization and Mapping: A Survey of Current Trends in Autonomous Driving," *IEEE Trans. Intell. Veh.*, vol. 2, no. 3, pp. 194-220, 2017.
 - [19] E. Yurtsever, J. Lambert, A. Carballo, and K. Takeda, "A Survey of Autonomous Driving: Common Practices and Emerging Technologies," *IEEE Access*, vol. 8, pp. 58443-58469, 2020.
 - [20] J. Deng, W. Dong, R. Socher, L.-J. Li, L. Kai, and F.-F. Li, "ImageNet: A large-scale hierarchical image database," in *2009 IEEE Conf. Comput. Vis. Pattern Recognit. (CVPR)*, Miami, FL, USA, 2009, pp. 248-255.
 - [21] P. Lichtsteiner, C. Posch, and T. Delbruck, "A 128 \times 128 120 dB 15 μ s Latency Asynchronous Temporal Contrast Vision Sensor," *IEEE J. Solid-State Circuit*, vol. 43, no. 2, pp. 566-576, 2008.
 - [22] Z. Zhang, "Microsoft Kinect Sensor and Its Effect," *IEEE Multimedia*, vol. 19, no. 2, pp. 4-10, 2012.
 - [23] Z. Zhang, "A flexible new technique for camera calibration," *IEEE Trans. Pattern Anal. Mach. Intell.*, vol. 22, no. 11, pp. 1330-1334, 2000.
 - [24] P. Furgale, J. Rehder, and R. Siegwart, "Unified temporal and spatial calibration for multi-sensor systems," in *2013 IEEE/RSJ Int. Conf. Intell. Robot. Sys. (IROS)*, Tokyo, Japan, 2013, pp. 1280-1286.
 - [25] P. Furgale, T. D. Barfoot, and G. Sibley, "Continuous-time batch estimation using temporal basis functions," in *2012 IEEE Int. Conf. Robot. Automat. (ICRA)*, Saint Paul, MN, USA, 2012, pp. 2088-2095.
 - [26] J. Maye, P. Furgale, and R. Siegwart, "Self-supervised calibration for robotic systems," in *2013 IEEE Intell. Veh. Symp. (IV)*, Gold Coast, QLD, Australia, 2013, pp. 473-480.
 - [27] Geiger, F. Moosmann, O. Car, and B. Schuster, "Automatic camera and range sensor calibration using a single shot," in *2012 IEEE Int. Conf. Robot. Automat. (ICRA)*, Saint Paul, MN, USA, 2012, pp. 3936-3943.
 - [28] S. Kato, E. Takeuchi, Y. Ishiguro, Y. Ninomiya, K. Takeda, and T. Hamada, "An Open Approach to Autonomous Vehicles," *IEEE Micro*, vol. 35, no. 6, pp. 60-68, 2015.
 - [29] J. Eidson, "IEEE-1588 standard for a precision clock synchronization protocol for networked measurement and control systems—A tutorial," in *2005 IEEE Works.*, 2005.
 - [30] OptiTrack. "OptiTrack Studio." Wikimedia Commons, the free media repository. https://commons.m.wikimedia.org/wiki/File:Opti_track_Studio.jpg (accessed Aug. 20th, 2020).
 - [31] Geiger, P. Lenz, C. Stiller, and R. Urtasun, "Vision meets robotics: The KITTI dataset," *Int. J. Robot. Res.*, vol. 32, no. 11, pp. 1231-1237, 2013.
 - [32] E. Olson, "AprilTag: A robust and flexible visual fiducial system," in *2011 IEEE Int. Conf. Robot. Automat. (ICRA)*, Shanghai, China, 2011, pp. 3400-3407.
 - [33] V. Otsason, A. Varshavsky, A. Lamarca, and E. De Lara, "Accurate GSM Indoor Localization," in *UbiComp 2005: Ubiquitous Computing*. Heidelberg, Berlin: Springer, 2005, pp. 141-158.
 - [34] Alarifi, A. Al-Salman, M. Alsaleh, A. Alnafessah, S. Al-Hadhrani, M. Al-Ammar, and H. Al-Khalifa, "Ultra Wideband Indoor Positioning Technologies: Analysis and Recent Advances," *Sensors*, vol. 16, no. 5, pp. 707-741, 2016.
 - [35] C. Yang and H.-R. Shao, "WiFi-based indoor positioning," *IEEE Commun. Mag.*, vol. 53, no. 3, pp. 150-157, 2015.
 - [36] J. Hallberg, M. Nilsson, and K. Synnes, "Positioning with Bluetooth," in *2003 10th Int. Conf. Telecommun. (ICT)*, Papeete, Tahiti, French Polynesia, 2003, pp. 954-958.
 - [37] J. Jeong, Y. Cho, Y.-S. Shin, H. Roh, and A. Kim, "Complex urban dataset with multi-level sensors from highly diverse urban environments," *Int. J. Robot. Res.*, vol. 38, no. 6, pp. 642-657, 2019.
 - [38] J. Engel, V. Usenko, and D. Cremers, "A photometrically calibrated benchmark for monocular visual odometry," 2016, *arXiv: 1607.02555*. [Online]. Available: <https://arxiv.org/abs/1607.02555>
 - [39] IRAP-Lab. "Complex Urban Data Set." Intelligent Robotic Autonomy and Perception (IRAP) Lab. <https://irap.kaist.ac.kr/dataset/system.html> (accessed Oct. 10th, 2020).
 - [40] W. Maddern, G. Pascoe, C. Linegar, and P. Newman, "1 year, 1000 km: The Oxford RobotCar dataset," *Int. J. Robot. Res.*, vol. 36, no. 1, pp. 3-15, 2017.
 - [41] X. Shi, D. Li, P. Zhao, Q. Tian, Y. Tian, Q. Long, C. Zhu, J. Song, F. Qiao, L. Song, Y. Guo, Z. Wang, Y. Zhang, B. Qin, W. Yang, F. Wang, R. H. M. Chan, and Q. She, "Are We Ready for Service Robots? The OpenLORIS-Scene Datasets for Lifelong SLAM," in *2020 IEEE Int. Conf. Robot. Automat. (ICRA)*, Paris, France, 2020, pp. 3139-3145.
 - [42] A. Pretto, E. Menegatti, M. Bennewitz, W. Burgard and E. Pagello, "A visual odometry framework robust to motion blur," in *2009 IEEE Int. Conf. Robot. Automat. (ICRA)*, Kobe, Japan, 2009, pp. 2250-2257.
 - [43] B. Zhang, X. Zhang, B. Wei and C. Qi, "A Point Cloud Distortion Removing and Mapping Algorithm based on Lidar and IMU UKF Fusion," in *2019 IEEE/ASME Int. Conf. Advanced Intell. Mechatron. (AIM)*, 2019, pp. 966-971.
 - [44] W. Hess, D. Kohler, H. Rapp and D. Andor, "Real-time loop closure in 2D LIDAR SLAM," in *2016 IEEE Int. Conf. Robot. Automat. (ICRA)*, Stockholm, Sweden, 2016, pp. 1271-1278.
 - [45] J. Zhang and S. Singh, "LOAM: Lidar Odometry and Mapping in Real-time," in *2014 10th Robot. Sci. Syst. (RSS)*, Berkeley, CA, USA, 2014.
 - [46] SPAR3D. "Velodyne cuts VLP-16 lidar price to \$4k." SPAR 3D. <https://www.spar3d.com/news/lidar/velodyne-cuts-vlp-16-lidar-price-4k/> (accessed May. 15th, 2020).
 - [47] G. Klein and D. Murray, "Parallel tracking and mapping for small AR workspaces," in *2007 6th IEEE and ACM Int. Symp. Mix. Augment. Real. (ISMAR)*, Nara, Japan, 2007, pp. 1-10.
 - [48] J. Engel, T. Schöps, and D. Cremers, "LSD-SLAM: Large-scale direct monocular SLAM," in *2014 13th Eur. Conf. Comput. Vis. (ECCV)*, Zürich, Switzerland, 2014, pp. 834-849.
 - [49] R. Mur-Artal and J. D. Tardos, "ORB-SLAM2: An Open-Source SLAM System for Monocular, Stereo, and RGB-D Cameras," *IEEE Trans. Robot.*, vol. 33, no. 5, pp. 1255-1262, 2017.
 - [50] A. R. Vidal, H. Rebecq, T. Horstschaefer and D. Scaramuzza, "Ultimate SLAM? Combining Events, Images, and IMU for Robust Visual SLAM in HDR and High-Speed Scenarios," *IEEE Robot. Automat. Lett.*, vol. 3, no. 2, pp. 994-1001.
 - [51] T. Shan and B. Englot, "LeGO-LOAM: Lightweight and Ground-Optimized Lidar Odometry and Mapping on Variable Terrain," in *2018 IEEE/RSJ Int. Conf. Intell. Robot. Syst. (IROS)*, Madrid, Spain, 2018, pp. 4758-4765.
 - [52] J.-E. Deschaud, "IMLS-SLAM: scan-to-model matching based on 3D data," in *2018 IEEE Int. Conf. Robot. Automat. (ICRA)*, Brisbane, QLD, Australia, 2018, pp. 2480-2485.
 - [53] C. Campos, R. Elvira, J. J. G. Rodríguez, J. M. Montiel, and J. D. Tardós, "ORB-SLAM3: An Accurate Open-Source Library for Visual, Visual-Inertial and Multi-Map SLAM," 2020, *arXiv:2007. 11898*. [Online]. Available: <https://arxiv.org/abs/2007. 11898>
 - [54] J. Zhang and S. Singh, "Visual-lidar odometry and mapping: Low-drift, robust, and fast," in *2015 IEEE Int. Conf. Robot. Automat. (ICRA)*, 2015, pp. 2174-2181.
 - [55] R. A. Newcombe, S. Izadi, O. Hilliges, D. Molyneaux, D. Kim, A. J. Davison, P. Kohli, J. Shotton, S. Hodges, and A. Fitzgibbon, "KinectFusion: Real-time dense surface mapping and tracking," in *2011 10th IEEE Int. Symp. Mix. Augment. Real. (ISMAR)*, Basel, Switzerland, 2011, pp. 127-136.
 - [56] T. Whelan, S. Leutenegger, R. Salas-Moreno, B. Glocker, and A. Davison, "ElasticFusion: Dense SLAM without a pose graph," in *2015 Robot. Sci. Sys. (RSS)*, Rome, Italy, 2015.
 - [57] D. Nistér, O. Naroditsky, and J. Bergen, "Visual odometry," in *2004 IEEE Comput. Soc. Conf. Comput. Vis. Pattern Recognit. (CVPR)*, Washington, DC, USA, 2004, pp. I-I.
 - [58] D. Fernandez and A. Price, "Visual odometry for an outdoor mobile robot," in *IEEE Conf. Robot. Automat. Mechatron.*, Singapore, Singapore, 2004, pp. 816-821.
 - [59] D. Scaramuzza and F. Fraundorfer, "Visual Odometry [Tutorial]," *IEEE Robot. Automat. Mag.*, vol. 18, no. 4, pp. 80-92, 2011.

- [60] L. Murphy, T. Morris, U. Fabrizi, M. Warren, M. Milford, B. Upcroft, M. Bosse, and P. Corke, "Experimental comparison of odometry approaches," in *Exp. Robot.*, 2013, pp. 877-890.
- [61] Wikipedia. "Mobile Mapping." Wikipedia, the free encyclopedia. https://en.wikipedia.org/wiki/Mobile_mapping (accessed Aug. 8th, 2020).
- [62] Wikipedia. "Simultaneous localization and mapping." Wikipedia, the free encyclopedia. https://en.wikipedia.org/wiki/Simultaneous_localization_and_mapping (accessed Nov. 16, 2019).
- [63] D. G. Lowe, "Distinctive image features from scale-invariant keypoints," *Int. J. Comput. Vis.*, vol. 60, no. 2, pp. 91-110, 2004.
- [64] E. Rublee, V. Rabaud, K. Konolige, and G. R. Bradski, "ORB: An efficient alternative to SIFT or SURF," in *2011 Int. Conf. Comput. Vis. (ICCV)*, 2011, pp. 2564-2571.
- [65] Ozyesil, V. Voroninski, R. Basri, and A. Singer, "A survey of structure from motion," 2017, *arXiv:1701.08493*. [Online]. Available: <https://arxiv.org/abs/1701.08493>
- [66] G. Verhoeven, C. Sevara, W. Karel, C. Ressel, M. Doneus, and C. Briese, "Undistorting the past: New techniques for orthorectification of archaeological aerial frame imagery," in *Good practice in archaeological diagnostics*. Cham, Switzerland: Springer, 2013, pp. 31-67.
- [67] H. Zhang, L. Jin and C. Ye, "The VCU-RVI Benchmark: Evaluating Visual Inertial Odometry for Indoor Navigation Applications with an RGB-D Camera," in *2020 IEEE/RSJ Int. Conf. Intell. Robot. Sys. (IROS)*, 2020, pp. 6209-6214.
- [68] J. Engel, J. Stuckler, and D. Cremers, "Large-scale direct SLAM with stereo cameras," in *2015 IEEE/RSJ Int. Conf. Intell. Robot. Syst. (IROS)*, Hamburg, Germany, 2015, pp. 1935-1942.
- [69] J.-C. Piao and S.-D. Kim, "Adaptive Monocular Visual-Inertial SLAM for Real-Time Augmented Reality Applications in Mobile Devices," *Sensors*, vol. 17, no. 11, pp. 2567-2591, 2017.
- [70] J. Delmerico, T. Cieslewski, H. Rebecq, M. Faessler, and D. Scaramuzza, "Are we ready for autonomous drone racing? the UZH-FPV drone racing dataset," in *2019 IEEE Int. Conf. Robot. Automat. (ICRA)*, Montreal, QC, Canada, 2019, pp. 6713-6719.
- [71] UZH FPV, "IROS 2020 FPV Drone Racing Competition Results", Robotics and Perception Group, <https://fpv.ifi.uzh.ch/iros-2020-fpv-drone-racing-vio-competition-results/> (accessed Dec. 15th, 2020)
- [72] W. Wang, D. Zhu, X. Wang, Y. Hu, Y. Qiu, C. Wang, Y. Hu, A. Kapoor, and S. Scherer, "TartanAir: A Dataset to Push the Limits of Visual SLAM," 2020, *arXiv:2003.14338*. [Online]. Available: <https://arxiv.org/abs/2003.14338>
- [73] A. Geiger. "The KITTI Vision Benchmark Suite." [cvlibs.net. http://www.cvlibs.net/datasets/kitti/eval_odometry.php](http://www.cvlibs.net/datasets/kitti/eval_odometry.php) (accessed Aug. 15th, 2020).
- [74] Oxford-Robotics-Institute. "Oxford RobotCar Dataset." Oxford Robotics Institute. <https://robotcar-dataset.robots.ox.ac.uk/> (accessed Aug. 16th, 2020).
- [75] W. Maddern, G. Pascoe, M. Gadd, D. Barnes, B. Yeomans, and P. Newman, "Real-time Kinematic Ground Truth for the Oxford RobotCar Dataset," 2020, *arXiv:2002.10152*. [Online]. Available: <https://arxiv.org/abs/2002.10152>
- [76] M. Kaess, A. Ranganathan, and F. Dellaert, "iSAM: Incremental smoothing and mapping," *IEEE Trans. Robot.*, vol. 24, no. 6, pp. 1365-1378, 2008.
- [77] M. Ramezani, Y. Wang, M. Camurri, D. Wisth, M. Mattamala, and M. Fallon, "The Newer College Dataset: Handheld LiDAR, Inertial and Vision with Ground Truth," 2020, *arXiv:2003.05691*. [Online]. Available: <https://arxiv.org/abs/2003.05691>
- [78] M. Smith, I. Baldwin, W. Churchill, R. Paul, and P. Newman, "The New College Vision and Laser Data Set," *Int. J. Robot. Res.*, vol. 28, no. 5, pp. 595-599, 2009.
- [79] Handa, T. Whelan, J. McDonald, and A. J. Davison, "A Benchmark for RGB-D Visual Odometry, 3D Reconstruction and SLAM," in *2014 IEEE Int. Conf. Robot. Automat. (ICRA)*, Hong Kong, China, 2014, pp. 1524-1531.
- [80] T. Whelan, M. Kaess, H. Johannsson, M. Fallon, J. J. Leonard, and J. McDonald, "Real-time large-scale dense RGB-D SLAM with volumetric fusion," *Int. J. Robot. Res.*, vol. 34, no. 4-5, pp. 598-626, 2015.
- [81] W. Li, S. Saeedi, J. McCormac, R. Clark, D. Tzoumanikas, Q. Ye, Y. Huang, R. Tang, and S. Leutenegger, "InteriorNet: Mega-scale multi-sensor photo-realistic indoor scenes dataset," 2018, *arXiv:1809.00716*. [Online]. Available: <https://arxiv.org/abs/1809.00716>
- [82] E. Palazzolo, J. Behley, P. Lottes, P. Giguère, and C. Stachniss, "ReFusion: 3D Reconstruction in Dynamic Environments for RGB-D Cameras Exploiting Residuals," in *2019 IEEE/RSJ Int. Conf. Intell. Robot. Sys. (IROS)*, Macau, China, 2019, pp. 7855-7862.
- [83] S. Agarwal, N. Snavely, I. Simon, S. M. Seitz, and R. Szeliski, "Building Rome in a day," in *2009 IEEE Int. Conf. Comput. Vis. (ICCV)*, Kyoto, Japan, 2009, pp. 72-79.
- [84] S. Agarwal, Y. Furukawa, N. Sna, B. Curless, S. M. Seitz, and R. Szeliski, "Reconstructing Rome," *Computer*, vol. 43, no. 6, pp. 40-47, 2010.
- [85] Y. Li, N. Snavely, and D. P. Huttenlocher, "Location Recognition Using Prioritized Feature Matching," in *2010 Eur. Conf. Comput. Vis. (ECCV)*, Heraklion, Crete, Greece, 2010, pp. 791-804.
- [86] N. Snavely, S. M. Seitz, and R. Szeliski, "Photo tourism: Exploring Photo Collections in 3D," in *2006 ACM SIGGRAPH*, New York, NY, USA, 2006, pp. 835-846.
- [87] Y. Li, N. Snavely, D. Huttenlocher, and P. Fua, "Worldwide Pose Estimation Using 3D Point Clouds," in *2012 Eur. Conf. Comput. Vis. (ECCV)*, Florence, Italy, 2012, pp. 15-29.
- [88] Knapitsch, J. Park, Q.-Y. Zhou, and V. Koltun, "Tanks and temples: Benchmarking Large-Scale Scene Reconstruction," *ACM Trans. Graph.*, vol. 36, no. 4, pp. 1-13, 2017.
- [89] M. Farenzena, A. Fusiello, and R. Gherardi, "Structure-and-motion pipeline on a hierarchical cluster tree," in *2009 IEEE Int. Conf. Comput. Vis. Works. (ICCVW)*, Kyoto, Japan, 2009, pp. 1489-1496.
- [90] J. L. Schonberger and J.-M. Frahm, "Structure-from-Motion Revisited," in *2016 IEEE Conf. Comput. Vis. Pattern Recognit. (CVPR)*, Las Vegas, NV, USA, 2016, pp. 4104-4113.
- [91] Tanks-and-Temples. "Tanks and Temples Benchmark." tanksandtemples.org/ (accessed Apr. 4th, 2020).
- [92] G. Ros, L. Sellart, J. Materzynska, D. Vazquez, and A. M. Lopez, "The SYNTHIA Dataset: A Large Collection of Synthetic Images for Semantic Segmentation of Urban Scenes," in *2016 IEEE Conf. Comput. Vis. Pattern Recognit. (CVPR)*, Las Vegas, NV, USA, 2016, pp. 3234-3243.
- [93] K. Y. Leung, Y. Halpern, T. D. Barfoot, and H. H. Liu, "The UTIAS multi-robot cooperative localization and mapping dataset," *Int. J. Robot. Res.*, vol. 30, no. 8, pp. 969-974, 2011.
- [94] K. Y. Leung, T. D. Barfoot, and H. H. Liu, "Decentralized cooperative slam for sparsely-communicating robot networks: A centralized-equivalent approach," *J. Intell. & Robot. Sys.*, vol. 66, no. 3, 2012, pp. 321-342.
- [95] Y. Huang, C. Xue, F. Zhu, W. Wang, Y. Zhang, and J. A. Chambers. "Adaptive Recursive Decentralized Cooperative Localization for Multirobot Systems With Time-Varying Measurement Accuracy," *IEEE Trans. Instrum. Meas.*, vol. 70, 2021, pp. 1-25.
- [96] P. Furgale, P. Carle, J. Enright, and T. D. Barfoot, "The Devon Island rover navigation dataset," *Int. J. Robot. Res.*, vol. 31, no. 6, pp. 707-713, 2012.
- [97] Jiang, Yanhua, Huiyan Chen, Guangming Xiong, and Davide Scaramuzza. "Icp stereo visual odometry for wheeled vehicles based on a 1dof motion prior." In *2014 IEEE Int. Conf. Robot. Automat. (ICRA)*, 2014, pp. 585-592.
- [98] Wu, Xiaolong, and Cédric Pradalier. "Illumination robust monocular direct visual odometry for outdoor environment mapping." In *2019 Int. Conf. Robot. Automat. (ICRA)*, Montreal, Canada, 2019, pp. 2392-2398.
- [99] D. Caruso, J. Engel, D. Cremers, and Ieee, "Large-Scale Direct SLAM for Omnidirectional Cameras," in *2015 IEEE Int. Conf. Intell. Robot. Sys. (IROS)*, Hamburg, Germany, 2015, pp. 141-148.
- [100] H. Matsuki, L. V. Stumberg, V. Usenko, J. Stückler, and D. Cremers. "Omnidirectional DSO: Direct sparse odometry with fisheye cameras." *IEEE Robot. Automat. Lett.* vol. 3, no. 4, 2018, pp. 3693-3700.
- [101] J. Engel, V. Koltun, and D. Cremers. "Direct sparse odometry." *IEEE Trans. Pattern Anal. Mach. Intell.*, vol. 40, no. 3, 2017, pp. 611-625.
- [102] T. Qin, P. Li, and S. Shen. "Vins-mono: A robust and versatile monocular visual-inertial state estimator." *IEEE Trans. Robot.*, vol. 34, no. 4, 2018, pp. 1004-1020.
- [103] N. Brasch, A. Bozic, J. Lallemand, and F. Tombari. "Semantic monocular SLAM for highly dynamic environments." In *2018 IEEE/RSJ Int. Conf. Intell. Robot. Sys. (IROS)*, Spain, 2018, pp. 393-400.
- [104] A. Sharma, R. Nett, and J. Ventura. "Unsupervised Learning of Depth and Ego-Motion from Cylindrical Panoramic Video with Applications for Virtual Reality." *Int. J. Semantic Comput.*, vol. 14, no. 03, pp. 333-356, 2020.
- [105] Gaidon, Q. Wang, Y. Cabon, and E. Vig, "Virtual worlds as proxy for multi-object tracking analysis," in *2016 IEEE Conf. Comput. Vis. Pattern Recognit. (CVPR)*, Las Vegas, NV, USA, 2016, pp. 4340-4349.

- [106] M. Henein, J. Zhang, R. Mahony, and V. Ila. "Dynamic SLAM: The need for speed." In *2020 IEEE Int. Conf. Robot. Automat. (ICRA)*, Paris, France, 2020, pp. 2123-2129.
- [107] B. Pfrommer, N. Sanket, K. Daniilidis, and J. Cleveland. "PennCOSYVIO: A challenging Visual Inertial Odometry benchmark," in *2017 IEEE Int. Conf. Robot. Automat. (ICRA)*, Singapore, Singapore, 2017, pp. 3847-3854.
- [108] Y. He, J. Zhao, Y. Guo, W. He, and K. Yuan. "PI-vio: Tightly-coupled monocular visual-inertial odometry using point and line features." *Sensors*, vol. 18, no. 4, 2018, pp. 1159-1183.
- [109] E. Mueggler, H. Rebecq, G. Gallego, T. Delbruck, and D. Scaramuzza. "The event-camera dataset and simulator: Event-based data for pose estimation, visual odometry, and SLAM," *Int. J. Robot. Res.*, vol. 36, no. 2, pp. 142-149, 2017.
- [110] E. Mueggler, G. Gallego, H. Rebecq, and D. Scaramuzza. "Continuous-time visual-inertial odometry for event cameras." *IEEE Trans. Robot.*, vol. 34, no. 6, 2018, pp. 1425-1440.
- [111] L. Majdik, C. Till, and D. Scaramuzza. "The Zurich urban micro aerial vehicle dataset," *Int. J. Robot. Res.*, vol. 36, no. 3, pp. 269-273, 2017.
- [112] S. Cortés, A. Solin, E. Rahtu, and J. Kannala. "ADVO: An Authentic Dataset for Visual-Inertial Odometry," in *2018 Eur. Conf. Comput. Vis. (ECCV)*, Munich, Germany, 2018, pp. 425-440.
- [113] M. Bloesch, S. Omari, M. Hutter, and R. Siegwart. "Robust visual inertial odometry using a direct EKF-based approach." In *2015 IEEE/RSJ Int. Conf. Intell. Robot. Syst. (IROS)*, Hamburg, Germany, 2015, pp. 298-304.
- [114] A. Solin, S. Cortes, E. Rahtu and J. Kannala, "PIVO: Probabilistic Inertial-Visual Odometry for Occlusion-Robust Navigation," *2018 IEEE Winter Conf. Appl. Comput. Vis. (WACV)*, Lake Tahoe, NV, USA, 2018, pp. 616-625.
- [115] P. Wang, R. Yang, B. Cao, W. Xu and Y. Lin, "DeLS-3D: Deep Localization and Segmentation with a 3D Semantic Map," *2018 IEEE/CVF Conf. Comput. Vis. Pattern Recognit. (CVPR)*, Salt Lake City, UT, USA, 2018, pp. 5860-5869.
- [116] R. Zhu, M. Yang, W. Liu, R. Song, B. Yan, and Z. Xiao. "DeepAVO: Efficient Pose Refining with Feature Distilling for Deep Visual Odometry." 2021, *arXiv:2105.09899*. [Online]. Available: <https://arxiv.org/abs/2105.09899>
- [117] Antonini, W. Guerra, V. Murali, T. Sayre-Mccord, and S. Karaman, "The Blackbird Dataset: A Large-Scale Dataset for UAV Perception in Aggressive Flight," in *2018 Int. Symp. Exp. Robot. (ISER)*, Buenos Aires, Argentina, 2018, pp. 130-139.
- [118] T. Qin, S. Cao, J. Pan, and S. Shen. "A general optimization-based framework for global pose estimation with multiple sensors." 2019, *arXiv:1901.03642*. [Online]. Available: <https://arxiv.org/abs/1901.03642>
- [119] M. Martin, S.-J. Chung, and S. Hutchinson. "The visual-inertial canoe dataset." *Int. J. Robot. Res.*, vol. 37, no. 1, pp. 13-20, 2018.
- [120] K. Meier, S. J. Chung, and S. Hutchinson. "River segmentation for autonomous surface vehicle localization and river boundary mapping." *J. Field Robot.*, vol. 38, no. 2, 2021, pp. 192-211.
- [121] M. Vayugundla, F. Steidle, M. Smisek, M. J. Schuster, K. Bussmann and A. Wedler, "Datasets of Long Range Navigation Experiments in a Moon Analogue Environment on Mount Etna," in *2018 Int. Symp. Robot. (ISR)*, Munich, Germany, 2018, pp. 1-7.
- [122] R. Giubilato, M. Vayugundla, W. Stürzl, M. J. Schuster, A. Wedler, and R. Triebel. "Multi-Modal Loop Closing in Unstructured Planetary Environments with Visually Enriched Submaps." 2021, *arXiv:2105.02020*. [Online]. Available: <https://arxiv.org/abs/2105.02020>
- [123] Z. Zhu, D. Thakur, D. Ozaslan, B. Pfrommer, V. Kumar, and K. Daniilidis, "The multivehicle stereo event camera dataset: an event camera dataset for 3D perception," *IEEE Robot. Automat. Lett.*, vol. 3, no. 3, pp. 2032-2039, 2018.
- [124] Y. Zhou, G. Gallego and S. Shen, "Event-Based Stereo Visual Odometry," *IEEE Trans. Robot.*, vol. 37, no. 5, pp. 1433-1450.
- [125] N. Zeller, F. Quint, and U. Stilla. "A synchronized stereo and plenoptic visual odometry dataset," 2018, *arXiv:1807.09372*. [Online]. Available: <https://arxiv.org/abs/1807.09372>
- [126] D. Schubert, T. Goll, N. Demmel, V. Usenko, J. Stuckler, and D. Cremers. "The TUM VI Benchmark for Evaluating Visual-Inertial Odometry," in *25th IEEE/RSJ Int. Conf. Intell. Robot. Syst. (IROS)*, Madrid, SPAIN, 2018, pp. 1680-1687.
- [127] K. Sun, K. Mohta, B. Pfrommer, M. Watterson, S. Liu, Y. Mulgaonkar, C. J. Taylor, and V. Kumar. "Robust Stereo Visual Inertial Odometry for Fast Autonomous Flight," *IEEE Robot. Automat. Lett.*, vol. 3, no. 2, pp. 965-972, 2018.
- [128] A. I. Mourikis and S. I. Roumeliotis, "A Multi-State Constraint Kalman Filter for Vision-aided Inertial Navigation," in *2007 IEEE Int. Conf. Robot. Automat. (ICRA)*, Rome, Italy, 2007, pp. 3565-3572.
- [129] M. Ferrera, V. Creuze, J. Moras, and P. Trouvé-Peloux, "AQUALOC: An underwater dataset for visual-inertial-pressure localization," *Int. J. Robot. Res.*, vol. 38, no. 14, pp. 1549-1559, 2019.
- [130] C. Hu, S. Zhu, Y. Liang, Z. Mu, and W. Song. Visual-Pressure Fusion for Underwater Robot Localization With Online Initialization. *IEEE Robot. Automat. Lett.*, 6(4), 2021, pp.8426-8433.
- [131] G. Zhang, X. Yan and Y. Ye, "Loop Closure Detection Via Maximization of Mutual Information," *IEEE Access*, vol. 7, pp. 124217-124232, 2019.
- [132] T. Pire, M. Mujica, J. Civera, and E. Kofman, "The Rosario dataset: Multisensor data for localization and mapping in agricultural environments," *Int. J. Robot. Res.*, vol. 38, no. 6, pp. 633-641, 2019.
- [133] Pire, T., Fischer, T., Castro, G., De Cristóforis, P., Civera, J. and Berles, J.J., S-ptam: Stereo parallel tracking and mapping. *Robot. Auton. Sys.*, 2017, vol. 93, pp.27-42.
- [134] D. Schubert, N. Demmel, L. v. Stumberg, V. Usenko, and D. Cremers, "Rolling-Shutter Modelling for Direct Visual-Inertial Odometry," in *2019 IEEE/RSJ Int. Conf. Intell. Robot. Syst. (IROS)*, Macau, China, 2019, pp. 2462-2469.
- [135] L. V. Stumberg, V. Usenko and D. Cremers, "Direct Sparse Visual-Inertial Odometry Using Dynamic Marginalization," in *2018 IEEE Int. Conf. Robot. Automat. (ICRA)*, Brisbane, Australia, 2018, pp. 2510-2517.
- [136] J. J. Yeong Sang Park, Youngsik Shin, Ayoung Kim, "ViViD: Vision for Visibility Dataset," in *2019 IEEE Int. Conf. Robot. Automat. Workshop (ICRAW)*, Montreal, Canada, 2019.
- [137] L. Jinyu, Y. Bangbang, C. Danpeng, W. Nan, Z. Guofeng, and B. Hujun, "Survey and evaluation of monocular visual-inertial SLAM algorithms for augmented reality," *Virtual Real. Intell. Hardw.*, vol. 1, no. 4, pp. 386-410, 2019.
- [138] Wenzel, Patrick, Rui Wang, Nan Yang, Qing Cheng, Qadeer Khan, Lukas von Stumberg, Niclas Zeller, and Daniel Cremers. "4Seasons: A cross-season dataset for multi-weather SLAM in autonomous driving." In *DAGM German Conf. Pattern Recognit. (GCPR)*, Cham, German, pp. 404-417, 2020.
- [139] Gladkova, M., Wang, R., Zeller, N. and Cremers, D., 2021. Tight Integration of Feature-based Relocalization in Monocular Direct Visual Odometry. *arXiv:2102.01191*. [Online]. Available: <https://arxiv.org/abs/2102.01191>
- [140] I. Ali, A. Durmush, O. Suominen, J. Yli-Hietanen, S. Peltonen, J. Collin, and A. Gotchev. "FinnForest dataset: A forest landscape for visual SLAM." *Robot. Auton. Syst.*, vol. 132, 2020.
- [141] H. E. Benseddik, F. Morbidi, and G. Caron. "PanoraMIS: An ultra-wide field of view image dataset for vision-based robot-motion estimation." *Int. J. Robot. Res.*, vol. 39, no. 9, pp. 1037-1051, 2020.
- [142] Y. Cabon, N. Murray, and M. Humenberger, "Virtual KITTI 2," 2020, *arXiv:2001.10773*. [Online]. Available: <https://arxiv.org/abs/2001.10773>
- [143] M. Gehrig, W. Aarents, D. Gehrig and D. Scaramuzza, "DSEC: A Stereo Event Camera Dataset for Driving Scenarios," *IEEE Robot. Automat. Lett.*, vol. 6, no. 3, pp. 4947-4954, 2021.
- [144] W. Jang, J. Hyun, J. An, M. Cho and E. Kim, "A Lane-Level Road Marking Map Using a Monocular Camera," *IEEE/CAA J. Autom. Sinica*, 2021, Early Access.
- [145] S. Huang, M. Antone, E. Olson, L. Fletcher, D. Moore, S. Teller, and J. Leonard, "A High-rate, Heterogeneous Data Set From The DARPA Urban Challenge," *Int. J. Robot. Res.*, vol. 29, no. 13, pp. 1595-1601, 2010.
- [146] R. Mur-Artal, J.M.M. Montiel, and J.D. Tardos, ORB-SLAM: a versatile and accurate monocular SLAM system. *IEEE Trans. Robot.*, vol. 31, no. 5, 2015, pp.1147-1163.
- [147] C. Berger, Toward rich geometric map for SLAM: online detection of planets in 2D LIDAR. *J. Automat. Mobile Robot. Intell. Sys.*, 2013, pp.35-41.
- [148] S. Ceriani, G. Fontana, A. Giusti, D. Marzorati, M. Matteucci, D. Migliore, D. Rizzi, D. G. Sorrenti, and P. Taddei, "Rawseeds ground truth collection systems for indoor self-localization and mapping," *Auton. Robot.*, vol. 27, no. 4, pp. 353-371, 2009.
- [149] T.A. Ciarfuglia, G. Costante, P. Valigi, and E. Ricci, Evaluation of non-geometric methods for visual odometry. *Robot. Auton. Sys.*, 2014, vol. 62, no.12, pp.1717-1730.
- [150] T. Peynot, S. Scheding, and S. Terho, "The Marulan Data Sets: Multi-sensor Perception in a Natural Environment with Challenging Conditions," *Int. J. Robot. Res.*, vol. 29, no. 13, pp. 1602-1607, 2010.

- [151] C. Brunner, T. Peynot, T. Vidal - Calleja, and J. Underwood, Selective combination of visual and thermal imaging for resilient localization in adverse conditions: Day and night, smoke and fire. *J. Field Robot.*, vol. 30 no. 4, 2013, pp.641-666.
- [152] G. Pandey, J. R. McBride, and R. M. Eustice, "Ford Campus vision and lidar data set," *Int. J. Robot. Res.*, vol. 30, no. 13, pp. 1543-1552, 2011.
- [153] K. Lenac, A. Kitanov, R. Cupec, and I. Petrović, Fast planar surface 3D SLAM using LIDAR. *Robot. Auton. Sys.*, vol. 92, 2017, pp.197-220.
- [154] X. Chen, T. Läbe, A. Milioto, T. Röhling, O. Vysotska, A. Haag, J. Behley, and C. Stachniss, OverlapNet: Loop closing for LiDAR-based SLAM. 2021, *arXiv:2105.11344*. [Online]. Available: <https://arxiv.org/abs/2105.11344>
- [155] F. Pomerleau, M. Liu, F. Colas, and R. Siegwart, "Challenging data sets for point cloud registration algorithms," *Int. J. Robot. Res.*, vol. 31, no. 14, pp. 1705-1711, 2012.
- [156] F. Pomerleau, F. Colas, R. Siegwart, and S. Magnenat, Comparing ICP variants on real-world data sets. *Auton. Robot.*, vol. 34, no.3, 2013, pp.133-148.
- [157] S. Anderson, C. McManus, H. Dong, E. Beerepoot, and T. D. Barfoot, "The gravel pit lidar-intensity imagery dataset," *Tech. Rep. ASRL-2012-ABLOOI, UTIAS*, 2012.
- [158] C.H. Tong, S. Anderson, H. Dong, and T. D. Barfoot, Pose interpolation for laser - based visual odometry. *J. Field Robot.*, vol. 31, no.5, 2014, pp.731-757.
- [159] C. H. Tong, D. Gingras, K. Larose, T. D. Barfoot, and É. Dupuis, "The Canadian planetary emulation terrain 3D mapping dataset," *Int. J. Robot. Res.*, vol. 32, no. 4, pp. 389-395, 2013.
- [160] S. Fontana, D. Cattaneo, A.L. Ballardini, M. Vaghi, and D.G. Sorrenti, A benchmark for point clouds registration algorithms. *Robot. Auton. Sys.*, vol. 140, 2021, p.103734.
- [161] H. Korrapati, J. Courbon, S. Alizon, and F. Marmoiton, "" The Institut Pascal Data Sets": un jeu de données en extérieur, multicapteurs et datées avec réalité terrain, données d'étalonnage et outils logiciels." In Orasis, Congrès des jeunes chercheurs en vision par ordinateur. 2013.
- [162] J. Mansouri, B. Seddik, S. Gazzah, and T. Chateau, Coarse localization using space-time and semantic-context representations of geo-referenced video sequences. In *2015 Int. Conf. Image Proc. Theory Tools Appl. (IPTA)*, 2015, pp. 355-359.
- [163] J.-L. Blanco-Claraco, F.-Á. Moreno-Dueñas, and J. González-Jiménez, "The Málaga urban dataset: High-rate stereo and LiDAR in a realistic urban scenario," *Int. J. Robot. Res.*, vol. 33, no. 2, pp. 207-214, 2014.
- [164] A. Jaenal, D. Zuñiga-Nöel, R. Gomez-Ojeda, and J. Gonzalez-Jimenez, Improving Visual SLAM in Car-Navigated Urban Environments with Appearance Maps. In *2020 IEEE/RSJ Int. Conf. Intell. Robot. Sys. (IROS)* 2020, pp. 4679-4685.
- [165] N. Carlevaris-Bianco, A. K. Ushani, and R. M. Eustice, "University of Michigan North Campus long-term vision and lidar dataset," *Int. J. Robot. Res.*, vol. 35, no. 9, pp. 1023-1035, 2016.
- [166] W. Xu, Y. Cai, D. He, J. Lin, and F. Zhang, Fast-lío2: Fast direct lidar-inertial odometry. 2021, *arXiv:2107.06829*. [Online]. Available: <https://arxiv.org/abs/2107.06829>
- [167] M. Dymczyk, E. Stumm, J. Nieto, R. Siegwart, and I. Gilitschenski, Will it last? learning stable features for long-term visual localization. In *2016 14th Int. Conf. 3D Vis. (3DV)* 2016, pp. 572-581.
- [168] N. Chebrolu, P. Lottes, A. Schaefer, W. Winterhalter, W. Burgard, and C. Stachniss, "Agricultural robot dataset for plant classification, localization and mapping on sugar beet fields," *Int. J. Robot. Res.*, vol. 36, no. 10, pp. 1045-1052, 2017.
- [169] F. Kraemer, A. Schaefer, A. Eitel, J. Vertens, and W. Burgard, From plants to landmarks: Time-invariant plant localization that uses deep pose regression in agricultural fields. 2017, *arXiv:1709.04751*. [Online]. Available: <https://arxiv.org/abs/1709.04751>
- [170] K. Leung, D. Lühr, H. Houshiar, F. Inostroza, D. Borrmann, M. Adams, A. Nüchter, and J. Ruiz del Solar, "Chilean underground mine dataset," *Int. J. Robot. Res.*, vol. 36, no. 1, pp. 16-23, 2017.
- [171] G. Pascoe, W. Maddern, M. Tanner, P., Piniés, and P. Newman, NID-SLAM: Robust monocular SLAM using normalised information distance. In *2017 IEEE Conf. Comput. Vis. Pattern Recognit. (CVPR)*, 2017, pp. 1435-1444.
- [172] Y. Cho, G. Kim, and A. Kim, Unsupervised geometry-aware deep lidar odometry. In *2020 IEEE Int. Conf. Robot. Automat. (ICRA)*, Paris, France, 2021, pp. 2145-2152.
- [173] Y. Choi, N. Kim, S. Hwang, K. Park, J. S. Yoon, K. An, and I. S. Kweon, "KAIST Multi-Spectral Day/Night Data Set for Autonomous and Assisted Driving," *IEEE Trans. Intell. Transp. Syst.*, vol. 19, no. 3, pp. 934-948, 2018.
- [174] K. Li, X. Zhang, L.I. Kun, and S. Zhang, Vision Global Localization with Semantic Segmentation and Interest Feature Points. In *2020 IEEE/RSJ Int. Conf. Intell. Robot. Sys. (IROS)*, 2020, pp. 4581-4587.
- [175] R. A. Hewitt, E. Boukas, M. Azkarate, M. Pagnamenta, J. A. Marshall, A. Gasteratos, and G. Visentin, "The Katwijk beach planetary rover dataset," *Int. J. Robot. Res.*, vol. 37, no. 1, pp. 3-12, 2018.
- [176] C. Wang, S. Hou, C. Wen, Z. Gong, Q. Li, X. Sun, J. Li, 2018. Semantic line framework-based indoor building modeling using backpacked laser scanning point cloud. *ISPRS J. Photogramm. Remote Sens.*, vol. 143, pp. 150-166, 2018.
- [177] C. Wen, Y. Dai, Y. Xia, Y. Lian, J. Tan, C. Wang, J. Li, Toward Efficient 3-D Colored Mapping in GPS-/GNSS-Denied Environments. *IEEE Geosci. Remote Sens. Lett.*, vol. 17, pp. 147-151, 2020.
- [178] P. Chen, W. Shi, W. Fan, H. Xiang, and S. Bao, RectMatch: A novel scan matching method using the rectangle-flattening representation for mobile LiDAR systems. *ISPRS J. Photogramm. Remote Sens.*, vol. 180, 2021, pp.191-208.
- [179] R. Gaspar, A. Nunes, A. M. Pinto, and A. Matos, "Urban@CRAS dataset: Benchmarking of visual odometry and SLAM techniques," *Robot. Auton. Syst.*, vol. 109, pp. 59-67, 2018.
- [180] J. J. Yeong Sang Park, Youngsik Shin, Ayoung Kim, "Radar Dataset for Robust Localization and Mapping in Urban Environment," in *2019 IEEE Int. Conf. Robot. Automat. Workshop (ICRAW)*, Montreal, Canada, 2019.
- [181] Y. S. Park, Y. -S. Shin and A. Kim, "PhaRaO: Direct Radar Odometry using Phase Correlation," in *2020 IEEE Int. Conf. Robot. Automat. (ICRA)*, Paris, France, 2020, pp. 2617-2623.
- [182] D. Wisth, M. Camurri and M. Fallon, "Robust Legged Robot State Estimation Using Factor Graph Optimization," in *IEEE Robot. Automat. Lett.*, vol. 4, no. 4, 2019, pp. 4507-4514.
- [183] M. Ramezani, G. Tinchev, E. Iuganov and M. Fallon, "Online LiDAR-SLAM for Legged Robots with Robust Registration and Deep-Learned Loop Closure," in *2020 IEEE Int. Conf. Robot. Automat. (ICRA)*, 2020, Paris, France, pp. 4158-4164.
- [184] D. Barnes, M. Gadd, P. Murcutt, P. Newman and I. Posner, "The Oxford Radar RobotCar Dataset: A Radar Extension to the Oxford RobotCar Dataset," in *2020 IEEE Int. Conf. Robot. Automat. (ICRA)*, Paris, France, 2020, pp. 6433-6438.
- [185] Z. Hong, Y. Petillot and S. Wang, "RadarSLAM: Radar based Large-Scale SLAM in All Weathers," in *2020 IEEE/RSJ Int. Conf. Intell. Robot. Sys. (IROS)*, Las Vegas, NV, USA, 2020, pp. 5164-5170.
- [186] W. Wen, Y. Zhou, G. Zhang, S. Fahandezh-Saadi, X. Bai, W. Zhan, M. Tomizuka, and L.T. Hsu, "UrbanLoco: A Full Sensor Suite Dataset for Mapping and Localization in Urban Scenes," in *2020 IEEE Int. Conf. Robot. Automat. (ICRA)*, Paris, France, 2020, pp. 2310-2316.
- [187] D. Lee, S. Ryu, S. Yeon, Y. Lee, D. Kim, C. Han, Y. Cabon, P. Weinzaepfel, N. Guérin, G. Csurka, and M. Humenberger, "Large-scale Localization Datasets in Crowded Indoor Spaces." in *2021 IEEE/CVF Conf. Comput. Vis. Pattern Recognit. (CVPR)*, pp. 3227-3236. 2021.
- [188] K. Lai, L. Bo, X. Ren, and D. Fox, "A large-scale hierarchical multi-view RGB-D object dataset," in *2011 IEEE Int. Conf. Robot. Automat. (ICRA)*, Shanghai, China, 2011, pp. 1817-1824.
- [189] S. Meister, S. Izadi, P. Kohli, M. Hämmerle, C. Rother, and D. Kondermann, "When can we use kinectfusion for ground truth acquisition," in *2012 IEEE/RSJ Int. Conf. Intell. Robot. Syst. Works. (IROSW)*, Vilamoura, Portugal, 2012, pp. 3-8.
- [190] A. Dai, M. Nießner, M. Zollhöfer, S. Izadi, and C. Theobalt, Bundlefusion: Real-time globally consistent 3d reconstruction using on-the-fly surface reintegration. *ACM Trans. Graph. (ToG)*, vol. 36, no. 4, 2017, p.1.
- [191] J. Shotton, B. Glocker, C. Zach, S. Izadi, A. Criminisi, and A. Fitzgibbon, "Scene coordinate regression forests for camera relocation in RGB-D images," in *2012 IEEE Conf. Comput. Vis. Pattern Recognit. (CVPR)*, Portland, OR, USA, 2013, pp. 2930-2937.
- [192] X. Li, and H. Ling, TransCamp: Graph Transformer for 6-DoF Camera Pose Estimation. 2021, *arXiv:2105.14065*. [Online]. Available: <https://arxiv.org/abs/2105.14065>
- [193] J. Xiao, A. Owens, and A. Torralba, "SUN3D: A Database of Big Spaces Reconstructed Using SfM and Object Labels," in *2013 IEEE Int. Conf. Comput. Vis. (ICCV)*, Sydney, NSW, Australia, 2013, pp. 1625-1632.
- [194] S. Choi, Q. Zhou and V. Koltun, "Robust reconstruction of indoor scenes," in *2015 IEEE Conf. Comput. Vis. Pattern Recognit. (CVPR)*, 2015, pp. 5556-5565.

- [195] Q.-Y. Zhou and V. Koltun, "Color map optimization for 3D reconstruction with consumer depth cameras," *ACM Trans. Graph.*, vol. 33, no. 4, pp. 1-10, 2014.
- [196] K. Lai, L. Bo, and D. Fox, "Unsupervised feature learning for 3D scene labeling," in *2014 IEEE Int. Conf. Robot. Automat. (ICRA)*, Hong Kong, China, 2014, pp. 3050-3057.
- [197] Wasenmüller, M. Meyer, and D. Stricker, "CoRBS: Comprehensive RGB-D benchmark for SLAM using Kinect v2," in *2016 IEEE Winter Conf. Appl. Comput. Vis. (WACV)*, Lake Placid, NY, USA, 2016, pp. 1-7.
- [198] O. Wasenmüller, M.D. Ansari, and D. Stricker, "Dna-slam: Dense noise aware slam for tof rgb-d cameras," in *Asian Conf. Comput. Vis. (ACCV)*, Cham, Switzerland, 2016, pp. 613-639.
- [199] B.-S. Hua, Q.-H. Pham, D. T. Nguyen, M.-K. Tran, L.-F. Yu, and S.-K. Yeung, "SceneNN: A Scene Meshes Dataset with aNnotations," in *2016 4th Int. Conf. 3D Vis. (3DV)*, Stanford, CA, USA, 2016, pp. 92-101.
- [200] M. Yazdampour, G. Fan and W. Sheng, "ManhattanFusion: Online Dense Reconstruction of Indoor Scenes from Depth Sequences," in *IEEE Trans. Vis. Comput. Graphics*, 2020, Early Access.
- [201] H. Oleynikova, Z. Taylor, M. Fehr, R. Siegwart, and J. Nieto, "Voxblox: Incremental 3D Euclidean Signed Distance Fields for on-board MAV planning," in *2017 IEEE/RSJ Int. Conf. Intell. Robot. Sys. (IROS)*, Vancouver, BC, Canada, 2017, pp. 1366-1373.
- [202] J. R. Ruiz-Sarmiento, C. Galindo, and J. Gonzalez-Jimenez, "Robot@Home, a robotic dataset for semantic mapping of home environments," *Int. J. Robot. Res.*, vol. 36, no. 2, pp. 131-141, 2017.
- [203] X. Qi, W. Wang, Z. Liao, X. Zhang, D. Yang, and R. Wei, "Object semantic grid mapping with 2D LiDAR and RGB-D camera for domestic robot navigation," *Appl. Sci.*, vol. 10, no. 17, p.5782.
- [204] J. McCormac, A. Handa, S. Leutenegger, and A. J. Davison, "SceneNet RGB-D: Can 5M Synthetic Images Beat Generic ImageNet Pre-training on Indoor Segmentation?," in *2017 IEEE Int. Conf. Comput. Vis. (ICCV)*, Venice, Italy, 2017, pp. 2678-2687.
- [205] M. Bloesch, J. Czamowski, R. Clark, S. Leutenegger and A. J. Davison, "CodeSLAM - Learning a Compact, Optimisable Representation for Dense Visual SLAM," in *2018 IEEE/CVF Conf. Comput. Vis. Pattern Recognit. (CVPR)*, Salt Lake City, UT, USA, 2018, pp. 2560-2568.
- [206] S. Song, F. Yu, A. Zeng, A. X. Chang, M. Savva, and T. Funkhouser, "Semantic Scene Completion from a Single Depth Image," in *2017 IEEE Conf. Comput. Vis. Pattern Recognit. (CVPR)*, Honolulu, HI, USA, 2017, pp. 1746-1754.
- [207] J. Huang, S. Yang, T. -J. Mu and S. -M. Hu, "ClusterVO: Clustering Moving Instances and Estimating Visual Odometry for Self and Surroundings," in *2020 IEEE/CVF Conf. Comput. Vis. Pattern Recognit. (CVPR)*, Seattle, WA, USA, 2020, pp. 2165-2174.
- [208] Dai, A. X. Chang, M. Savva, M. Halber, T. Funkhouser, and M. Nießner, "ScanNet: Richly-annotated 3d reconstructions of indoor scenes," in *2017 IEEE Conf. Comput. Vis. Pattern Recognit. (CVPR)*, Honolulu, HI, USA, 2017, pp. 5828-5839.
- [209] H. Mahé, D. Marraud and A. I. Comport, "Semantic-only Visual Odometry based on dense class-level segmentation," in *2018 Int. Conf. Pattern Recognit. (ICPR)*, Beijing, China, 2018, pp. 1989-1995.
- [210] B. Bescos, J.M. Fàcil, J. Civera, and J. Neira, DynaSLAM: Tracking, mapping, and inpainting in dynamic scenes. *IEEE Robot. Automat. Lett.*, vol. 3, no. 4, 2018, pp.4076-4083.
- [211] R. Scona, M. Jaimez, Y.R. Petillot, M. Fallon, and D. Cremers, "Staticfusion: Background reconstruction for dense rgb-d slam in dynamic environments," in *2018 IEEE Int. Conf. Robot. Automat. (ICRA)*, Brisbane, Australia, 2018, pp. 3849-3856.
- [212] T. Schops, T. Sattler, and M. Pollefeys, "BAD SLAM: Bundle Adjusted Direct RGB-D SLAM," in *2019 IEEE/CVF Conf. Comput. Vis. Pattern Recognit. (CVPR)*, Long Beach, CA, USA, 2019, pp. 134-144.
- [213] J. Straub, T. Whelan, L. Ma, Y. Chen, E. Wijmans, S. Green, J. J. Engel, R. Mur-Artal, C. Ren, and S. Verma, "The Replica dataset: A digital replica of indoor spaces," 2019, *arXiv:1906.05797*. [Online]. Available: <https://arxiv.org/abs/1906.05797>
- [214] X. Hu, and J. Lang, DOE-SLAM: Dynamic Object Enhanced Visual SLAM. 2021, *Sensors*, vol. 21, no. 9, p.3091.
- [215] Z. Shan, R. Li, and S. Schwertfeger, "RGBD-inertial trajectory estimation and mapping for ground robots," *Sensors*, vol. 19, no. 10, pp. 2251-2279, 2019.
- [216] H. Zhang and C. Ye, "DUI-VIO: Depth Uncertainty Incorporated Visual Inertial Odometry based on an RGB-D Camera," in *2020 IEEE/RSJ Int. Conf. Intell. Robot. Sys. (IROS)*, Las Vegas, NV, USA, 2020, pp. 5002-5008
- [217] M. Goesele, B. Curless and S. M. Seitz, "Multi-View Stereo Revisited," in *2006 IEEE Comput. Soc. Conf. Comput. Vis. Pattern Recognit. (CVPR)*, New York, NY, USA, 2006, pp. 2402-2409.
- [218] Schönberger, J.L., Zheng, E., Frahm, J.M. and Pollefeys, M., "Pixelwise view selection for unstructured multi-view stereo," in *2016 Eur. Conf. Comput. Vis. (ECCV)*, pp. 501-518.
- [219] Y. Furukawa and J. Ponce, "Accurate, Dense, and Robust Multiview Stereopsis," *IEEE Trans. Pattern Anal. Mach. Intell.*, vol. 32, no. 8, 2010, pp. 1362-1376.
- [220] C. Strecha, W. Von Hansen, L. Van Gool, P. Fua, and U. Thoennessen, "On benchmarking camera calibration and multi-view stereo for high resolution imagery," in *2008 IEEE Conf. Comput. Vis. Pattern Recognit. (CVPR)*, Anchorage, AK, USA, 2008, pp. 1-8.
- [221] K. Kolev, M. Klodt, T. Brox, and D. Cremers, "Continuous Global Optimization in Multiview 3D Reconstruction," *Int. J. Comput. Vis.*, vol. 84, no. 1, pp. 80-96, 2009.
- [222] D. Cremers and K. Kolev, "Multiview Stereo and Silhouette Consistency via Convex Functionals over Convex Domains," *IEEE Trans. Pattern Anal. Mach. Intell.*, vol. 33, no. 6, 2011, pp. 1161-1174.
- [223] D. Crandall, A. Owens, N. Snavely, and D. Huttenlocher, "Discrete-continuous optimization for large-scale structure from motion," in *2011 IEEE Conf. Comput. Vis. Pattern Recognit. (CVPR)*, Providence, RI, USA, 2011, pp. 3001-3008.
- [224] D. M. Chen, G. Baatz, K. Koser, S. S. Tsai, R. Vedantham, T. Pylvanainen, K. Roimela, X. Chen, J. Bach, M. Pollefeys, B. Girod, and R. Grzeszczuk, "City-scale landmark identification on mobile devices," in *2011 IEEE Conf. Comput. Vis. Pattern Recognit. (CVPR)*, Providence, RI, USA, 2011, pp. 737-744.
- [225] D. J. Crandall, A. Owens, N. Snavely and D. P. Huttenlocher, "SfM with MRFs: Discrete-Continuous Optimization for Large-Scale Structure from Motion," *IEEE Trans. Pattern Anal. Mach. Intell.*, vol. 35, no. 12, 2013, pp. 2841-2853.
- [226] S. Shuhan, "Accurate Multiple View 3D Reconstruction Using Patch-Based Stereo for Large-Scale Scenes," *IEEE Trans. Image Process.*, vol. 22, no. 5, pp. 1901-1914, 2013.
- [227] S. Cao and N. Snavely, "Learning to Match Images in Large-Scale Collections," in *2012 Eur. Conf. Comput. Vis. Works. (ECCVW)*, Florence, Italy, 2012, pp. 259-270.
- [228] J. L. Schönberger, A. C. Berg and J. Frahm, "PAIGE: PAirwise Image Geometry Encoding for improved efficiency in Structure-from-Motion," in *2015 IEEE Conf. Comput. Vis. Pattern Recognit. (CVPR)*, Boston, MA, USA, 2015, pp. 1009-1018.
- [229] K. Wilson and N. Snavely, "Network Principles for SfM: Disambiguating Repeated Structures with Local Context," in *2013 IEEE Int. Conf. Comput. Vis. (ICCV)*, Sydney, NSW, Australia, 2013, pp. 513-520.
- [230] R. Jensen, A. Dahl, G. Vogiatzis, E. Tola, and H. Aanaes, "Large Scale Multi-view Stereopsis Evaluation," in *2014 IEEE Conf. Comput. Vis. Pattern Recognit. (CVPR)*, Columbus, OH, USA, 2014, pp. 406-413.
- [231] N.D. Campbell, G. Vogiatzis, C. Hernández, and R. Cipolla, "Using multiple hypotheses to improve depth-maps for multi-view stereo," in *2008 Eur. Conf. Comput. Vis. (ECCV)*, 2008, pp. 766-779.
- [232] K. Wilson and N. Snavely, "Robust Global Translations with 1DSfM," in *2014 Eur. Conf. Comput. Vis. (ECCV)*, Zurich, Switzerland, 2014, pp. 61-75.
- [233] T. Schops, J. L. Schonberger, S. Galliani, T. Sattler, K. Schindler, M. Pollefeys, and A. Geiger, "A Multi-view Stereo Benchmark with High-Resolution Images and Multi-camera Videos," in *2017 IEEE Conf. Comput. Vis. Pattern Recognit. (CVPR)*, Honolulu, HI, USA, 2017, pp. 3260-3269.
- [234] L. Nardi, B. Bodin, M. Z. Zia, J. Mawer, A. Nisbet, P. H. J. Kelly, A. J. Davison, M. Lujan, M. F. P. O'Boyle, G. Riley, N. Topham, and S. Furber, "Introducing SLAMBench, a performance and accuracy benchmarking methodology for SLAM," in *2015 IEEE Int. Conf. Robot. Automat. (ICRA)*, Seattle, WA, USA, 2015, pp. 5783-5790.
- [235] B. Bodin, H. Wagstaff, S. Saedi, L. Nardi, E. Vespa, J. Mawer, A. Nisbet, M. Lujan, S. Furber, A. J. Davison, P. H. J. Kelly, and M. F. P. O'Boyle, "SLAMBench2: Multi-Objective Head-to-Head Benchmarking for Visual SLAM," in *2018 IEEE Int. Conf. Robot. Automat. (ICRA)*, Brisbane, QLD, Australia, 2018, pp. 1-8.
- [236] M. Bujanca, P. Gafton, S. Saedi, A. Nisbet, B. Bodin, O. Michael F.P. A. J. Davison, K. Paul H.J., G. Riley, B. Lennox, M. Lujan, and S. Furber, "SLAMBench 3.0: Systematic Automated Reproducible Evaluation of SLAM Systems for Robot Vision Challenges and Scene Understanding," in *2019 Int. Conf. Robot. Automat. (ICRA)*, Montreal, QC, Canada, 2019, pp. 6351-6358.

- [237] CloudCompare. "CloudCompare - 3D point cloud and mesh processing software." CloudCompare - Open Source Project. <https://www.danielgm.net/cc/> (accessed Aug. 8th, 2020).
- [238] Uzh-rpg. "Video to events: Recycling video datasets for event cameras", uzh-rpg. https://github.com/uzh-rpg/rpg_vid2e/ (accessed Sep. 5th, 2021)
- [239] AirLab. "TartanAir: A Dataset to Push the Limits of Visual SLAM." AirLab. <https://theairlab.org/tartanair-dataset/> (accessed Mar. 5th, 2020).
- [240] C. Kerl, J. Sturm, and D. Cremers, "Dense visual SLAM for RGB-D cameras," in *2013 IEEE/RSJ Int. Conf. Intell. Robot. Syst. (IROS)*, Tokyo, Japan, 2013, pp. 2100-2106.
- [241] F. Endres, J. Hess, J. Sturm, D. Cremers, and W. Burgard, "3-D Mapping With an RGB-D Camera," *IEEE Trans. Robot.*, vol. 30, no. 1, pp. 177-187, 2014.
- [242] R. Mur-Artal and J. D. Tardos, "Visual-Inertial Monocular SLAM With Map Reuse," *IEEE Robot. Automat. Lett.*, vol. 2, no. 2, pp. 796-803, 2017.
- [243] S. Sacedi, L. Nardi, E. Johns, B. Bodin, P. H. J. Kelly, and A. J. Davison, "Application-oriented design space exploration for SLAM algorithms," in *2017 IEEE Int. Conf. Robot. Automat. (ICRA)*, Singapore, Singapore, 2017, pp. 5716-5723.
- [244] T. Qin, Y. Zheng, T. Chen, Y. Chen, and Q. Su, RoadMap: A Light-Weight Semantic Map for Visual Localization towards Autonomous Driving. 2021, *arXiv:2106.02527*. [Online]. Available: <https://arxiv.org/abs/2106.02527>
- [245] D. Gershgorin. "The data that transformed AI research—and possibly the world." Quartz. <https://qz.com/1034972/the-data-that-changed-the-direction-of-ai-research-and-possibly-the-world/> (accessed Apr. 16, 2020).
- [246] Savva, M., Kadian, A., Maksymets, O., Zhao, Y., Wijmans, E., Jain, B., Straub, J., Liu, J., Koltun, V., Malik, J. and Parikh, D., Habitat: A platform for embodied ai research. In *2019 IEEE/CVF Int. Conf. Comput. Vis. (CVPR)*, 2019, pp. 9339-9347.
- [247] NVIDIA, "RTX Technology", NVIDIA, <https://developer.nvidia.com/rtx/raytracing/> (accessed Sep. 16, 2021).
- [248] Bang4BuckPC Gamer, "Red Dead Redemption 2 Ultra Settings 4K | RTX 3090 | Ryzen 3950X OC", Bang4BuckPC Gamer, https://www.youtube.com/watch?v=hUzmTnKrLA&t=1306s&ab_channel=Bang4BuckPCGamer/ (accessed Sep. 16, 2021).